Fluid migration and porosity evolution in the Buda Hills, Hungary – selected examples from Triassic and Paleogene carbonate rocks

Zsófia Poros

Dissertation submitted to the Ph.D. program for Geology and Geophysics at the Ph.D. School of Earth Sciences, Eötvös Loránd University, Budapest
in partial fulfilment of the requirements for the degree of
Philosophiae Doctor

Supervisors:
Prof. **Andrea Mindszenty**
Department of Physical and Applied Geology, Eötvös Loránd University, Budapest

Ferenc Molnár, associate professor
Department of Mineralogy, Eötvös Loránd University, Budapest

Head of the Ph.D. School: Prof. **Gyula Gábris**
Chair of the Ph.D. Program: Prof. **Andrea Mindszenty**

on contract with ENI S.p.A.
Industrial advisor: **Paola Ronchi**, Ph.D.
ENI Exploration and Production Division, Milan, Italy

2011
Eötvös Loránd University
Budapest, Hungary

Acknowledgements

First of all I would like to thank the continuous help and support of my supervisor, **Andrea Mindszenty**. Her immense enthusiasm on the topic always made me motivated in doing my research. I really enjoyed our discussions and the way how we could think together. I also acknowledge her efforts to improve my English skills.

I am grateful to my co-supervisor, **Ferenc Molnár** for his help, especially for introducing me to the field of fluid inclusions and hydrothermal processes in the Buda Hills already during my undergraduate research project.

Paola Ronchi, the industrial advisor at the ENI (Milan, Italy), is thanked for her useful advices. I learned a lot from her about the industrial approach in geological research.

I am very grateful to **Jacques Pironon** (Université de Lorraine, Nancy, France) for the opportunity to investigate my oil inclusions in Nancy by numerous different methods. He taught me very important things about the petrography of hydrocarbon-bearing fluid inclusions, too.

I am very thankful to **Hans G. Machel**, (University of Alberta, Edmonton, Canada) for working together on the enigmatic powderization of dolomites. I appreciate that he spent considerable time visiting the field and discussing about this topic.

I am very grateful to **Orsolya Győri** for the effective cooperation, for the useful discussions and also for her assistance in the field work and in the illustration of my thesis.

Participants of the twin-project sponsored by the SHELL, namely **Anita Erőss, Judit Mádl-Szőnyi** and **Anita Csoma**, are acknowledged for the fruitful cooperation. I especially thank the help of Anita Erőss to understand the hydrogeology of the Buda Karst.

I thank to **János Haas** and **Kinga Hips** the correction of certain parts of the text. I am grateful to Kinga for her help in interpreting my data concerning the dolomitization.

I appreciate the thoughtful discussions with **László Fodor** about the structural geology of the area. Discussion with **Csaba Szabó** about rare earth elements is highly appreciated. I thank the help of **Kornél Torkos** at the initial stage of gas chromatographic measurements. **Zoltán Szekeres** is acknowledged for the fulfilment of the gas chromatographic measurements. I am grateful to **Csanád Sajgó** for the discussion about the organic geochemical part of the work. I thank the help of **Balázs Brunner** to understand the GC method. I am thankful to **Ádám Vadas** for his help in the modification of the geological map. I thank the help of **Zsolt Bendő** in the SEM work and of **Judit Tóthné Király** in the XRD

measurements. **Szabolcs Leél-Őssy** and **Sándor Krausz** are acknowledged for drilling and sampling in the Szemlőhegy Cave.

I am very grateful to my geologist friends for their support and help during my work, namely to **Márta Berkesi** and **Tibor Guzmics** for their help in Raman analysis, to **Róbert Part, Attila Péntek, Györgyi Tuba, Péter Kiss** and **Richárd Orbán** for the assistance in the field work and sampling and to **Péter Pekker** for his assistance in XRD measurements.

I am particularly grateful to **Benedek Gál** for his endless support and patience. I thank his help in the field work, in sample preparation, and in making figures. I also thank his help in revising my English writing and I am grateful for the discussions about my research almost every day.

I would like to thank **my parents** for bringing me up in an ambience that always inspired me for thinking and working hard. I am thankful to **my aunt** for encouraging me to do a PhD research. I am very grateful to **my sisters** for their support and for showing interest in my work all along my PhD research.

Financial support for the project was provided by **ENI S.p.A.** Contract number: 4700006937/ST 1.

Table of contents

List of figures

Chapter I – Introduction

To improve the tools and methodologies of distinguishing meteoric and hydrothermal effects on carbonate reservoirs, a collaboration was initiated by ENI S.p.A. and Eötvös Loránd University. The 'Buda Thermal Karst' area was selected for an outcrop-based case study focussing on the effects of burial diagenesis, tectonics, fracturing, subaerial exposure, hydrothermal events and recent groundwater flow on the porosity of karstified carbonates. The general aim was to provide an analogue for carbonate reservoir systems that underwent multiphase diagenetic evolution including multiple phases of karstification and also hydrothermal events.

In most karst systems porosity creation is due to the interaction of carbonates with meteoric waters containing atmospheric CO_2. However, there are karst systems where non-atmospheric CO_2 plays important role in dissolution, i.e. hydrothermal sources, organic matter, etc. Rocks that suffered dissolution in the deep-burial setting are called 'hydrothermal karsts' by some authors (Fritz et al. 1993). The term 'hydrothermal' was defined by White (1957) as follows: "water that is considerably warmer (5°C or more) than the surrounding environment". Hydrothermal karst is also called 'hypogenic karst'. It is defined as influenced by deep energy and gas sources, associated with regional flow systems (Klimchouk 2007). Whilst epigenic systems are directly influenced by the infiltration of meteoric water and CO_2 from the atmosphere and soil and they are often associated with local–to–intermediate flow systems (Goldscheider et al. 2010). Cooling corrosion, pressure corrosion and biocorrosion also may result in significant dissolution. In addition, mixing corrosion has extreme importance in porosity creation that is the result of mixing of waters of different partial CO_2 pressures. In order to be able to predict the volume and distribution of porosity in a karst system it is very important to understand the porosity-creating processes and the controlling factors (Esteban and Wilson 1993).

Aim of the study

The Buda Hills, hosting the famous Pleistocene-Recent thermal karst with actual hot springs and caves, are built up by Mesozoic-Tertiary carbonates and to a lesser extent also by siliciclastic rocks. This rock suite was affected by several events of meteoric karstification related to repeated, tectonically controlled uplift and erosion throughout late Mesozoic to Tertiary times. Previous studies showed that in addition to obviously meteoric karstification, Buda Hills have been affected by multiple hydrothermal events and the interaction of

hydrothermal and meteoric solutions was also possible. Therefore the project aimed to see the impact of these superimposed meteoric- and hydrothermal processes on the porosity evolution of the affected marine carbonates.

The working hypothesis was that porosity evolution of carbonates in the Buda Hills must have been closely related to the stages of Alpine tectogenesis, namely to:

- Middle Triassic to Jurassic extension and subsidence
- Cretaceous/Early Tertiary deformation (thrusting, strike-slip faulting, uplift and exposure)
- Neogene extension and subsidence
- Plio/Pleistocene inversion (uplift and exposure)

The aim was to reveal whether the above specified tectogenetic events had any recognizable contribution to the ultimate porosity of the studied rock suite. As a result of the preliminary field work two major, still open, secondary porosity types could be recognized in the exposed carbonate rock suite:

1) Cavernous/fracture porosity represented by the famous hypogenic cave-system formed along former calcite-barite-sulphide veins

2) Extensive diffuse micro-porosity of powdered Triassic dolomites.

Both porosity types are known as hosts of hydrocarbons, not in the Buda Hills but elsewhere in the world. Karst-controlled cavernous reservoirs are very common. Dolomite powder is also known to be a hydrocarbon reservoir (e.g. the Grosmont reservoir, Canada). Therefore special attention was focussed to those processes which could be responsible for the formation of these two porosity types.

The present project deals with the Mesozoic-Tertiary part of the diagenetic history, whereas a twin-project – sponsored by SHELL – studied the Pleistocene to recent elements of the evolution with a hydrogeological approach. As a result of this cooperation we had the possibility to investigate the whole complex evolution of fluid flow systems of the Buda Hills/Buda Karst and also to study the possible link between the paleo- and the recent hydrogeological settings.

Structure of the Thesis

In accordance with the two different types of large-scale porosity detected in the Buda Karst, the results are presented here in two separate sections. “Geological background” is followed by the first main chapter (Chapter III) which deals with the diagenetic evolution of

the oldest rocks exposed in the Buda Hills, namely the Triassic platform dolomites including both the details of shallow to burial dolomitization and the discussion of the unique powderization of dolomites with the emphasize on the powderization history. The next main chapter (Chapter IV) is a summary of the early stages of the evolution of the Buda Thermal Karst focussing on the first signs of the contribution of hydrocarbon-bearing, basinal fluids to the hypogenic karst system. The relationship between the paleo- and recent hydrogeology is also discussed in this chapter. After the discussion of the implications of these results to hydrocarbon exploration, the effect of all the detected diagenetic phases on porosity evolution is summarized as final conclusions.

Chapter II – Geology and structural evolution of the Buda Hills

The Buda Hills is located in the neighbourhood of Budapest (Fig. 1), in the northeastern part of the Transdanubian Range (TR), in the central part of the Pannonian Basin. The Pannonian Basin is a Neogene structure formed as a result of extension related attenuation of the lithosphere in late Early to Late Miocene times (Royden and Horváth 1988). Due to the thin lithosphere, the whole area is characterized, by elevated heat flux (averaging to 100 mW/m^2) as compared to the surrounding regions (Lenkey et al. 2002). Inversion of the basin began in the latest Miocene and resulted in the uplift of certain blocks. The TR, including the Buda Hills, is one of the uplifted Mesozoic-Tertiary basement blocks of the Pannonian Basin. Due to the uplift and concomitant erosion, Triassic and Paleogene formations are exposed in the Buda Hills. They are stepwise down-faulted to the SE, towards the Pannonian Basin proper (Fig. 2).

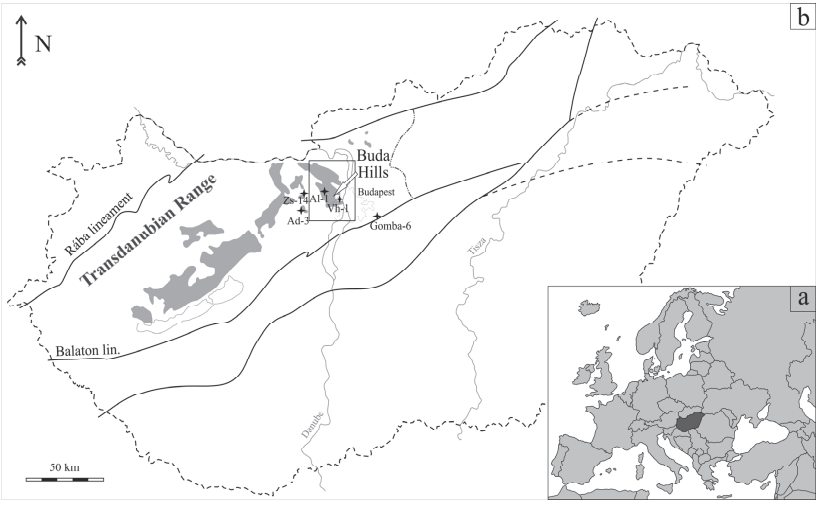

Fig. 1: (a) Location of Hungary within Europe (b) Location of the Buda Hills after Haas et al. (2010). Grey colour: Outcropping Triassic formations. Locations of boreholes mentioned in the text are indicated.

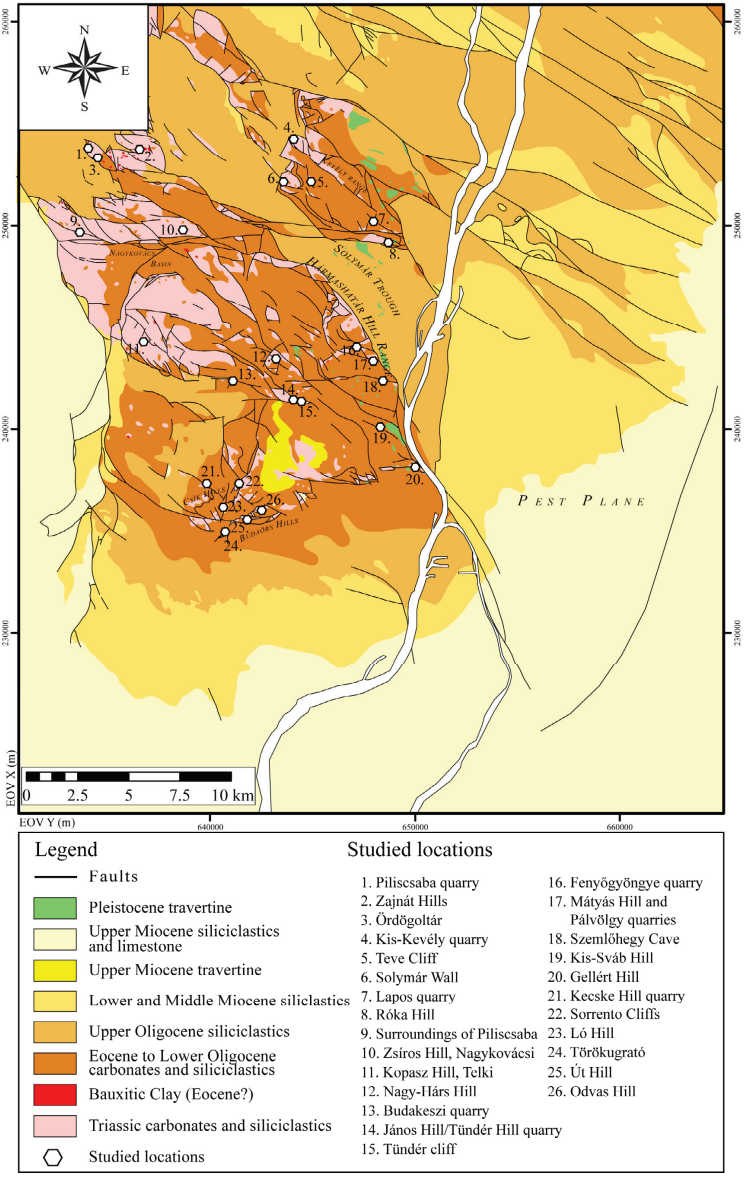

Fig. 2: Studied locations indicated on the simplified geological map of the Buda Hills (modified after Fodor, unpublished). See detailed maps of each locality in the Appendix.

Mesozoic

In the Triassic, the TR was part of the shelf of Neotethys located between the South Alpine and Upper Austroalpine Units (Haas et al. 1995). Westward propagating Neotethys rifting reached the studied region in the Middle Anisian which led to disintegration of the former carbonate ramp and the development of platform and intraplatform basins. In the Ladinian to the Early Carnian interval dolomitized platform carbonates (diplopora dolomite-Budaörs Formation; Fig. 3) formed in the Buda Hills. They are the oldest formations exposed in the Buda Hills. Thickness of this formation is estimated to be 1000-1200 m in this area (Haas et al. 2001). By Carnian times segmentation of the Budaörs platform resulted in the development of intrashelf basins where pelagic, cherty nodular, bituminous limestones and dolomites formed (Mátyáshegy Formation). Cherty dolomites (Sashegy Dolomite Member) crop out in the Hármashatár and Sashegy Ranges. Core drilling Vh-1, within the town of Budapest, exposed the upper part of the Mátyáshegy Formation of Late Norian to Early Rhaetian age which is made up of limestone and marl. Thickness of this formation ranges between 50 and 200 m. Detailed petrography of the rocks revealed that this limestone (representing the Mátyáshegy Limestone Member of Mátyáshegy Formation) locally contains calcareous marl intercalations rich in organic material (Haas et al. 2000). On the higher elevated blocks, the shallow-water carbonate platform development was continuous throughout the Carnian, Norian and Rhaetian, represented by Hauptdolomit and Dachstein Limestone Formations (Wein 1977, Haas et al. 2000; Fig. 3). Total thickness of the Hauptdolomit and the thick-bedded, oncoidal Dachstein Limestone is estimated to be ca. 1500 m in the Buda Hills (Wein 1977).

One of the peculiarities of the TR unit is the pervasive dolomitization of both the Middle Triassic and the lower part of the Upper Triassic platforms represented by the Budaörs and the Hauptdolomit Formations, respectively (Balog et al. 1999). There is a transitional interval between the completely dolomitized (Hauptdolomit) and undolomitized carbonate sequences (Dachstein Limestone). This interval was penetrated by the Ady-liget borehole (Ad-1) in a thickness of 120 m. In the transitional zone, which belongs to the Dachstein Limestone Formation (Fenyőfő Member), the alternation of dolomitized and undolomitized intervals and the presence of partially dolomitized carbonates are common (Haas and Demény 2002). More detailed description of dolomitization of the carbonates in the TR is given in Chapter III.

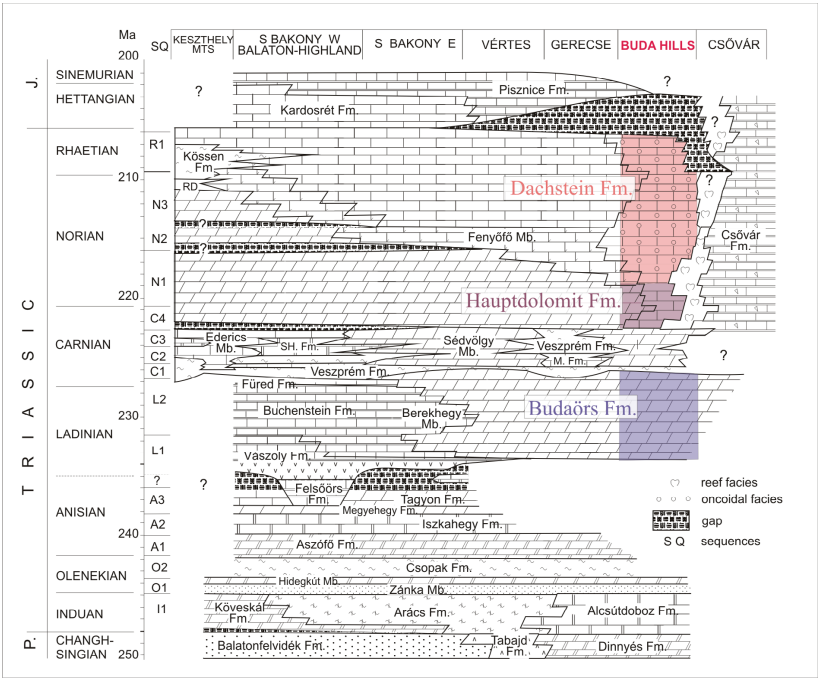

Fig. 3: Triassic formations and their time and space relationship along a conceptual SW–NE cross-section of the Transdanubian Range (Haas and Budai 1999). (Carbonates of basinal facies in the Buda Hills (e.g. Mátyáshegy Fm, the coeval facies of Hauptdolomit and Dachstein Limestone) are not indicated.)

Jurassic and Cretaceous sediments are altogether missing in the area of the Buda Hills. However, since continuity of the deep-marine Triassic-Jurassic sedimentation was proved at Csővár, in the NE part of the TR, it is assumed, that the basins survived also in the area of the Buda Hills and the sediments were removed later by erosion. From Middle Cretaceous times on, the TR became involved in thrusting, nappe-movements and related deformation (Tari, 1994). The TR was uplifted and became subaerially exposed in Early Albian times. As a result, at places younger Mesozoic formations were stripped by erosion and bauxite was formed. This subaerial episode was followed by subsidence thus the unconformity became covered by several hundreds of metres of sediments. The next phase of uplift and erosion in Turonian – Early Senonian times, resulted in the formation of extensive bauxite deposits on the surface of the exposed Late Triassic carbonates. After that, another subaerial exposure led to the formation of the third − Paleocene to Early Eocene − bauxitiferous unconformity with

an apparent gap between Upper Triassic and Middle Eocene formations in most cases. To sum up, although in the TR three different major subaerial exposure periods are known, there is only one single bauxite horizon exposed in the Buda Hills at the base of the Eocene transgression sequence (Szantner et al. 1986; Mindszenty et al. 2001). Lithologically the bauxite/bauxitic clay of the Buda Hills looks similar to the Eocene bauxites rather than to the Cretaceous ones (Mindszenty et al. 1991).

Wein (1977) recognized some SE-NW striking synclinal structures and also some thrust faults which have not affected the Tertiary and post-Tertiary formations. The orientation of the fold axes suggests a NE-SW oriented compressional stress field for this supposedly Middle to Late Cretaceous deformation, which – according to the observations of Wein (1977) and confirmed also by Fodor et al. (1994) – resulted in intense brecciation in the affected, rigid, Triassic dolomites.

Paleogene

According to the continental escape model of Kázmér and Kovács (1985), in Middle Eocene to Late Oligocene times, the bulk of the northern part of the Pannonian Basin (including the TR) was squeezed out from the Alpine realm between the southern right-lateral Periadriatic-Balaton Line and the northern left-lateral Rába Line (Fig. 1). According to Tari (1994) the Rába Line is not a major subvertical strike-slip fault but, instead a low-angle normal fault. According to the latest models the continental escape from the Alpine sector, started in the Late Eocene (Fodor et al. 1992) but best developed in the Oligocene and has not occurred along the Rába Line but affected the whole Alcapa unit which is bordered by the Periadriatic-Balaton Line to the south and by the Pieniny Klippenbelt to the north (e.g. Csontos et al. 1992, Csontos 1995, Fodor et al. 1998, Kovács et al. 2007). Associated with these large-scale movements there were also rotations. It has to be kept in mind therefore, that the interpretation of all pre-Tertiary directions requires a compensation for an anticlockwise rotation of about 30 degrees (Márton and Fodor 2003) resulted by the tectonic emplacement of the TR unit to its present position.

Based on detailed tectonic measurements, Fodor et al. (1994) recognized two major dextral strike-slip zones within the Buda Hills, each of roughly E-W orientation: (1) the Budaörs strike-slip zone at the southern boundary, and (2) the Nagykovácsi zone close to the northern boundary of the Buda Hills. In between these two zones, in order to accommodate lateral movements, antiforms and SE oriented flexural folds were formed and simultaneously also faulting along NW-SE oriented normal faults has intensified. The highest of the

antiforms – the so called 'János Hill ridge' – can be traced from Budaörs almost to Csillaghegy spanning most of the distance between the two major dextral strike-slip zones. In the János Hill section of the ridge the fault is not detectable on the surface since ─ according to Fodor et al. (1994) ─ it is a blind fault. That means that the János Hill antiform is a 'fault propagation anticline' (sensu Suppe 1983), having been active from late Middle Eocene to Middle Miocene times. It is one of the most prominent Tertiary paleogeographic features of the Buda Hills (called also the Buda Line) which controlled the Oligocene facies pattern (see details below). The Buda Line also affected the erosion – which may have reached even the Mesozoic basement – due to the intense uplift along this structure during the Early Oligocene ('infraoligocene denudation'; Telegdi-Roth 1927, Jaskó 1979).

The eroded surface of the Triassic sediments, locally covered by bauxitic clays, is overlain by the Paleogene transgression sequence. As a result of the first transgression period in Late Lutetian-Bartonian times, the karstic surface of the Triassic carbonates became locally covered by dolomite breccia, variegated clay or coal-bearing layers, the latter exposed in the Nagykovácsi and Solymár basins (Rozlozsnik 1935, Szőts 1948). The second transgression reached only the northwestern part of the Buda Hills. In Priabonian times, due to the third transgression which already reached the whole area of the Buda Hills, the deposition of shallow marine sediments initiated with basal conglomerate ─ alluvial fan, according to Kósa et al. (2003) ─ and breccia members, containing dolomite, andesite and chert pebbles (Wein 1977) followed by the shallow marine Szépvölgy Limestone Formation of 50-80 m average thickness (Báldi and Báldi-Beke 1986). As a result of gradual changes in the depositional environment the formation of limestone was gradually replaced by the calcareous 'Bryozoan marl' and then by the Buda Marl Formation (Fig. 4). The fauna of the 60-120 m thick Buda Marl already represents deep-marine, i.e. bathyal conditions (Báldi 1983). At those parts where the 'infraoligocene denudation' had no effect, SE of the Buda Line, the Upper Eocene-Lower Oligocene marl is overlain by anoxic clay of 100 m thickness (Tard Clay Formation). There is no hiatus between the two formations. Since Tard Clay is a potential source rock it was subject to detailed organic geochemical studies by Brukner-Wein et al. (1990). They distinguished four different intervals within the formation: 1) lower part consisting of anoxic shale and marl (TOC= 0.5-5%; type III kerogen); 2) middle part which is characterized by laminated marl and siltstone (TOC= 0.5-5%; type II kerogen); 3) upper part consisting of laminated clayey marl and siltstone (TOC= 2%; type III kerogen); 4) top marl (TOC< 1%). From all these intervals the middle part of the formation is the most prone to produce liquid hydrocarbons.

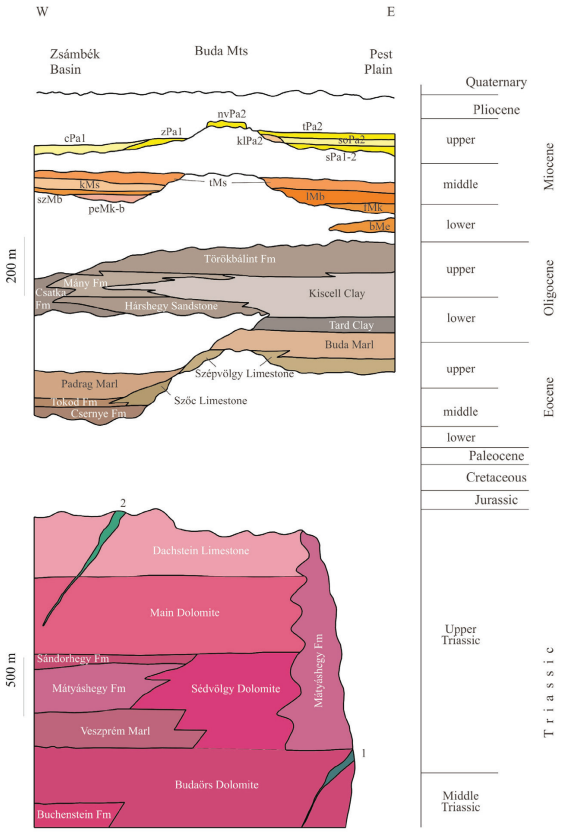

Fig. 4: General stratigraphic column of the Buda Hills (Esteban et al. 2009): 1. Middle Triassic volcanic dykes; 2. Upper Cretaceous subvolcanic dykes; [b]Me: Budafoki Fm; [f]Mk: Fóti Fm; [l]Mb: Lajta Limestone Fm; [t]Ms: Tinnyei Fm; [sz]Mb: Szilágyi Fm; [k]Ms: Kozárdi Fm; [s]Pa_{1-2} Száki Fm; [so]Pa_2: Somlói Fm; [t]Pa_2: Tihanyi Fm; [kl]Pa_2: Kállai Fm; [nv]Pa_2: Nagyvázsony Freshwater Limestone; [z]Pa_1: Zámori Fm; [c]Pa_1: Csákvári Fm.

At the northwestern part of the Buda Hills, Lower Oligocene sediments are represented by marine, coastal sandstone, the so called Hárshegy Sandstone Formation (Báldi and Nagymarosy 1976), which locally may directly overlay the Triassic formations. This sandstone has both silicified and non-silicified facies. Early diagenetic (Late Kiscellien) silicification of the sandstone by hydrothermal fluids is supposedly related to the Paleogene

volcanism (Báldi and Nagymarosy 1976; Gál et al. 2008) even though Paleogene volcanic rocks are not exposed in the area of the Buda Hills. (The closest known occurrences of Paleogene volcanic rocks are located ~60 km away from the Buda Hills, in the Velence Mts. and in the Mátra Mts.) The Tard Clay and certain parts of the Hárshegy Sandstone are covered by the pelagic Kiscell Clay of Late Kiscellien (Lower Oligocene) age which represents the greatest water depth within the transgressional sequence. Thickness of the Kiscell Clay is up to 800 m in the inner parts of the basin. Contemporaneity of the lower part of the Kiscell Clay and the Hárshegy Sandstone was proved by Báldi and Nagymarosy (1976) (Fig. 4). Sedimentation continued up to the end of the Oligocene. The Upper Oligocene is represented by shallow marine, sublittoral sandstone, called Törökbálint Sandstone Formation followed by the Lower Miocene Budafok Formation representing the final stage of the basin filling (Báldi 1983).

Neogene to Quaternary

By Miocene times, parts of the Buda Hills became subaerially exposed and the erosion of Paleogene rocks initiated (Wein 1977). Integrated paleomagnetic and structural geological studies in the TR revealed several counterclockwise rotation events during Tertiary times (Márton and Fodor 2003). Counterclockwise rotation of the TR resulted in clockwise rotation in the observed stress field. Thus, the orientation of maximum compression gradually changed from WNW-SES to N-S between Early Miocene and Late Miocene (Márton and Fodor 2003; Fig. 5). Due to changes in the orientation of the stress field by the Middle Miocene, NW–SE trending normal faults became activated and the sense of motion of the Budaörs strike-slip zone changed from dextral to sinistral (Fodor et al. 1994). Simultaneously, due to NW–SE trending normal faulting, sedimentation continued in the subsiding basinal sectors.

In the Badenian, sedimentation continued along the margins of the Buda Hills. It is represented by the shallow-marine Rákos Limestone Formation rich in macrofauna. In the latest Miocene (Pannonian Stage), at the top and on the slopes of the Sváb Hill, in the southern part of the Buda Hills freshwater limestone was deposited on the eroded surface of the Triassic and/or Eocene formations (Müller and Magyar 2008). In the SE part of the Buda Hills, the Pannonian is represented by siliciclastic sediments, i.e. sand, quartz pebble, and clay (Wein 1977). From the latest Miocene–Pliocene on, the area of the Buda Hills underwent differential uplift and erosion due to compressional tectonics having prevailed in the Pannonian Basin.

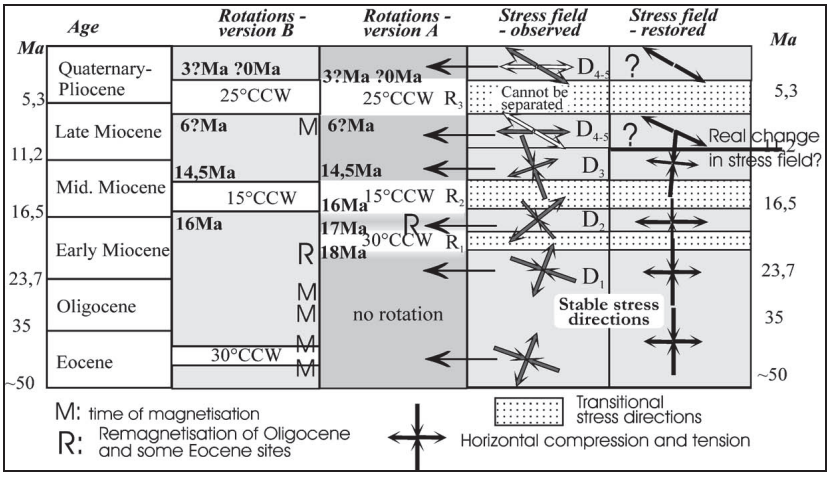

Fig 5: Observed stress field variations in the Transdanubian Range (Márton and Fodor 2003)

By the Pleistocene the whole area of the Buda Hills became subaerially exposed. In Pleistocene times, travertines formed at the margins of the uplifting Buda Hills mainly along NW–SE trending faults. They reflect the hydrological change associated with the uplift since younger travertines occur at lower topographic positions in comparison with the older ones (Scheuer and Schweitzer 1988). Simultaneously with the formation of travertines, hypogenic, fracture related cave systems were formed, hosted mostly in Upper Eocene carbonates and subordinately also in Triassic carbonates. Formation of those cave-systems and related hydrothermal processes are described in details in Chapter IV.

The uplift of the Buda Hills is still active. According to Ruszkiczay-Rüdiger et al. (2005) based on the ages of different travertine horizons an average uplift rate of 0.18 mm/year during the last 360 Ky could be calculated. According to Szanyi et al. (2009) between 500 Ka and 310 Ka the area was characterized by a relatively slow uplift. It may have accelerated 310-320 K years ago reaching an estimated rate of 0.16 mm/year based on uranium-series dating of speleothemes.

Chapter III – Porosity evolution of the dolomitized platform carbonates – with emphasis on the powderization of dolomite

III/1 Introduction

As mentioned above, the bulk of the Buda Hills is comprised of Middle and Upper Triassic carbonates of both platform and basinal facies that were dolomitized to variable degrees. This research focussed on the completely dolomitized Triassic platform carbonates, i.e. Budaörs Dolomite Formation of Ladinian to Early Carnian age and Hauptdolomit Formation of Middle Carnian to Early (?) Norian age (Fig. 3). Dolomitization in the Buda Hills has not been studied so far, and only a limited number of studies were carried out on dolomitization in the whole Transdanubian Range (TR) (Balog et al. 1999; Haas and Demény 2002). According to Balog et al. (1999) most of the dolomitization of the Hauptdolomit occurred early, in tidal-flat setting and it was mostly controlled by climate. Geochemical data revealed that dolomitization continued in the burial realm. Norian and Rhaetian carbonates, represented by Dachstein Limestone in the TR, are unaffected by dolomitization here because the climate became cooler and wetter through time. A transitional member consisting of partially dolomitized carbonates between dolomitized (Hauptdolomit) and undolomitized (Dachstein Limestone) platform carbonates was studied in details by Haas and Demény (2002) on two sections in the Gerecse Hills, at the northeastern part of the TR. Even though, there are no evaporites in the Dachstein-type platform carbonates, they suggested that early dolomitization of the subtidal lime mud in the case of Hauptdolomit was a result of downward seepage and reflux of higher-density evaporated seawater. They concluded that increasing humidity and gradual extension of the platform led to cessation of early dolomitization in Middle to Late Norian times.

Powderization of the above dolomites is a general phenomenon in the TR, especially in the Buda Hills, where its areal extent is exceptionally large compared to similar occurrences elsewhere in the world. Several studies have tried to reveal the causes of the peculiar powderization of dolomite in the Buda Hills and its surroundings, although, this topic is not frequently discussed in the international literature. Previous researchers proposed the following three possible mechanisms, as responsible for the peculiar disintegration of dolomite in the TR.

Recent weathering induced powderization

Initially, powderization of dolomite in the Buda Hills was explained, merely, by recent weathering, including both chemical and physical weathering. This concept was based on the following observation: there is a grain size decrease from depth towards the surface, namely dolomite powder on the surface is underlain by fractured dolomite and intact dolomite follows underneath (Szabó 1858; Hofmann 1871; Koch 1871; Schafarzik 1884, 1902; Timkó 1909). Nendtvich (1859) found no difference in the $CaCO_3/MgCO_3$ ratio of powdered and non-powdered dolomite. He emphasized that powderization was not caused merely by chemical weathering because the similar chemical compositions of disintegrated and intact rocks contradicts to the s. str. definition of chemical weathering.

Hydrothermal powderization

Scherf (1922) discarded the former explanation – the simple weathering – because of the presence of the powdered and non-powdered dolomite occurrences next to each other. He suggested that powderization was due to the 'silicic-acid-bearing' thermal water circulation along fractured zones because he found a strong correlation between the areal distribution of powderization and fractures filled by hydrothermal minerals. He emphasized that powderization often occurred together with iron-oxi-hydroxide precipitates which were thought to be hydrothermal in origin; therefore, these minerals represent the pathways of former hydrothermal fluid migration. According to this model, dolomite pillars may represent the central part of former upwelling zones of hydrothermal fluids because these towers are cemented by hydrothermal minerals, mainly silica, calcite, and iron oxides. According to him these towers are cliff-like because of the increased resistance against erosion due to the cementation, while the surroundings became disintegrated due to the supposed thermal effect. This hydrothermal explanation for disintegration was later accepted by several authors, e.g. Schafarzik and Vendl (1929), Brugger (1940), Jakucs (1950), and Nagy (1979). Brugger (1940) investigated the powderization process also from the point of view of bauxite-formation. He concluded that powderization is hydrothermal related but in addition to the dissolution effect of the hydrothermal fluids he discussed also the potential effect of the elevated temperature on disintegration. Jakucs (1950) pointed out that powderization is not only a surficial phenomenon since powdered dolomite occurs even at 110–120 m depth below ground surface. He explains the powderization by the following process: hydrothermal fluid infiltrates into the micro-cracks of the dolomite and causes precipitation of aragonite. He thought that later disintegration was due to the subsequent recrystallization of aragonite to

calcite characterized by volume increase. Nagy (1979) confirmed the hydrothermal origin of the powderization by presenting some trace elements (Ag, Ba, Cr, Co, Cu, Ga, Mn, Ni, Pb, Sr, Ti, V) analysis results which—according to him—showed enrichment in the powdered dolomite as compared to the fresh rock. The theory of hydrothermal powderization was also adopted in a paper published most recently by Esteban et al. (2009). In the latter paper powderization of dolomite is interpreted as being a micro-dissolution process. According to them pulverization of dolomite is associated with silicification and mineralization which is considered to be a diagenetic facies association, namely the "PSM facies".

Pre-Mid-Eocene unconformity related powderization

The third approach is that disintegration of dolomite is somehow related to the unconformities. According to Földvári (1933) powderization is restricted to the boundary zone of the pre-Mid-Eocene unconformity related Mn-crust and the carbonates (limestone or dolomite). Based on the experiments of Gedeon (in Földvári 1933) powderization may be related to downward percolating waters through the overlying bauxite. He also described that the powdered dolomite under the bauxite has elevated iron- and calcite-content. Bárdossy (1977) describes that powdered dolomite zones, of maximum few m thickness, commonly occur right below bauxite lenses not in the Buda Hills, but at other localities in the TR. Kleb et al. (1993) describe that there are several porous/powdered zones in the Hauptdolomit Formation which are commonly related to fracture-systems or rather to the Triassic/Eocene unconformity in the Buda Hills.

Powderization of dolomite elsewhere

Only a few dolomite powder occurrences are published in the international literature. Powdered dolomite occurrences related to structural elements are described from nappe-boundaries and also related to low-angle normal faults (e.g. Pappone and Ferranti 1995). These powdered dolomites are interpreted being the results of pure mechanical disintegration due to tectonic shearing. Few cm wide powdered dolomite zone was observed at the contact aureole of the Adamello pluton, Italy (personal communication, Ronchi 2009) which is the largest Tertiary intrusion in the Alps. In this case country rocks (including dolomite) were subject to thermal alteration during magma emplacement (Piane et al. 2008). Horizontally extensive but only a few metres thick 'flour dolomite layer' was described below red residua underlain by cracked dolomite and further down by fresh dolomite from South China (Ji et al. 2004). This karst related dolomite powder occurrence is interpreted as being the result of

chemical weathering. Powdered dolomite is also known to host heavy oil in the Grosmont reservoir, Canada. Details of the process of powderization of Grosmont dolomite are still unclear (personal communication, Machel 2010).

Because – as it was shown above – the exact process of powderization is still open to debate, I started out with the aim to reconstruct the triggering mechanism of powderization by comparing textures, mineralogy and geochemistry of intact and disintegrated dolomite samples. Since in the Buda Hills powdered and intact dolomites occur together, investigation of disintegrated and non-disintegrated rock samples were carried out simultaneously. I also studied the dolomitization process – however not in details – in order to see whether the texture and type of dolomitization had any influence on the disintegration. In addition, I wanted to understand whether dolomitization was of particular importance from the point of view of the porosity evolution of the studied formations.

III/2 Applied methods

Micropetrography was done on thin-sections of 30 μm thickness. In order to distinguish between calcite, dolomite, and their ferroan variants thin sections were stained with alizarin red-S and potassium ferricyanide as described by Dickson (1966). CL-petrography was performed on a MAAS – Nuclide ELM-3 type cold cathode luminoscope on polished thin-sections at the Department of Physical and Applied Geology, Eötvös L. University.

For Scanning Electron Microscopic investigations an Amray 1830i SEM equipped with INCA EDS was used at the Department of Petrology and Geochemistry, Eötvös L. University. Both secondary electron (SE) and backscattered electron (BSE) modes were used. For SE images dolomite grains were put on carbon adhesive tape and then they were carbon coated. For BSE images thin sections of powdered dolomite were prepared according to the following steps: 1) a thin layer of rapid glue (Super Bond) was placed on the top of a glass slide 2) dolomite mound was dispersed on the top of the glue layer 3) another layer of the glue on the top of the dolomite powder ensured total immersion of the powder grains. 4) After solidification 200–250 μm thick polished sections were prepared of the impregnated dolomite powder.

80–100 μm thick, doubly polished thin sections were prepared for the fluid inclusion studies. Fluid inclusion microthermometry was performed on a Linkam FTIR 600 heating–freezing stage at the Department of Mineralogy, Eötvös L. University. Standardization was carried out on –56.6, 0 and 385°C temperatures using quartz wafers containing synthetic H_2O

and H_2O–CO_2 fluid inclusions. Accuracy of the measurements during freezing experiments and heating up to 150°C was 0.1°C.

X-ray powder diffraction was completed on a Siemens D 5000 type diffractometer at the Department of Mineralogy, Eötvös L. University.

Stable carbon and oxygen isotope analyses were done in the Institute for Geochemical Research, Hungarian Academy of Sciences. Monomineralic samples were measured by a Finnigan MAT delta S type mass spectrometer after being pulverized and using the conventional anhydrous phosphoric acid digestion method, under vacuum (McCrea 1950). In the case of heterogeneous samples (e.g. dolomite associated with calcite) different phases were separated either by micro-drilling or the sequential calcite-dolomite separation method was used. These samples were measured by a Finnigan delta+XP equipment. Digestion was done by anhydrous phosphoric acid using continuous flow technique (Spötl and Vennemann 2003).

Major, trace and rare earth elements of bulk rock samples were measured by ICP-AES and ICP-MS (FIMS was used for Hg) by a commercial analytical laboratory. Detection limits for each element are noted in the Appendix-Table 1.

III/3 Results

III/3.1 Field observations

Powderization of Triassic dolomites is a common phenomenon in the Buda Hills but also non-powdered dolomites are exposed in the area. In addition, there are some quarries where both powdered and non-powdered dolomites occur next to each other. Degree and general appearance of disintegration also varies by outcrops. Both platform dolomites (i.e. Budaörs Dolomite and Hauptdolomit) have non-powdered and powdered varieties in the Buda Hills.

III/3.1.1 Non-powdered dolomites

During the field work two types of non-powdered platform dolomites were observed: #1 '*intact dolomite*' is a term used for those dolomites of which the supposedly original bedding or lamination is still visible and which are not significantly affected by other diagenetic processes (e.g. calcite cementation, disintegration) after dolomitization. Nevertheless, it has to be mentioned that even intact dolomites are generally highly fractured in the Buda Hills. #2 *non-powdered dolomites associated with other mineral phases*, most

commonly with calcite. In these cases, the original structure of dolomite is usually destroyed by intense brecciation, but in a few cases it is still recognizable (Ördögoltár, Piliscsaba; Fig. 2). This type of rocks has either a pillar-like appearance or forms prominent elongated zones.

Intact dolomite samples were studied in details from Odvas Hill where Budaörs Dolomite is exposed and from Tündér Cliff where Hauptdolomit occurs (Fig. 2). Odvas Hill belongs to Budaörs Hills which forms the southern boundary of the Buda Hills. Triassic dolomite is overlain at Odvas Hill by Eocene sedimentary rocks (Buda Marl). Scattered remnants of Oligocene sandstone (Hárshegy Sandstone) also occur at some places. Budaörs Dolomite was studied at a quarry located at the northeastern part of Odvas Hill. Although, dolomite is not powdered here, it is generally highly fractured, showing fitted (crackle) breccia texture. Brecciation is even more intense along fractures where breccia clasts moved away from each other. These fractures and brecciated zones are partially filled by dolomite powder and/or cemented by coarse crystalline hydrothermal calcite and barite (Poros et al. 2011; see detailed description of this assemblage in Chapter IV). Infiltration of the overlying marl into the fractures of dolomite was also observed. Where brecciation was less intense, cyclic succession with massive and thin laminated beds was still recognizable. The dip of beds changes from place to place within the quarry so they are interpreted as tilted blocks (Fig. 6a) or megabreccia clasts of an Eocene slope-complex (described by Magyari 1991). Dolomite is generally finely crystalline but coarsely crystalline (1–3 mm) euhedral dolomite crystals were also observed partially cementing the small, oval-shaped pores of the rock. Within the area of Odvas Hill a few meters tall, scattered pillars were also found. They are made up by dolomite of fitted breccia fabric associated with reddish coloured calcite. Hydrochloric acid was used to detect calcite in those pillars where calcite was not visible for the naked eye.

Non-powdered dolomites associated with other mineral phases and also *intact dolomite*s were studied in details at János Hill and at Tündér Cliff, which are members of the Sváb Hill group, located in the central part of Buda Hills (Fig. 2). Tündér Cliff area is made up by the Carnian–Norian Hauptdolomit Formation which is unconformably overlain by Eocene formations. It forms a part of the so called Tündér Cliff–Hunyadorom Range identified as a right lateral synsedimentary strike slip zone of Late Eocene age by Fodor et al. (1994). Tündér Cliff itself is a ca. 20 m high resistant cliff which is made up by both intact dolomite − where the original thick-bedding is still visible − and brecciated dolomite cemented by calcite (Fig. 6b). Vuggy porosity, partially filled by coarse euhedral dolomite crystals (1–2 mm), was observed in the finely crystalline intact dolomite-type. Pores are oval-

shaped with the longer diameter ranging between 1 and 5 mm. At Piliscsaba quarry also biomoldic cavities of few cm in size after gastropods partially cemented by the above mentioned euhedral dolomite crystals were rarely detected (Fig. 6f). In the brecciated parts of the Tündér Cliff, reddish/yellowish calcite occurs between the breccia clasts. Coarse-crystalline white calcite cement, associated with limonitic patches of 0.5 to 2 cm size, along fractures and voids is also common. In the near surroundings of the so called Tündér Cliff, some smaller (up to 5 m high) pillars of peculiar mushroom shape were also found (Fig. 6c). These pillars are made predominantly of dolomite associated with calcite. Voids (a few cm in size) and fractures within these pillars are filled with white calcite with partially oxidized pyrite along the margins of the voids (Fig. 6e). In addition to the pillars, there were also straight zones, i.e. 'small-scale ridges' of maximum few cm widths which consisting of dolomite impregnated by calcite (Fig. 6d). Orientation of these ridges is variable. At the foot of the Tündér Cliff, small-scale ridges and pillars are surrounded by dolomite powder.

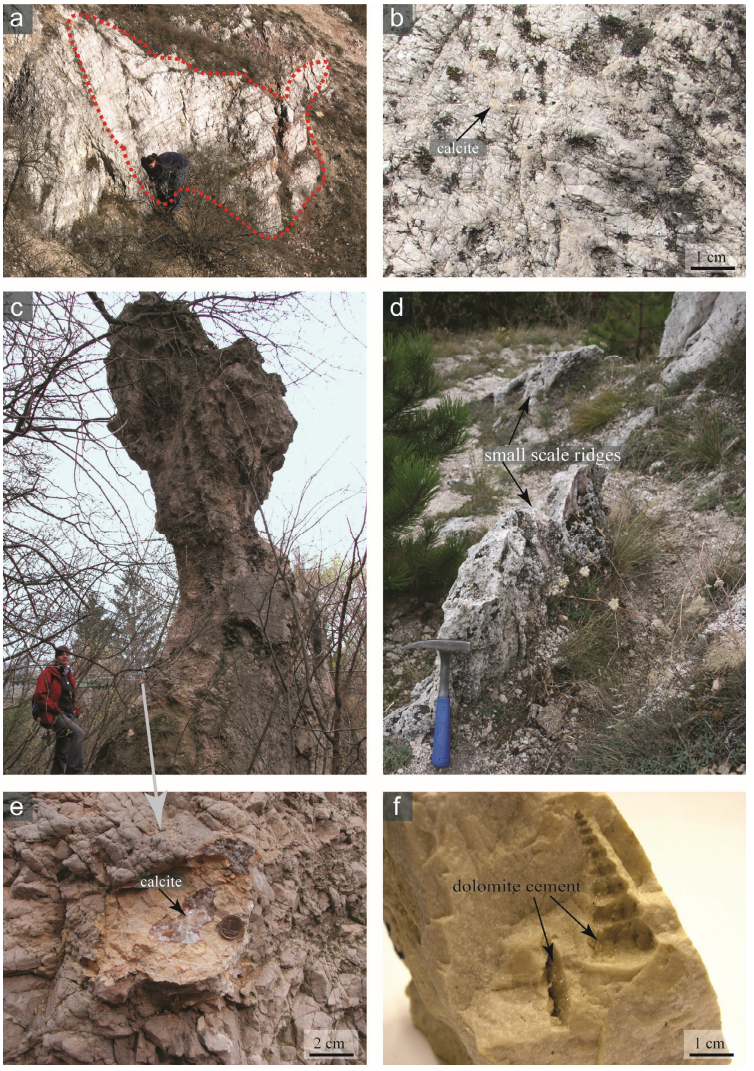

Fig. 6: (a) Tilted megabreccia clast in the Budaörs Dolomite. Original bedding is still visible. Odvas Hill (b) Dolomite breccia with minor amounts of yellowish-reddish calcite in between the clasts, Tündér Cliff (c) Protruding pillar of mushroom shape, consisting of dolomite and calcite at the foot of the Tündér Cliff (d) Erosion-resistant small-scale ridges consisting of dolomite associated with calcite, Zsíros Hill (e) Calcite cement in a void of the pillar of picture c (f) Euhedral dolomite crystals filling biomoldic pores of intact dolomite, Piliscsaba quarry.

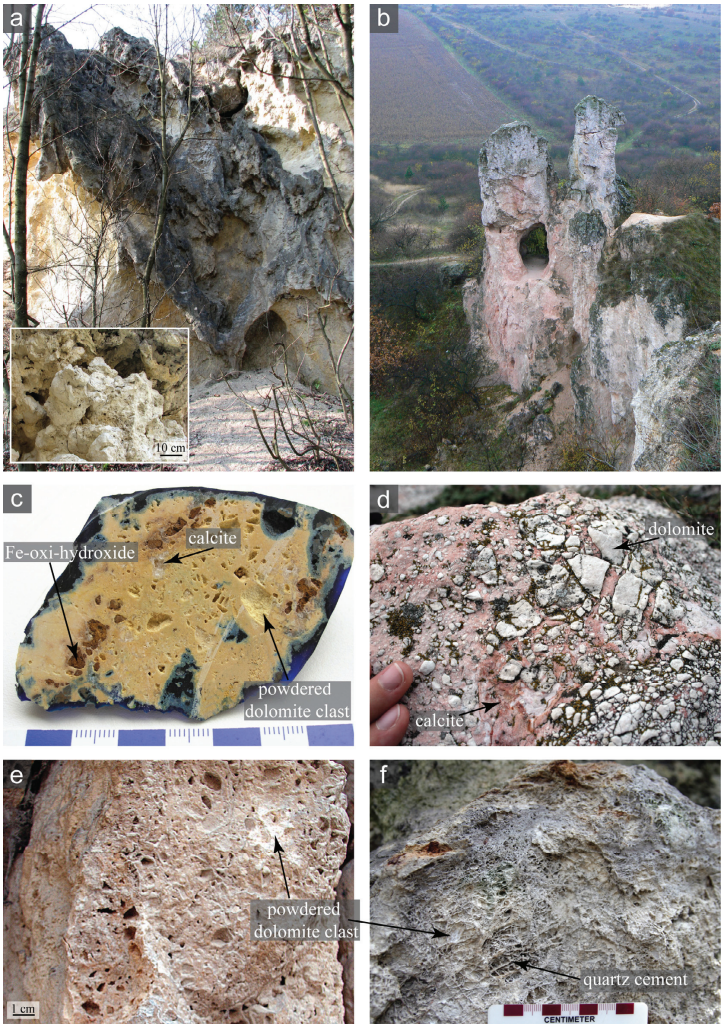

Fig. 7: (a) 'Mega-concretion' in dolomite powder at János Hill, Tündér Hill quarry. Note that the morphology points to cementation from descending fluids (b) Teve Cliff itself represents the erosion-resistant cliff-zone that consists of dolomite and red calcite (c) Hand specimen from the 'mega-concretion' (from picture a): dolomite powder and limonitic clasts impregnated by calcite (sample J-05). (d) dolomite breccia clasts floating in red calcite, Zsíros Hill (e) Boxwork texture made by calcite frame and dolomite clasts, János Hill (f) Boxwork texture made by quartz frame and dolomite clasts at Sorrento Cliffs (e-f) Boxwork texture is due to post-cementation powderization of the dolomite breccia clasts.

At János Hill (in the Tündér Hill quarry) the very same coarse-crystalline white calcite associated with limonitic patches was observed cementing the fractures and voids of dolomite. At the northwestern side of the quarry, few mm wide calcite veinlets were found in the central part of 10 to 20 cm wide prominent breccia zones. The proportion of white calcite to dolomite in these zones is gradually decreasing towards the host rock. In addition, there is a unique rock type exposed in the southern side of this quarry showing a 'flowstone-like' morphology which points to precipitation from descending, gravitationally-controlled fluids (Fig. 7a). This rock type is called "Hunyad-type speleo-concretion" by Esteban (2009). This 'mega-concretion' is made up by dolomite powder, breccia clasts and limonitic fragments impregnated by transparent white calcite (Fig. 7c). It is of spongy texture characterized by significant porosity. Box-work structure was detected (Fig. 7e) at the basal segment of this rock type, at those parts of the rock, where former dolomite breccia clasts became powdered after calcite cementation. The pore space thus created is partially cemented by a latest generation of euhedral transparent calcite crystals. Non-cemented parts of the dolomite are disintegrated to different degrees in this quarry. Yellowish, tabular barite crystals (0.5–1 cm) were also found along one single fracture within the partially disintegrated dolomite.

In addition to the above mentioned occurrences dolomite pillars and prominent zones, made up by predominantly calcite-impregnated dolomite, are exposed in several other outcrops, e.g. in the northern part of the Buda Hills at Teve Cliff, Solymár Wall and Zsíros Hill as well as in the southernmost part, at Csík Hills. All these dolomite pillars and prominent zones are surrounded by highly disintegrated dolomite. At the above listed three occurrences from the northern part of the Buda Hills, dolomite was associated with non-transparent, red-coloured calcite forming few meters wide, more than 10 m tall prominent zones, hereinafter called cliff zones, e.g. Teve Cliff (Fig. 7b). Those rocks, exposed at Zsíros Hill and Solymár Wall, look like being a dolomite breccia cemented by red-coloured calcite (Fig. 7d). Breccia clasts are sub-angular and their size ranges from a few mm up to 5 cm. At Teve Cliff, it is not possible to differentiate between calcite and dolomite phases macroscopically. At Sorrento Cliffs (Csík Hills), brecciated dolomite is either crosscut by brown-coloured silicified veins or cemented by white quartz showing box-work structure; however, all the former dolomite clasts are now powdered (Fig. 7f). The most intense quartz cementation occurs along fractures but the cementation front infiltrates laterally, as well, when fractures crosscut beds of significant permeability. Peculiar-shaped dolomite pillars of flat top are also common here. At Sorrento Cliffs, some small scale ridges and 'flowstone-like' structures were also observed in dolomite in those particular zones where dolomite is

impregnated by calcite, very similar to those ones found at the foot of Tündér Cliff and at János Hill.

Orientation of calcite veinlets, small-scale ridges and cliff zones is not uniform, however, there are some locations where the orientation of these zones shows great similarities with the closest major structural elements. For example in the János Hill quarry the strike of calcite veins is consistently NE–SW which is parallel to the Buda Line. At the Teve Cliff, the prominent zones impregnated by red calcite are of WNW–ESE strike which is very similar to that of the Nagykovácsi Line. Nevertheless, there are some exceptions, e.g. at Zsíros Hill, where the distribution of the vein-orientations is bimodal (NW–SE and NE–SW), and no obvious relationship can be found with either of the known major fault zones.

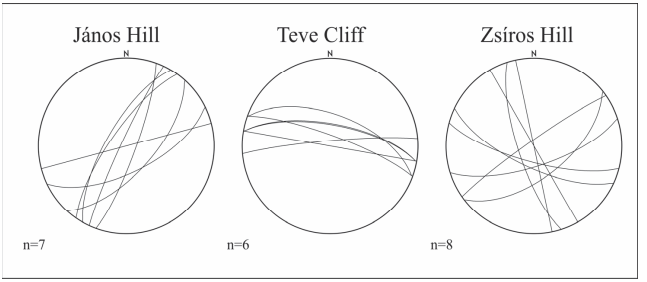

Fig. 8: Orientation of small-scale ridges/cliff zones in dolomite impregnated with red calcite (Teve Cliff, Zsíros Hill) or white calcite (János Hill)

III/3.1.2 Disintegrated dolomites

Disintegrated dolomite occurrences, observed right below the actual surface, are common in the Buda Hills and also in the whole Transdanubian Range. However, it is not a homogeneous phenomenon and the degree of disintegration is also highly variable. As far as the degree of disintegration is concerned, there is no difference between Budaörs Dolomite and Hauptdolomit Formation.

Four stages of dolomite disintegration were established that correspond to a gradual decrease in grain size:

1. from parent dolomite to *crackle/fitted breccia* (equal to intact dolomite) where dolomite is highly fractured but the original structure and bedding of the rock is still recognizable (e.g. Odvas Hill). (Fig. 9a).
2. *mosaic breccia* is used for that stage of disintegration where the breccias clasts are already moved away from each other (clast size: a few mm up to about 2 cm) (Fig. 9b)

3. *mosaic breccia blocks* (up to several meters width and height) *floating in powdered dolomite* (e.g. Zsíros Hill) (Fig. 9c)
4. *powdered dolomite* is generally very fine-grained (100–300 μm) therefore it has a flour-like appearance (Fig. 9d), small amount of breccia clasts of a few cm diameter are very commonly associated with powdered dolomite (Fig. 9e).

Fig. 9: Stages of disintegration: (a) Crackle breccia, Odvas Hill (b) Mosaic breccia, Kopasz Hill (c) Mosaic breccia blocks floating in dolomite powder, Zsíros Hill (d) Flour-like dolomite powder (e) Dolomite powder quarry at Kopasz Hill, Telki

The most obvious occurrence of gradual decrease in clast size from the intact dolomite towards the totally powdered dolomites was observed on cm/m-scale in the surroundings of open fractures. It was commonly observed that dolomite powder partially occludes the open fractures and the grain size gradually increases towards the host rock.

Not only the degree of disintegration but also the extent of it varies by outcrops. 'Regional' and 'local' types of powderization were distinguished in the field. *Regional powderization* occurs within areas of a few km^2 in size while local type of powderization was observed on meter-scale. Usually regional-type dolomite powder is characterized by smaller and more uniform grain size while in the dolomite subject to local-type disintegration, wider range of grain size was observed. Based on our field observations, the following two subgroups were established in the case of regional type powderization:

a) First type of dolomite powder is commonly associated with the major pre-Late Eocene regional unconformity (between Triassic and Upper Eocene sedimentary rocks) marked by bauxites and bauxitic clays. This type is known to be generally structure-destructive. In this case, powdered dolomite is overlain by thin layers of bauxitic clay exposed for example in the Budakeszi quarry and Kopasz Hill, Telki. Powdered dolomite was found also a few tens of metres below the actual surface, in a construction pit in Budakeszi, covered by an alluvial fan-type Eocene succession (Kósa et al. 2003). At this exposure meter-scale underground karstic cavities filled with bauxite are hosted by totally powdered dolomite (Fig. 10a) suggesting that powderization must have post-dated the formation and infilling of karstic cavities since it is not possible to create karstic cavities in dolomite powder. (This pit is not exposed anymore.) Boundary of bauxite and powdered dolomite is sharp both in the latter case and also when powdered dolomite is just covered by bauxite. It was also observed that powdered dolomite is directly overlain by the Lower Oligocene Hárshegy Sandstone at Teve Cliff where the Eocene rocks are altogether missing. At the same quarry, thin barite–limonite veinlets crosscutting both the disintegrated dolomite and the overlying Oligocene sediments were observed. Moreover, dolomite pebbles, which became powdered after deposition, are enclosed by the siliciclastic cover here. These observations together are pointing to the fact that powderization is most probably younger than the formation of sandstone and also the formation of the barite veins.

b) Regional powderization was also observed right below the present-day surface with no associated bauxite. At one locality, in a 2-3 metres high road cut at NW side of Ló Hill in Csík Hills, powderization is structure-preserving. Even though dolomite became completely powdered, the fitted breccia structure of the parent rock was clearly recognizable (Fig. 10b).

In the case of *local-type powderization* the following four subgroups were established:

a) Fault/fracture related powderization can form powdered zones of a thickness from a few cm up to several metres (Fig. 10c). Gradual increase in grain size was commonly observed towards the host rock.

b) Few cm thick powdered dolomite layers were observed in between ca. 1 metre thick dolomite beds (Fig. 10d). These latter two types of powderization are very common and exposed at several outcrops in the Buda Hills.

c) Alternation of powdered and non-powdered beds/layers was observed both in the northernmost part (at Piliscsaba quarry) and southernmost part (at the quarry north to Kecske Hill, Csík Hills) of the Buda Hills. In the Piliscsaba quarry disintegrated layers were not totally powdered, and the thickness of disintegrated and non-disintegrated beds was uniformly around 1 metre. At the quarry next to Kecske Hill the alternation of 1 m thick beds and 10 cm thick layers were observed and only the thin layers are powdered (Fig. 10e, f).

d) Powdered dolomite was found related to an undulating surface, too, in the same quarry at Kecske Hill where thin powdered layers and thick non-powdered beds alternate. In this quarry dolomite is overlain by loess. It was observed that above the undulating surface of several meters amplitude, not only the thin layers but also the thick beds are disintegrated, while below this surface thick beds are usually non-disintegrated. Total thickness of dolomites that suffered pervasive powderization (i.e. disintegration which affected both thin layers and thick beds) is approximately 15-20 m in this quarry. This boundary is not always sharp and the sub-horizontal bedding, identical to that one of the underlying dolomite, is still recognizable in the powder, especially close to the undulating surface. In addition, it was commonly observed in this quarry that disintegration of dolomite is the most intense along fractures. These fractures usually do not cross the above undulating surface but gradually fade as approaching it (Fig. 10e). The original bedding of dolomite is slightly perturbed in these fractured zones.

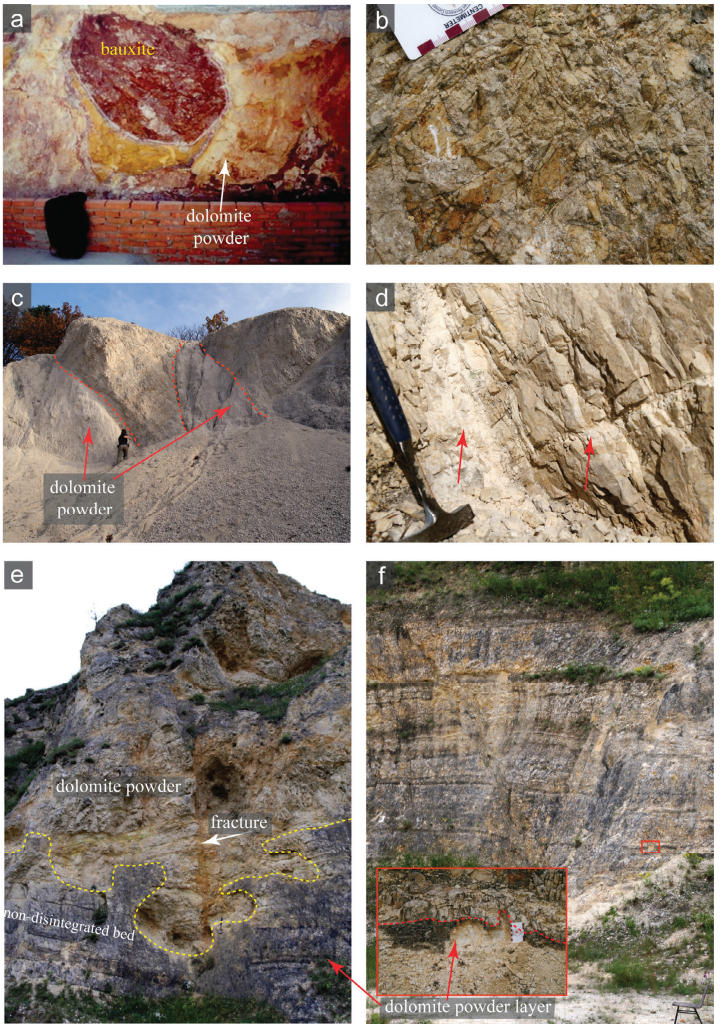

Fig. 10: (a) Karstic cavity filled with bauxite hosted by powdered dolomite, construction pit at Budakeszi (not exposed anymore) (b) Texture-preserving dolomite powder at Ló Hill. Note that even the breccia clasts are totally powdered (c) Local powderization related to fractures at the surroundings of Piliscsaba (d) Local powderization along fracture and along bedding planes, surroundings of Piliscsaba (e) Dolomite powder above an undulating surface. Note that dolomite powder occurs below the undulating surface as well but only locally, represented by dolomite powder layers, Kecske Hill quarry, Csík Hills (f) Alternation of dolomite powder layers and non-disintegrated dolomite beds exposed in the same quarry.

III/3.1.3 Subsurface occurrence of dolomite powder

Powderization is not only a surficial phenomenon but it was observed also below the actual ground surface within the area of the Buda Hills. According to Alföldi et al. (1968), disintegrated dolomite consistently occurs above 200 m depth from present actual land surface (Fig. 11). Disintegration is restricted to dolomites since it was not observed in the case of the other rock types in the boreholes. For example in the case of the Ady-liget borehole (Al-1) disintegrated dolomite was observed as overlain by intact Dachstein Formation (Haas 1989). Subsurface powderization was generally observed also in the other parts of the TR. Powdered dolomite zones, from few cm up to 2-3 metres in thickness, were commonly observed right below bauxite lenses known from underground mines at 150-300 m depth (Bárdossy 1977).

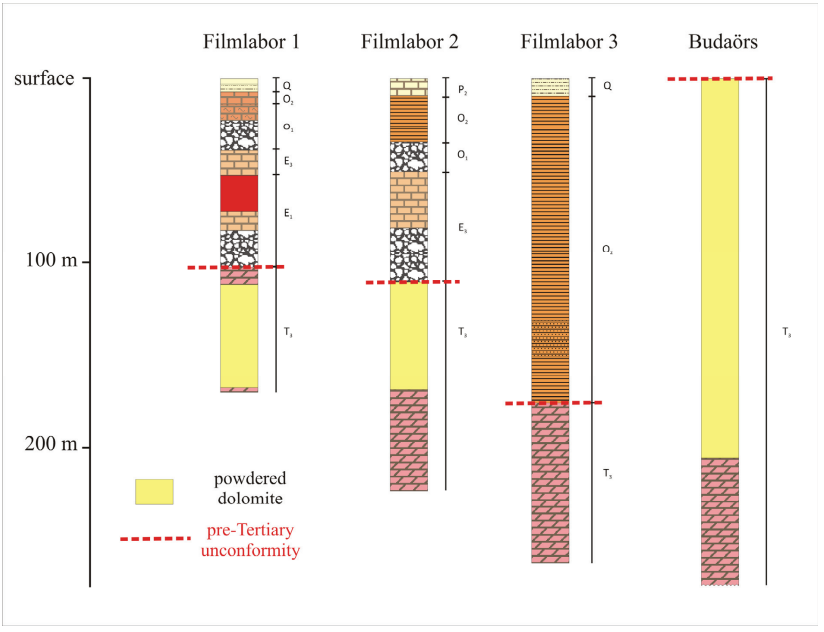

Fig. 11: Subsurface extent of powderization in the Buda Hills (simplified after Alföldi et al. 1968). Boreholes named *Filmlabor* are located in the near surroundings of Hárshegy. Borehole *Budaörs* is located in the SE side of the Tűzköves Hill, Budaörs

III/3.2 Micropetrography and mineralogy

Micropetrography of the studied rock samples is described according to the rock-types observed in the field.

III/3.2.1 Intact dolomites (with no other minerals associated)

Dolomitization was commonly fabric-destructive in the studied samples but subordinately, fabric-selective dolomites (Fig. 12a) occur, too. In the case of fabric-destructive dolomite samples, two dolomite populations (Fig. 12b) were identified in both studied formations distinguished by their remarkably different crystal sizes: 1) replacive, nonplanar-anhedral fine dolomite crystals of 30 μm size on the average (dolomite-I). These crystals are usually cloudy due to the presence of abundant inclusions. 2) Dolomite-II commonly forms an overgrowth rim on dolomite-I (Fig. 12c) resulting in planar-euhedral (rarely subhedral) crystals of clear rim (equivalent to dolomite-II) and cloudy centre (equivalent to dolomite-I). In other cases, dolomite-II phase forms planar-euhedral crystals without cloudy centre. Both types of planar-euhedral phases are coarsely crystalline (average crystal size is 200-250 μm), sometimes with crystals up to 1-2 mm. These crystals commonly cement elongated, oversize vuggy pores but significant amount of intercrystalline porosity remains open between these crystals. A bright luminescent zone (Fig. 12d) marks the irregular-shaped boundary between the dull luminescent cloudy centre (dolomite-I) and the clear rim (dolomite-II). This bright zone represents the first zone of dolomite-II phase; subsequent zones of dolomite-II show dull luminescence. Alternation of fluid inclusion-rich and fluid inclusion-free growth zones were also observed within the dolomite-II phase in the case of Hauptdolomit. Minor amount of saddle dolomite (Fig. 12e) was also found both as void-filling phase and sporadically in between nonplanar crystals.

Fabric-selective dolomitization was detected in the case of laminated layers from the Odvas Hill. Microbial boundstone texture is still recognizable that consists of clotted micrite and irregular-shaped fenestral pores cemented by drusy crystals (Fig. 12a). Irregular-shaped pores are of various sizes (up to several mm) and they are parallel to the macroscopically observed lamination. Fabric-selective dolomite was also detected as breccia clasts occurring together with fabric-destructive dolomite clasts (Fig. 12f). Pore space between the breccia clasts is occluded by fine, ‘milled’ dolomite material. Fabric-selective clasts are so small that the identification of the precursor fabric is ambiguous. However, clotted micrite and rounded structures filled by microspar with micrite rim was detected. No recognizable carbonate grains were found suggesting that this texture may be already of diagenetic origin, similar to that one

detected in the above described laminated layers. Although in the case of Tündér Cliff fabric-selective dolomite was not observed, probably relict fabric does occur represented by oval-shaped structures (up 5 mm in size) outlined by abundant inclusions.

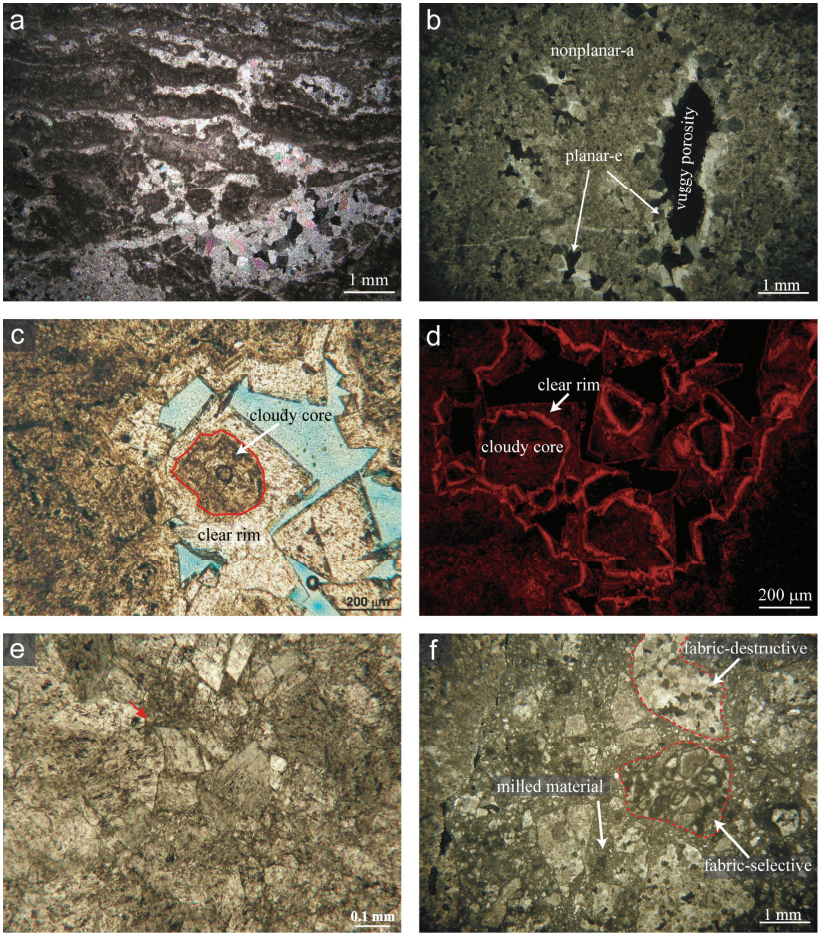

Fig. 12: (a) Fabric-selective dolomitization texture (sample O-05) +N (b) Fabric-destructive dolomitization of two dolomite populations (sample O-02) +N (c) Planar-euhedral dolomite of clear rim and cloudy centre (sample Tu-01) 1N (d) CL pattern of the same dolomite crystal (sample Tu-01) (e) Saddle dolomite (sample Tu-03) 1N (f) Dolomite breccia (sample O-09) +N

III/3.2.2 Non-powdered dolomites associated with other minerals

Stained thin sections revealed that most of the samples either from small scale ridge/cliff zones or from pillars contain calcite. Calcite is the most common mineral associated with dolomite. Two different types of calcite were observed already on the field associated with dolomite, i.e. transparent white calcite and non-transparent red calcite.

Coarsely crystalline, red calcite (calcite-I) shows poikilotopic texture by enclosing abundant irregular-shaped, rounded dolomite crystals (Fig. 14a) of various sizes (from 50 μm up to several cm). Cleavage planes of calcite are very pronounced. These observations suggest that red calcite is not a simple calcite cement but rather a dolomite-replacing phase, i.e. dedolomite (sensu Lucia 1961). This phase does not show any luminescence. Dissolution residue of calcite was investigated by XRD in order to find out the origin the red colour of it. Typical minerals of bauxite, i.e. kaolinite, hematite and gibbsite were detected (Fig. 13); therefore, the red colour of calcite is supposed to be the result of the hematite-rich bauxite or bauxitic clay inclusions.

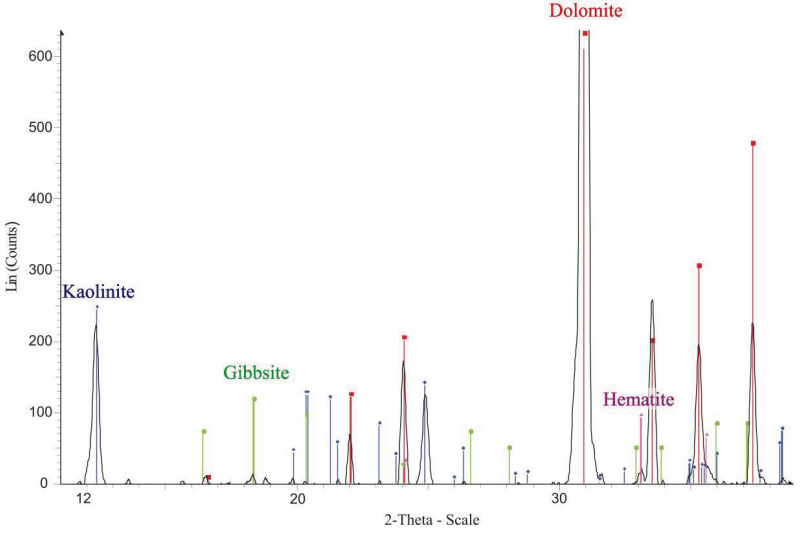

Fig. 13: X-ray powder diffractogram of dissolution residue of red calcite (sample Nk-06)

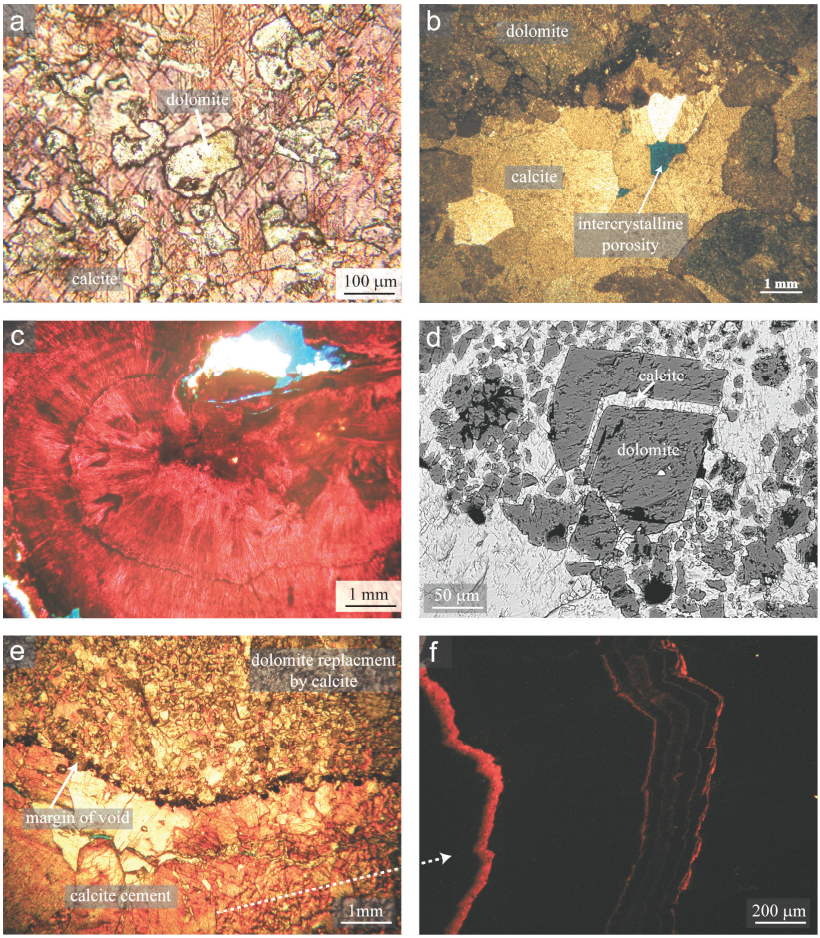

Fig. 14: (a) Corroded dolomite grains enclosed by poikilotopic red calcite (sample K-07) (b) Dolomite breccia cemented by white calcite (sample J-03) (c) Iron-oxi-hydroxide occurring together with white calcite (sample Tu-04) (d) BSE image of calcite replacement of dolomite along a zone and calcite cementation by the very same phase (sample J-02) (e) Margin of a calcite-cemented void (same void on Fig. 6 e); calcite cementation in the void, dolomite replacement by calcite in the host rock (f) CL pattern of the calcite that occludes the void (e-f) sample Tu-06.

White calcite (calcite-II) is limpid in thin section and free of fluid inclusions. Sparry calcite occurs as cement growing on the wall of fractures or voids. Where calcite cement does not occlude the whole pore space, minor intercrystalline porosity was observed (Fig. 14b). Calcite is commonly associated with 'limonitic' patches that consist of an iron-oxi-hydroxide mineral of concentric structure, with radially oriented crystals within each concentric zone (Fig. 14c). Replacement of dolomite by calcite (i.e. dedolomitization) was also observed by SEM along growth zones (Fig. 14d) and rarely in patches in the central, cloudy part of the dolomite rhombs. The frequently observed poikilotopic texture of calcite, enclosing irregular-shaped, rounded remnants of dolomite crystals, also points to dedolomitization. Dedolomitization is the most significant in the few cm wide zones next to fractures or voids cemented by the very same white calcite (Fig. 14e). No petrographic differences were observed between replacing and cementing calcite. It was also observed that only the outermost part of the dolomite breccia clasts is cemented/replaced by calcite while the central part of them is porous or missing (Fig. 15a). Using the SEM revealed that in the case of samples from János Hill (Tündér Hill quarry), barite crystals, containing dolomite inclusions, were also enclosed by the same calcite phase (Fig. 15b). Cathodoluminescence pattern of white calcite is the following: non-luminescent calcite is rarely interrupted by 'clusters' of bright luminescent zones. One cluster consists of one thicker and 4 to 5 very thin zones (Fig. 14f).

In addition to the above described red and white calcite phases there was a third, very late limpid, transparent calcite (calcite-III) observed in the case of the so-called "Hunyad-type concretions". Euhedral crystals (200-500 μm in size) of this late calcite partially occlude the open pore spaces, especially the space of former dolomite breccia clasts (Fig. 15c). This is a fluid-inclusion-free calcite but dolomite powder inclusions frequently occur along growth zones of it. This phase is usually non-luminescent, however, in one single sample (J-05) from this 'mega-concretion' the non-luminescent calcite was interrupted by two, very thin bright luminescent zones (Fig. 15d). There is an apparent conflict between the field observations and micropetrography: based on the 'flowstone-like' morphology of the huge 'concretion', exposed in the Tündér Hill quarry, one would expect to see vadose instead of phreatic calcite cement in this rock type.

Detailed petrographic studies on stained thin sections were carried out where alternation of disintegrated and non-disintegrated beds was observed (e.g. Kecske Hill and Piliscsaba quarry). Samples from non-disintegrated beds, as a rule, are partially dedolomitized and/or a very minor calcite cementation (calcite-I or II) was detected occluding the intercrystalline

pore space between planar-euhedral dolomite crystals (Fig. 15e). In the quarry, close to Kecske Hill, calcite associated with dolomite was commonly detected in the case of samples taken from those thick beds that are below the above-mentioned undulating surface.

Quartz cementation was observed only at the Sorrento Cliffs, Csík Hills. Micropetrography supplemented by XRD analyses revealed that the brown coloured siliceous veins, found also in between the dolomite breccia clasts, are of mainly very fine-crystalline quartz and goethite. Quartz cementation without goethite was also observed. In this case the individual quartz crystals are of various sizes, up to 0.1 mm. In samples showing box-work texture, significant intercrystalline porosity was observed in the partially disintegrated dolomite breccia clasts (Fig. 15f).

Hydrothermal barite and calcite cementation along fractures were also observed both in the intact (e.g. Törökugrató) and partially disintegrated dolomites (e.g. Teve Cliff). No dedolomitization was observed in the host dolomite related to fractures cemented by hydrothermal calcite. (See detailed description of this hydrothermal mineral assemblage in Chapter VI.)

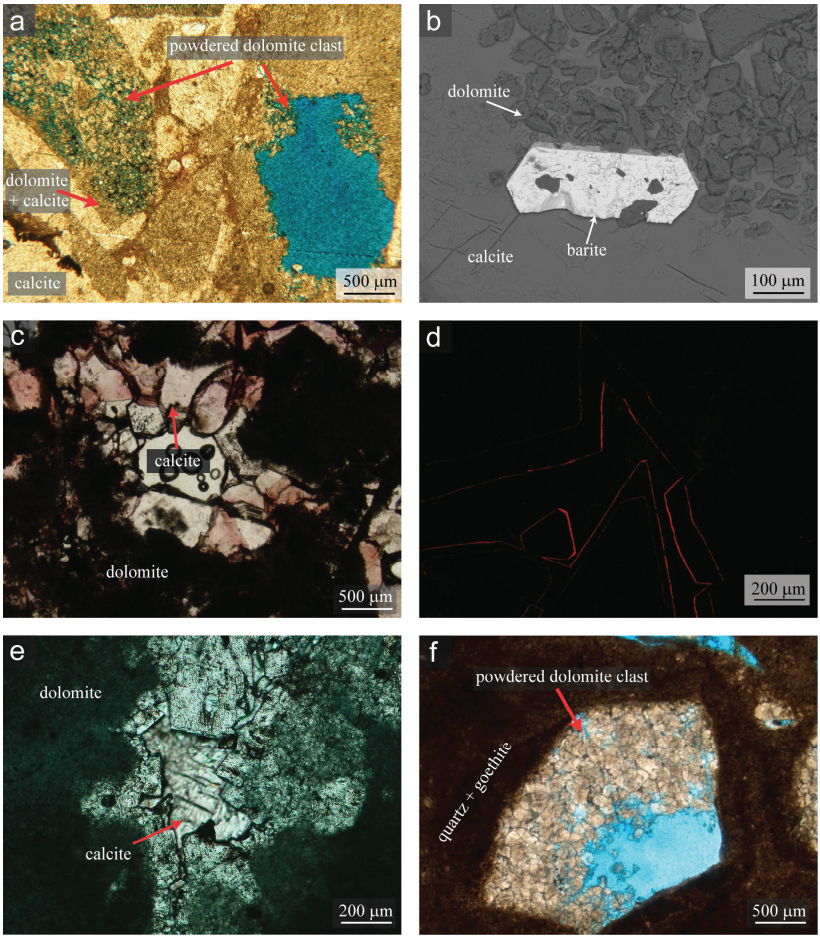

Fig. 15: Porous dolomite breccia clasts surrounded by calcite. Note that the margin of the clasts is more resistant to disintegration because of the presence of calcite (sample J-03; thin section made with blue epoxy) (b) BSE image of barite and dolomite grains enclosed by white calcite (sample J-02) (c) Post-powderization calcite cement (calcite-III) occluding the pore space after former dolomite clasts (sample J-02; stained thin section) (d) CL pattern of calcite-III in sample J-05. In most cases calcite-III is non-luminescent (e) Calcite occluding the intercrystalline pores in between dolomite crystals. This sample is from the non-disintegrated bed from Piliscsaba quarry (sample P-06; stained thin section). (f) Boxwork texture in dolomite cemented by quartz and goethite. Note that the powdered dolomite grain is characterized by significant intercrystalline porosity (sample Cs-10, thin section made with blue epoxy).

III/3.2.3 Powdered dolomite

Mineralogy of powdered dolomite was investigated both by XRD and SEM. According to XRD data powdered dolomite samples are monomineralic in most cases but very minor contribution of magnesium-bearing calcite and quartz was detected especially in those powdered dolomite samples that occur next to either small scale ridges/cliff zones or pillars.

SEM confirms the XRD data. It was observed on BSE images that grain size distribution is bimodal (Fig. 16a), rarely polymodal (determined only visually) in the case of local-type powdered dolomite and unimodal (Fig. 16b) in the case of dolomite powder associated with the bauxitiferous unconformity. Average grain size of the powder fraction is commonly larger in the case of fracture related powder (up to 1-2 mm) than in the case of the regional type powder (maximum 200 μm). In both cases the grains are generally angular. Occurrence of dolomite clasts (0.2-1 mm in size) impregnated by red calcite (calcite-I) along their margin was rarely observed in powdered dolomite (Fig. 16c) adjoining a ridge structure (e.g. Teve Cliff).

Surface of dolomite crystals of both powdered and all kind of non-powdered dolomite samples were investigated by using SE images. Although no quantitative analysis was carried out on these images, it can be stated that the surface of the crystals and grains is predominantly sharp in all kind of dolomite powder samples. Most commonly dolomite powder grains are characterized by sharp-edges that do not follow the orientation of crystal faces or cleavage planes of dolomite (Fig. 16d). Presence of rhombohedron-shaped grains was, however, also detected because of the disintegration along the cleavage planes of dolomite crystals. In dolomite powder samples, it was rarely observed that some of the crystals/grains were characterized by rounded surface and contained elongate pores along former cracks or cleavage planes. Rounded grains and rounded surfaces of dolomite were commonly observed in those samples where calcite replacement of dolomite was present (Fig. 16e). In those samples, representing the first three stages of disintegration of dolomite, the surface of planar-euhedral coarse crystals was always intact (Fig. 16f).

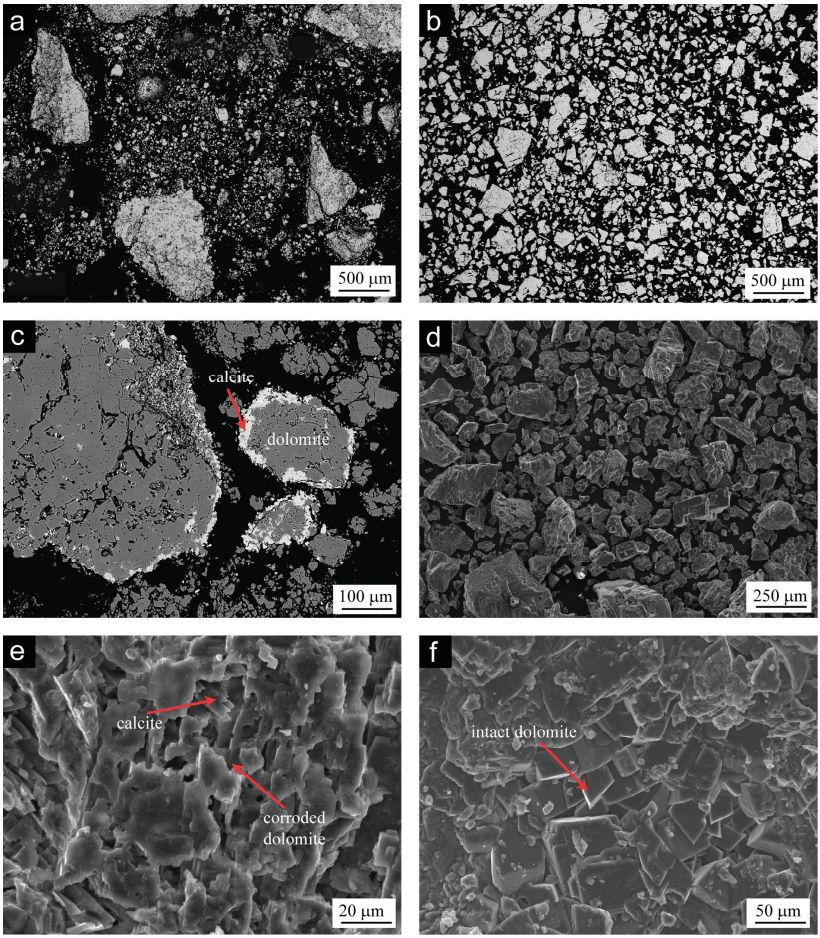

Fig. 16: SEM images of dolomite powder: (a) Bimodal grain size distribution of local type dolomite powder (sample J-09) (b) Unimodal grain size distribution of regional type dolomite powder (sample Z-03) (c) Dolomite breccia clasts with calcite cement and replacement on the margin, that makes them more resistant against disintegration, associated with dolomite powder grains (sample T-07) (d) SE image of the surface of the dolomite powder grains that are characterized by sharp edges (sample Bu-03). (e) SE images of corroded dolomite crystals occurring together with calcite (sample P-01) (f) Intact surface of dolomite crystals in non-disintegrated dolomite (sample P-19).

III/3.3 Fluid inclusion petrography and microthermometry

Fluid inclusions of fabric-destructive dolomite were measured in the case of Budaörs Dolomite from Odvas Hill, (sample O-02) and in Hauptdolomit from Tündér Cliff (sample Tu-01). Both nonplanar-anhedral (Fig. 17a) and planar-euhedral dolomite crystals contained measurable fluid inclusions (Fig. 17b) in the Budaörs Dolomite samples from the Odvas Hill. Nevertheless, it has to be noted that only the cloudy central part of the planar crystals contained measurable fluid inclusion. Planar-euhedral crystals without cloudy core were free of inclusions.

In the case of the Hauptdolomit sample from Tündér Cliff, fluid inclusions were measured both from dolomite-I and dolomite-II phases. In planar-euhedral dolomites, inclusions were measured both from the cloudy central part of the crystals (dolomite-I) and also from the inclusion-rich growth zones within the dolomite-II phase (Fig. 17c).

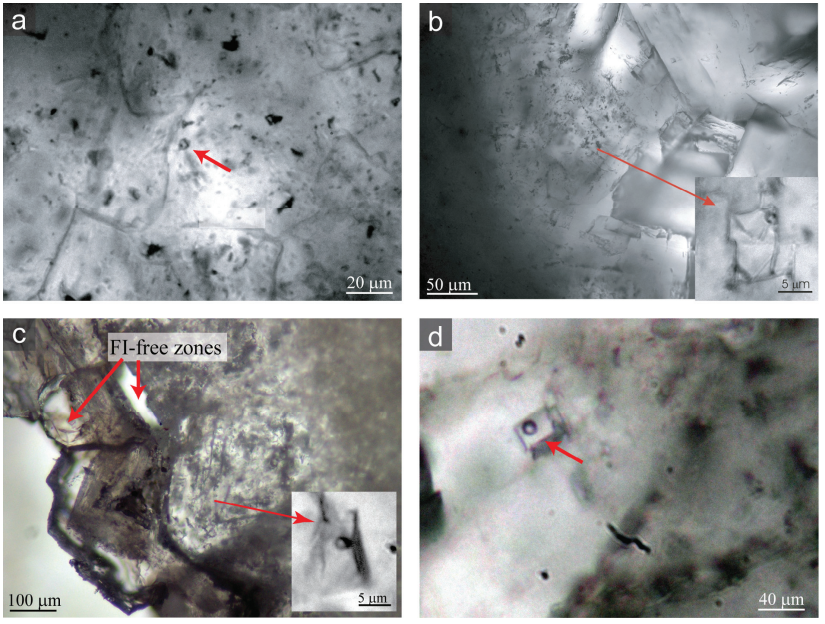

Fig. 17: Fluid inclusions in dolomite (a) Two-phase (L-V) fluid inclusions in nonplanar-anhedral dolomite (sample O-02) (b) Two-phase (L-V) fluid inclusions in the cloudy core of planar-euhedral dolomite (sample O-02) (c) Fluid inclusion-rich and FI-free zones alternate in planar-euhedral crystals (sample Tu-01) (d) Two-phase (L-V) fluid inclusion in sample Tu-01. (L/V ratio: ca. 70:30)

All the measured aqueous inclusions were primary in origin and contained both liquid (L) and vapour (V) phases. Size of the measured inclusions is ranging between 5-15 μm. Visually-determined liquid-vapour ratio is highly variable from 99:1 up to 70:30 (Fig. 17d) but no gas-rich inclusions occur. This observation points to the fact that the volume of some of the inclusions may have changed after entrapment, this process in known as thermal reequilibration (Goldstein 2001). Cryoscopic and heating measurements were not possible to be completed on the same inclusion because after homogenization or freezing of the inclusion the vapour phase became metastable and the vapour bubble disappeared because of its small size (<10 vol. %). Therefore homogenization temperature was measured mainly from those inclusions containing small (ca. 5%) gas phases because these inclusions were thought to be non-stretched. Melting temperature was measured from those inclusions containing larger gas bubble (ca. 20%), assuming that these inclusions were not refilled but only stretched.

Melting temperature and homogenization temperatures are similar in dolomites of different textures (Appendix-Table 2, 3). NaCl-H_2O system is assumed for the entrapped fluid since it was not possible to detect the eutectic temperature because of the very small size of the inclusions. Inclusions in Budaörs Dolomite are characterized by a salinity of 3.4 up to 7.9 NaCl equiv. w% (T_{melt}=-2 to -5°C) and Hauptdolomit showed a salinity of 3.4 up to 5 w% (T_{melt}=-2 to -3°C). Homogenization temperatures are in the same range both in the inclusions of the planar-euhedral and nonplanar-anhedral crystals but slight differences were detected between the two formations. Minimum value of homogenization temperature interval is 70°C (Fig. 18) in the case of the older (Budaörs Fm) dolomite while younger (Hauptdolomit Fm) dolomite is characterized by a minimum temperature value of 62°C (Fig. 19).

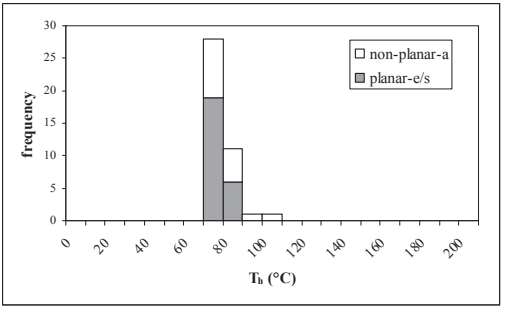

Fig. 18: Distribution of homogenization temperatures measured in Budaörs Dolomite, Odvas Hill

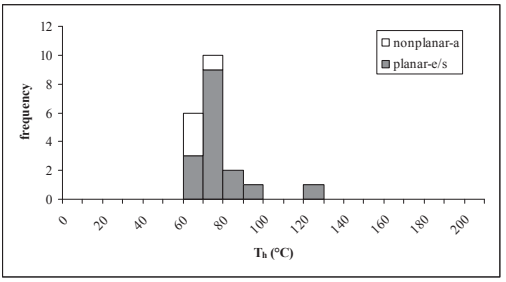

Fig. 19: Distribution of homogenization temperatures measured in Hauptdolomit, Tündér Cliff

III/3.4 Geochemistry

III/3.4.1 Stable isotope geochemistry

Two different dolomite populations (i.e. nonplanar-anhedral and planar-euhedral) of fabric-destructive dolomite samples were measured separately when it was possible both from Budaörs and Hauptdolomit Formations. Nonplanar-anhedral and planar-euhedral dolomites were separated by micro-drilling. However, separation was not always perfect due to the fine crystal size. It was not possible to measure separately the clear rim and cloudy centre in the case of planar-euhedral crystals in absence of appropriately fine drilling equipment. Therefore it is important to mention that in the case of planar-euhedral crystals of clear rim and cloudy core, both dolomite-I and dolomite-II phases are present within one and the same crystal.

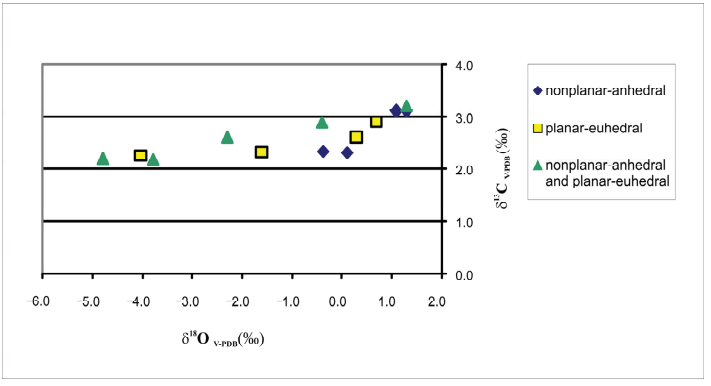

Fig. 20: Stable carbon and oxygen isotope data of different types of dolomite

All carbon isotope values are restricted to a narrow interval between +2.2 and +3.2 while oxygen values fall within a much wider interval from +1.3 down to -4.8. Intervals of both oxygen and carbon isotopes related to the two different types of dolomite partially overlap. Planar-euhedral crystals are generally more depleted in heavy oxygen isotope than nonplanar-anhedral crystals (Fig. 20).

Regarding all the data, including the values of calcite and dolomite phases, a trend can be observed from white calcite towards dolomite (Fig. 21). It has to be emphasized, however, that this is only the effect of physical mixing of dolomite and calcite phases during sample preparation because in many cases, it was not possible to measure pure calcite or dolomite, only the mixture of them, because of the very fine crystal size. The following sequential calcite-dolomite separation method was used to measure the isotopes of calcite and dolomite separately when it was not possible to separate them physically by drilling: CO_2 produced by acid treatment was measured after different duration of etching: *10 minutes, 1 hour* and *1 day*. The data belonging to '*10 minutes'* are representative for the calcite because dolomite is more resistant against the acid attack than calcite is. The '*1 hour'*-test represents the mixture of the two components and the values after '*1 day'* acid treatment are considered much more representative of the dolomite phase. The original proportion of calcite and dolomite was also taken into consideration during the interpretation. Thus I could differentiate between those isotope values representing the mixture of calcite and dolomite and those values related to separate mineral phase. Excluding the values of mixed samples facilitates the distinction between isotopic composition of dolomite and calcite.

All the dolomite samples, independent from the stage of disintegration, show essentially the same isotope signal. Stable isotope values of calcite phases of different colours are similar because both show negative carbon and oxygen isotope values, however, red calcite is characterized by slightly less negative $\delta^{13}C$ isotope value, as compared to white calcite (Appendix-Table 4). It has to be noted, however, that only one data-pair was measured for the pure red calcite (Fig. 21). Isotopic composition of calcite from the 'mega-concretion' (calcite-III) is the same as that of the white calcite.

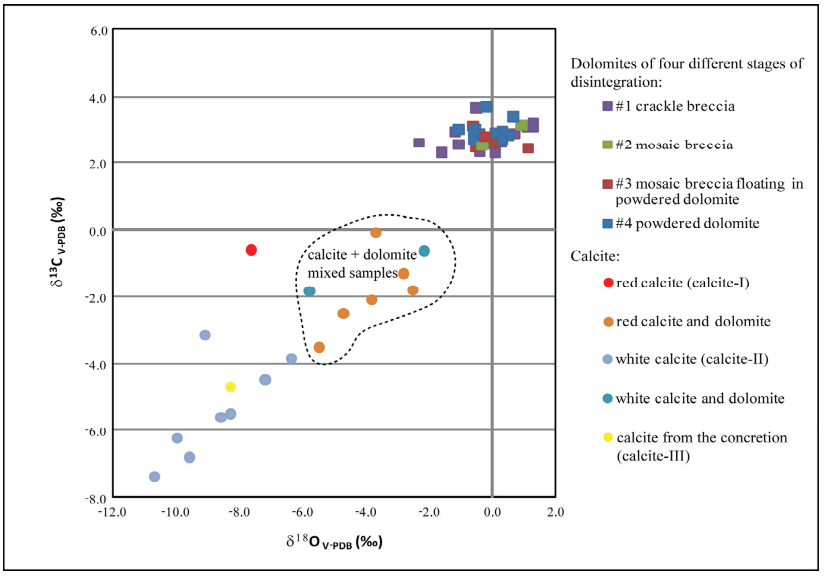

Fig. 21: Carbon vs. oxygen isotope values of bulk samples of different types of dolomite and separated samples of different calcite phases

III/3.4.2 Major and trace elements

In addition to the mineralogy and stable isotopic composition of different types of dolomites bulk samples were measured both for major and trace elements by ICP-AES and ICP-MS. Disintegrated and non-disintegrated dolomite samples were measured as well as dedolomite samples. As to the Ca/Mg ratio there are no differences between disintegrated and non-disintegrated dolomite (Appendix-Table 1). Dolomite containing calcite shows enrichment in Ca at the expense of Mg which is an obvious sign not only of calcite cementation but also of dedolomitization observed on the microscopic scale. In the case of the other measured major elements (Si, Al, Fe) no remarkable anomalies and differences were detected even if the sample was collected from under the unconformity (Appendix-Table 1). Dolomite partially replaced by red calcite (DC-01) has the highest Fe-content which is in accordance with the presence of iron-bearing solid inclusions mentioned before.

Regarding the rare-earth elements (REE) no significant differences could be detected in the studied samples (Appendix-Table 1). All samples are depleted in each REE as compared to the PAAS (Fig. 22). All the normalized REE-patterns are flat (with the exception

of Tm) with no significant differences between the concentrations of light, medium and heavy rare earth elements.

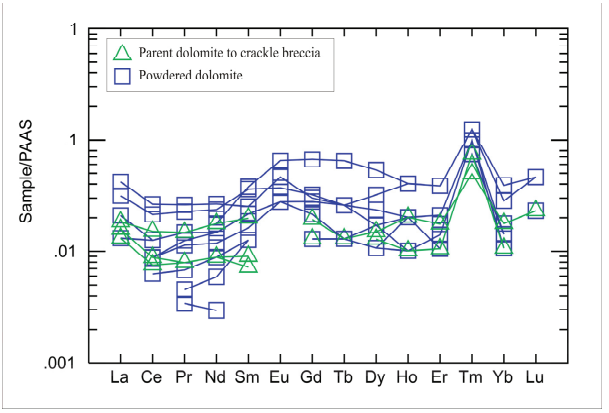

Fig. 22: Rare Earth Elements normalized to PAAS (Taylor and Mc-Lennan 1985). Nine samples of powdered dolomite and three samples of intact dolomite were measured. (Missing data points are below detection limit)

REE and certain additional trace elements, generally related to low-T hydrothermal fluids (e.g. Ba, Hg), were normalized to the average value of the three intact dolomite samples in order to trace the possible changes in concentrations during either disintegration or dedolomitization of dolomite. In the case of REE no systematic enrichment or depletion was detected as compared to parent dolomite. All curves are flat and deviation from value 1 is very minor in each case (Fig. 23). Normalized REE data show very similar values in the case of local and regional type powders as well as in dedolomite samples.

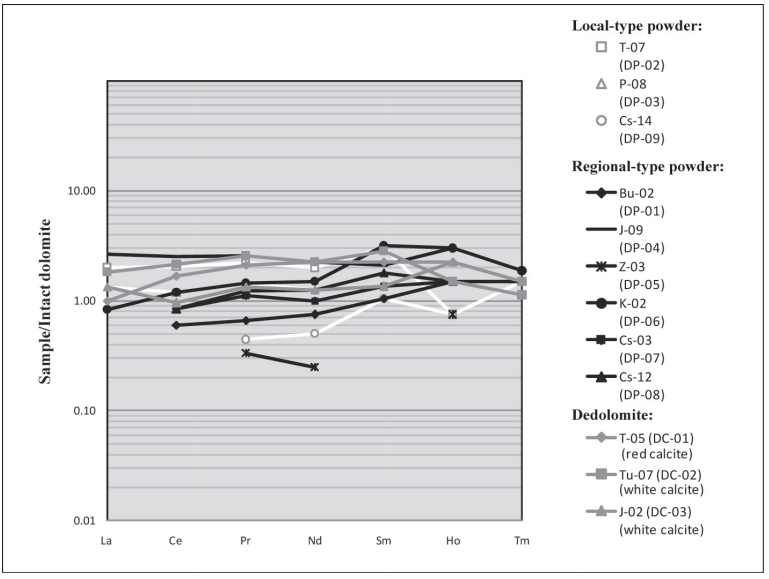

Fig. 23: REE concentrations normalized to the average value of three intact dolomite samples (D-01, 02, 03). Note those REE are not illustrated that remain below the detection limit in intact samples.

Other trace elements, i.e. P, Mn, Zn, Pb, Ba, etc., were also normalized to the average value of intact samples. As opposed to previous studies I could not detect systematic enrichment or depletion in powdered samples relative to the intact samples (Fig. 24). However, occasionally some samples characterized by significantly different concentrations relative to intact samples were also found. For example elevated Ba-content accompanied by positive S anomaly can be explained by the presence of barite enclosed by the calcite formed due to dedolomitization (sample J-02). The sample impregnated by red calcite (T-05) shows enrichment in Ba, Hg and S which can easily be explained by the above mentioned field observation, i.e. that there are some barite-limonite veins crosscutting the dolomite exposed in Teve Cliff quarry. All types of dolomite, i.e. locally and regionally powdered dolomite as well as dedolomites show similar trace element concentrations. However, it is important to mention that in the case of dedolomite samples calcite and dolomite phases were not measured separately and the samples are predominantly of dolomite with variable amounts of calcite.

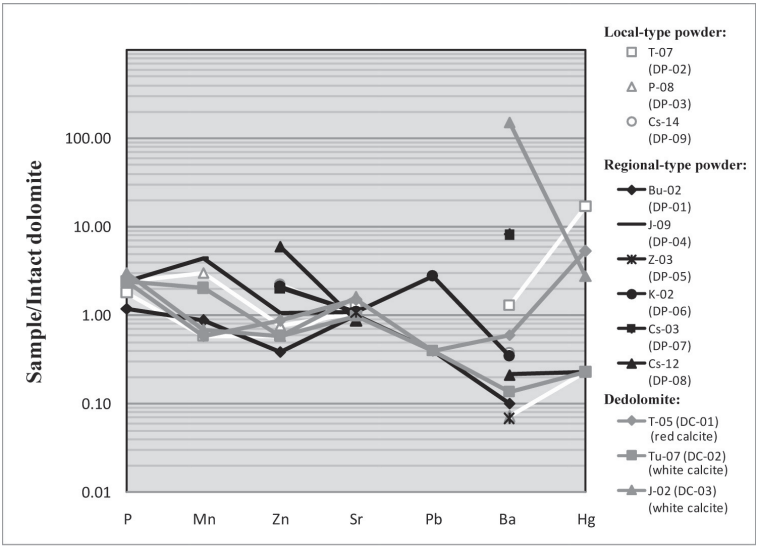

Fig. 24: Trace element concentrations normalized to the average value of three intact dolomite samples (D-01, 02, 03).

III/4 Discussion (dolomitization, dedolomitization, powderization)

Based on field observations and petrography, relative timing of the diagenetic events affecting the Triassic dolomites was established. Dolomitization was followed by intense fracturing of dolomite and breccia formation, by dedolomitization/calcitization and cementation along fractures. Samples of box-work texture are one of the obvious evidences for powderization of dolomite being younger than all these processes. Subsequent to powderization (or with partial overlap) a very late calcite cementation must have occurred, however, only locally, resulting in 'mega-concretions'. In this chapter, the above processes are discussed according to the established paragenetic sequence.

III/4.1 Dolomitization

Stable isotope values of nonplanar-anhedral crystals fall within broadly the same interval, measured in Upper Triassic dolomites in the TR ($\delta^{13}C$: 1 to 3‰; $\delta^{18}O$: -1 to 3‰; Balog et al. 1999, Haas et al. 2000, Haas and Demény 2002). These oxygen isotope values are slightly heavier than those of the calcite precipitated in equilibrium with Late Triassic

seawater since the $\delta^{18}O$ values measured from well-preserved Triassic brachiopods from the Tethyan realm is ranging between -3.9 and -0.6‰ V-PDB (Korte et al. 2005). The observed slight difference in $\delta^{18}O$ values of Late Triassic calcite and dolomite is in accordance with results of Woronick and Land (1985) who claim that dolomite will be about 3 to 6 ‰ heavier than coprecipitated calcite, due to differences in fractionation between dolomite-water and calcite-water.

According to the uniformly high homogenization temperature values (> ~60°C) of dolomite-I and II phases it is suggested that both phases precipitated at elevated temperature. Fluid inclusion data are in accordance with the observed nonplanar-anhedral texture in the case of dolomite-I, since this texture is considered to develop at higher temperatures (>50-60°C), i.e. above the so called 'critical roughening temperature' (Gregg and Sibley 1984). Presence of saddle dolomite also points to elevated temperature conditions during precipitation. Gradual decrease in $\delta^{18}O$ values form dolomite-I towards dolomite-II shows that that the temperature of dolomitizing fluid gradually increased with time. Fluid inclusion data do not confirm this but it has to be emphasized that there are no homogenization temperature data from the outermost part of the planar-euhedral crystals.

According to Machel (2004) fabric-destructive texture of two different dolomite populations may be the result either of one single phase of dolomitization or of dolomite recrystallization. Recrystallization means that metastable phases, namely the precursor of the central cloudy part of larger crystals, apparently undergo intracrystalline recrystallization during or after formation of the stable overgrowths (e.g. Sibley 1990).

In this case, there may be significant differences in the geochemical composition of the two dolomite populations. In this latter case, geochemical compositions of both dolomite populations would be similar (Machel 1997, 2004). Having seen the differences in oxygen isotopic composition of the two dolomite populations, the case of one single dolomitization event is less likely. It cannot be decided, however, if dolomite-I underwent intracrystalline recrystallization during formation of the stable overgrowth or not. Identical fluid inclusion data in the nonplanar-anhedral crystals and in the cloudy core of planar-euhedral crystals may point to that dolomite-I phase was not affected by recrystallization. (If there were recrystallization fluid inclusions in the cloudy core of a planar-euhedral crystal may have been replaced by that fluid which was responsible for the formation of dolomite-II. It is suggested because recrystallized dolomite commonly contains fluid inclusions that have been trapped during recrystallization (Goldstein and Reynolds 1994).) Nevertheless, because of the similar fluid inclusion data in the case of dolomite-I and II, the case of recrystallization cannot be

ruled out. It is also possible that replacive dolomitization at elevated temperatures already resulted in stable dolomite phases (dolomite-I) and the subsequent dolomite cementation process had no effect on the fluid inclusions and stable isotopic compositions of the dolomite-I.

Petrography, stable isotope and fluid inclusion data together suggest that in the case of the studied platform carbonates from the Buda Hills there was a minor near-surface fabric-selective dolomitization first which was restricted to the thin laminated layers. This was followed by a pervasive replacive dolomitization in the burial realm, above 60°C, which has affected also the thick beds and resulted in the dolomite-I phase. During continued subsidence the same fluid became slightly warmer and precipitated dolomite overgrowth cement (dolomite-II) in the open pore space resulting in coarse planar-euhedral crystals of clear rim and cloudy centre. There may have been also a minor dissolution event before precipitation of dolomite-II phase because the surface of dolomite-I phase is often corroded shown by the first bright luminescent zone of dolomite-II phase (Fig. 12d).

It is important to emphasize that minimum temperature values of the inclusions were taken into consideration and scattered higher homogenization temperature values (up to 124°C) were thought to be invalid because of the supposed volume change of the inclusions after entrapment. Minor differences in minimum homogenization temperature values in the two studied formations may represent the differences in the burial depth. The younger Hauptdolomit is supposed to have reached shallower depth than the underlying Budaörs Fm (T_h min= 70°C) which is in accordance with lower homogenization temperatures measured from Hauptdolomit (T_h min= 62°C). Homogenization temperature interval and salinity values are in good agreement with the results of Balog et al. (1999) who also carried out FI investigations in the Hauptdolomit Fm from several different localities within the TR. They concluded that these salinity data were characteristic of normal to slightly hypersaline seawater. However, salinity values as high as 7.9 wt% are considered to be much more saline than the seawater pointing to highly modified pore-waters responsible for the dolomitization.

Although, it is not yet possible to delineate an adequate dolomitization model for this case, it can be concluded that the dolomitizing fluid that resulted in fabric-destructive textures was not merely the heated and evaporated seawater but there might have been some additional fluid contribution to the system based on the calculated oxygen isotopic composition of the fluid (Fig. 25).

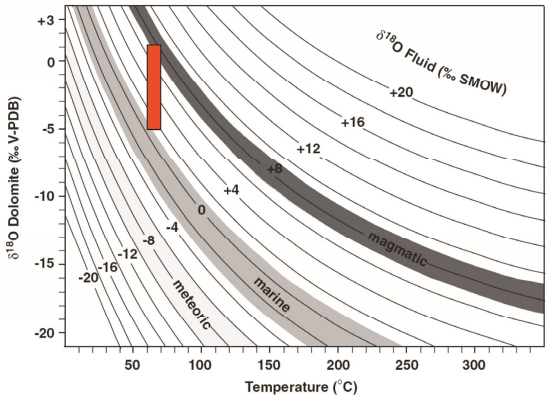

Fig. 25: Precipitation temperature vs. oxygen isotopic composition of the studied dolomite, marked by red rectangle. The $\delta^{18}O$ of the fluid in equilibrium with dolomite was calculated using the fractionation equation of Land (1983)

III/4.2 Dedolomitization/calcitization of dolomite

According to the earliest studies, dedolomitization requires the following conditions: high Ca/Mg ratio; high rate of water flow; relatively low P_{CO_2}; and temperature less than 50°C (de Groot 1967). Therefore dedolomitization is most commonly a near-surface phenomenon commonly observed related to unconformities and karst phenomena (e.g. Evamy 1967, Folkman 1969, Ronchi et al. 2004, Nader et al. 2003). This process can be areally extensive resulting in dramatic change in the amount and distribution of both porosity and permeability (Fritz 1967; Hanshaw and William 1985). Other studies revealed that dedolomitization occurs in the burial realm as well, commonly associated with dissolution of Ca-sulphate phases (e.g. Budai et al. 1984, Fu et al. 2008).

Dedolomitization of the Hauptdolomit Fm has been reported from several localities of the TR and also from the Alps in Italy, however, such observations from the Buda Hills were lacking. Tóth and T. Gecse (1981) described 10 to 20 metres thick dedolomitized 'dykes' in the Upper Triassic basement of the TR from under bauxite lenses. According to their description those 'dykes' are very similar to the surface occurrences of dedolomitized zones with red calcite in the Buda Hills. The strike of the 'dedolomite-dykes' is mainly NW-SE, subordinately WNW-ESE but with a great scatter to essentially all directions. Variable orientations were measured in the Buda Hills as well. In the Norian *Dolomia Principale* (equivalent to Hauptdolomit) similar phenomena were described by Ronchi et al. (2004) from

the Southern Alps, Italy who also found calcite-cementation and dedolomitization related to fracture-networks. This was interpreted as the result of Quaternary subaerial diagenesis.

Two types of dedolomite were observed in the studied samples: red calcite and white calcite. In the case of white calcite both dolomite-replacing calcite (s. str. dedolomite) and calcite cement was detected. It is suggested that dedolomitization occurred as mole per mole calcite replacement of dolomite, i.e. the rock underwent the so called *one step process* when dolomite dissolution and calcite precipitation were coeval (Fu et al. 2008). Since no petrographic (including CL) differences were found of the replacing and the cementing calcite phases, the calcite cement phase is considered to be a primary precipitate from the very same fluid, which occludes the open fractures and vugs of the dolomite rock.

Stable isotope study revealed that both detected calcites (calcite-I and II) are of meteoric origin based on the negative $\delta^{13}C$ (-0.6 to -7.4 ‰) and $\delta^{18}O$ (-6.3 to -10.7 ‰) values. Therefore, it can be interpreted as karst related dedolomitization, i.e. the result of near-surface calcitization processes caused by meteoric flushing below an erosional unconformity. The effects of freshwater diagenesis was detected on Upper Triassic carbonates (limestone and dolomite) in the TR from other location (Halimba), too, based on fluid inclusions and stable isotope studies (Mindszenty et al. 2001). Minor meteoric signal of calcite in Triassic dolomites of the Buda Hills were also detected by stable isotope study (by negative $\delta^{13}C$ and $\delta^{18}O$ values) by Haas et al. (2000). Dolomite-replacing calcite in the *Dolomia Principale* is characterized by similar carbon (~ -4 to -6 ‰) and oxygen isotope intervals (Ronchi et al. 2004). Similar, however slightly less depleted, isotopic composition ($\delta^{13}C$= ~ 2.4‰; $\delta^{18}O$= ~ -5.5‰) was measured in karst related dedolomite in Jurassic carbonates from Lebanon (Nader et al. 2003).

Since red calcite does not show any luminescence it can be stated that this phase precipitated under oxidizing conditions. The observed cathodoluminescence pattern of white calcite points to precipitation in the upper part of the meteoric phreatic zone. This zone is mainly characterized by oxidizing conditions which results in dull or non-luminescent calcite containing a few bright, thin luminescent zones pointing to slight redox fluctuations (James and Choquette 1989). Redox fluctuation may also explain the presence of high amounts of iron-oxi-hydroxides. It can be stated that both calcites (calcite-I and II) formed in the meteoric phreatic zone under predominantly oxidizing conditions during the telogenetic phase of the studied dolomite formations. There are two periods when the studied dolomite formations may have been in such situation, namely during the pre-Mid-Eocene subaerial exposure and during the sub-recent to recent exposure.

Even though, the crosscutting relationship of the white and red calcite/dedolomite phases was not observed, it was possible to estimate the relative ages of them based on detailed petrography. Since minerals typical in bauxite were detected in the dissolution residue of the red calcite, bauxite was most probably yet unconsolidated during the precipitation of this calcite, because the flushing out of such finely dispersed bauxite minerals would not have been possible from an already lithified rock. Red calcite therefore is very likely coeval or only slightly younger than the bauxite (~Early/Middle Eocene of age). The subsurface occurrences of very similar dedolomite bodies (that were obviously not affected by the subsequent sub-recent subaerial exposure) in other parts of the TR may confirm the above assumption, namely that the precipitation of red calcite is related to the first telogenetic phase of the dolomite.

In the white calcite detrital barite inclusions were found which confines the maximum age of this cement phase as post-Miocene. Namely the age of the oldest known barite-veins in the Buda Hills is Miocene (Fodor et al. 1994, Gál et al. 2008) thus the white calcite must be younger than that. Minimum age of this calcite phase was established by U-Th age determination of samples from Tündér Cliff (sample Tu-06) and János Hill (sample J-04). It revealed that the white calcite must be older than ca. 1.5 M years (personal communication, Surányi 2010). Red calcite is not appropriate for U-Th measurements because of the abundant bauxite inclusions. Since the barite encloses also dolomite powder grains it can be supposed that disintegration of dolomite along fractures must have started before barite precipitation. Thus, the above texture can be interpreted by supposing the following series of events: 1st: fracturing of dolomite producing minor amount of dolomite powder along fractures; 2nd barite cementation along fractures of dolomite; 3rd highly fractured dolomite, containing barite veins, was later subject to dedolomitization. The red calcite never contains any barite inclusions which may confirm its pre-Miocene age. Thus the two types of calcite of different ages may reflect the two separate subaerial exposure periods of the Buda Hills, i.e. Cretaceous to Middle Eocene and Pliocene to recent, respectively (Wein 1977).

Although, in the absence of exact ages of the studied calcite phases it still cannot be ruled out that red calcite and white calcite are the results of one and the same karst related process and that the above mineralogical differences only reflect the differences of the host rocks in different outcrops. Accepting this idea, would mean that both red calcite and white calcite must have been precipitated during the last subaerial exposure period. Red calcite might have precipitated in dolomites where minor bauxite infiltration occurred while white calcite could be the representative for those dolomites that had no bauxite infiltration.

III/4.3 Powderization of dolomite

III/4.3.1 Previous models vs results of the present study

Based on the results of the recent study none of the previously published models (described in details in the Chapter III/1) can be entirely accepted. In accordance with Nendtvich (1859), powderization cannot be explained by merely recent chemical weathering because there was no change detected in chemistry and mineralogy between samples representing the different stages of disintegration. Even though, powderization occurs also ca. 100 m below the ground surface (Jakucs 1950), it is clearly controlled by the depth from recent land surface, since disintegrated dolomite consistently occurs above 200 m depth from the present actual land surface (Fig. 11). This is in accordance with the idea of recent weathering induced powderization.

Although, the spatial relationship between the distribution of powdered dolomite and the bauxitic unconformity is obvious, it has to be mentioned that in the area of Buda Hills, pre-Mid-Eocene and sub-recent/recent unconformities often overlap. Therefore the differentiation between their effects is ambiguous. In the case of the Buda Hills, the significant effect of pre-Mid-Eocene subaerial exposure on intense disintegration cannot be proved. It has to be noted, however, that in other parts of TR minor powderization related to bauxitic unconformity was observed in deep boreholes and underground mines, as well. These dolomite powders may be the result of the pre-Mid-Eocene subaerial exposure period, but the study of these occurrences was beyond the scope of present study.

The effect of hydrothermal fluids on powderization can be excluded, too based on the followings. Firstly, disintegration of dolomite is usually not restricted to the narrow surroundings of areas that have been affected by hydrothermal fluids. For example the whole area (~2 km^2) of Zajnát Hills consists of disintegrated dolomite but no hydrothermal mineralization was observed at all at that locality. In contrast, Törökugrató quarry exposes non-disintegrated dolomite (Budaörs Fm) that hosts more than one metre wide hydrothermal veins (Poros et al. 2011). In addition, this study revealed that even if disintegrated dolomite and hydrothermal minerals occur in the same place, there is very likely no genetic relationship between them. For example at Sorrento Cliffs, powdered dolomite and associated quartz cementation is independent since powderization is clearly younger than quartz precipitation.

Secondly, as opposed to some of the former studies, no systematic chemical differences were detected between disintegrated and non-disintegrated dolomite samples, regarding neither the major nor the trace element contents. Stable isotopic compositions also remained

unaffected during the gradual disintegration process. Moreover, if there were any systematic changes in composition, e.g. trace element enrichment in the powdered dolomite, it wouldn't necessarily imply causal relationship because, theoretically, hydrothermal fluids might have migrated through the dolomite powder even after the disintegration using the elevated porosity of this zone. X-ray powder diffraction and petrography show that mineralogy has not changed during disintegration, either: both non-disintegrated and disintegrated samples predominantly consist of dolomite.

Absence of aragonite and/or calcite, in vast majority of dolomite powder samples, excludes the model of Jakucs (1950) who suggested that powderization was due to the volume increase during recrystallization of aragonite to calcite. Furthermore, lack of calcite and other cement phases in powdered dolomite suggests the followings: either that dedolomites and cemented dolomites were less prone to disintegration, or powderization predated calcitization and cementation. Field observations showed that the second alternative is less likely since powderization of dolomite must be younger than either of the followings: 1) accumulation of Eocene bauxite 2) formation of the basal member of the Lower Oligocene Hárshegy Sandstone 3) quartz cementation most probably Early Oligocene in age (related to the Paleogene volcanism) 4) formation of barite veins in the Miocene 5) dedolomitization events of pre-Mid-Eocene and/or Pliocene-Pleistocene (>1.5 My) ages. Regarding the young age of powderization, the above observations are in agreement with Esteban et al. (2009). They claim that powderization must be post-Pannonian (Late Miocene) in age since sandstone-dykes of Pannonian age were found in the disintegrated dolomite at Ördög Cliff.

III/4.3.2 New model: Sub-recent physical weathering

It can be stated thus, that powderization must have post-dated dedolomitization and cementation and only those dolomites have suffered intense disintegration that were not affected by dedolomitization/cementation before. Peculiar-shaped dolomite pillars, cliff zones and ridges are all the results of later differential erosion. This explains the occasional juxtaposition of disintegrated and non-disintegrated dolomite occurrences on the actual surface. Non-cemented and non-calcitized dolomite was more prone to disintegration; therefore it was more prone to erosion as well (Fig. 29).

At Kecske Hill, such juxtaposition is preserved at a stage when partially dedolomitized structures are not yet protruding above the recent topography: the irregular-shaped, undulating surface is still overlain by several metres of dolomite powder. This outcrop can be interpreted as the representative of the next to last (pre-erosional) stage of dolomite pillar formation (Fig.

29c). The undulating surface can be interpreted either being simply a powderization front or perhaps a dedolomitization front (Fig. 29c). These two fronts may or may not overlap in this case. Having seen the high amplitude of this uneven surface, it can be supposed that the dedolomitization front was rather horizontal. Dedolomitization, affecting preferentially the thick beds, was followed by fracturing resulting in the rough, undulating surface. Later powderization was the most intense in the surroundings of these fractures having affected mainly the non-calcitized/non-dedolomitized beds as well as the uppermost part of the calcitized/dedolomitized zone. Based on the vertical distribution of powdered and calcitized dolomite beds it can be stated that the powderization front has been progressing towards the depth from the land surface while the dedolomitization front moved in the opposite direction.

The results of this study suggest that disintegration of dolomite in the Buda Hills was a process:

- which resulted in gradual grain size diminution,
- which resulted in no chemical and mineralogical changes,
- which had no significant dissolution associated with it, since only those samples contain dolomite crystals characterized by significant corrosion that were subject to dedolomitization,
- which preferentially affected dolomite along fractures (described also by Scherf 1922 and Jakucs 1950),
- against which calcitized dolomite/dedolomite and cemented dolomite has been more resistant,
- which was/is strongly related to the recent or sub-recent land-surface,
- which was/is effective below maximum 200 m from the present-day land-surface,
- which is younger than the last karst related dedolomitization event, i.e. it occurred sometime in Pliocene to Pleistocene (?).

Based on the above points, the observed disintegration of dolomite must be a sub-recent, near-surface process that results in mechanical disintegration, i.e. physical rather than chemical weathering. Thus this interpretation is a variant of the oldest model, namely of the recent weathering induced powderization.

Near-surface physical weathering processes, known to commonly result in internal stress and subsequent disintegration of the rocks, were recently summarized by Cueto et al. (2009). These are the followings: 1) water freeze-thaw 2) crystallization of soluble salts, i.e. salt-weathering (e.g. Benavente et al. 2007), 3) swelling-contraction cycle of clays. In addition, contribution of thermal expansion to physical weathering is also common. Salt-

weathering and swelling-contraction cycle of clays can be ruled out in this case because of the clear, monomineralic composition of the studied powdered dolomite samples. Water freeze-thaw mechanism, however, may be an adequate mechanism triggering powderization in the case of the Buda Hills, as well. Recent disintegration of dolomite, and also other rock types (e.g. granites, gneisses), under cold-climate conditions was studied in Canada, by Mackay (1999). In the case of dolomites, explosive shattering due to frost-weathering was observed resulting in smaller fragments (but not powder), from one year to another, that were scattered around the parent rock (Mackay 1999).

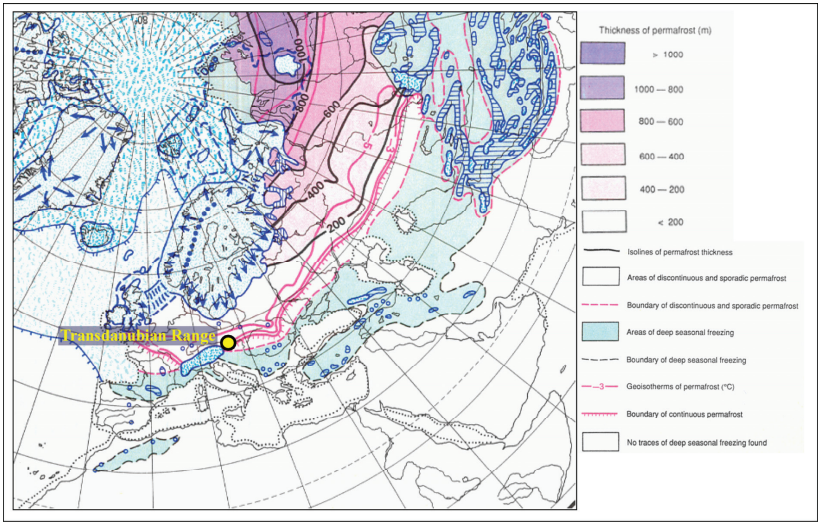

Fig. 26: Extension of permafrost during the maximum cooling of the last glaciation (18-20 000 years ago) (Frenzel et al. 1992). Note that TR is located close to the boundary of continuous permafrost.

To be able to adopt the water freeze-thaw mechanism as possible triggering effect of powderization also in the Buda Hills raises the question, whether there were such cold climate conditions in the studied area in the sub-recent period. According to Frenzel et al. (1992) Buda Hills was close to the boundary of continuous permafrost (Fig. 26) during the maximum cooling of the last glaciation period (ca. 18-20 K years ago). The thickness of the permafrost is considered as maximum 200 m in this zone which fits to the observation of powdered dolomites down to maximum 200 m from the actual surface. There is also field evidence for the presence of permafrost related features in the Pleistocene of the Buda Hills, e.g.

cryoturbated Eocene marl overlain by loess is exposed right below the recent surface by construction pits, close to the Hármashatár Hill (Fig. 27). However, when accepting frost-weathering as one of the adequate explanations, the question arises why powderization of dolomite is not ubiquitous at all those places in the world where permafrost affected dolomites.

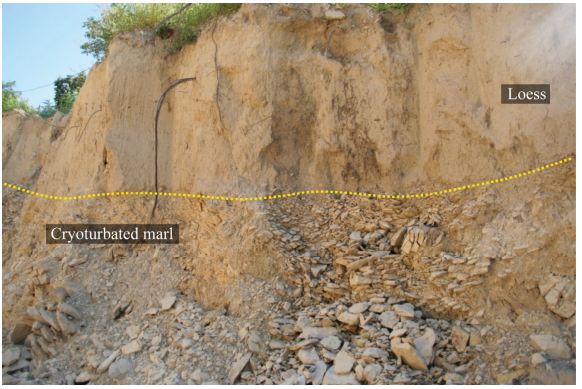

Fig. 27: Photograph of cryoturbated Eocene marl overlain by loess, Szépvölgy str., Rózsadomb (photo by M. Virág)

III/4.3.3. Laboratory experiment

In order to see whether the wedging-effect of ice is indeed a possible explanation for disintegration of dolomite samples from the Buda Hills, a very simple laboratory freezing experiment was carried out. Two different samples representing the same Hauptdolomit Formation were chosen, one from the Buda Hills (sample P-05) and one from the Southern Alps (Tre Cime, Italy, sample TC-01) because I also wanted to see whether dolomite samples from different localities behave similarly to freeze-and-thaw or not. P-05 sample represents the 2nd stage of disintegration and characterized by dual-porosity, i.e. intercrystalline porosity and fracture porosity, which is very common in the studied samples. The randomly selected sample from the Tre Cime representing the Dolomia Principale Formation is characterized by very significant dolomite overgrowth cementation and vuggy porosity. I put both samples of identical sizes (d ~3-4 cm) into two separate plastic bottles filled with water and put the bottles in the deep-freezer (at constant T= –18°C). After the entire amount of water became frozen I let the water thaw on room temperature (T=+22°C). After having completed four freezing-thawing cycles, the sample from Buda Hills became totally disintegrated,

characterized by very wide range of grain size from 1 mm up to 1 cm, while the sample from the Alps remained intact (Fig. 28). The different behaviour of the two samples can be explained by the well-known fact that the durability of dolomites is strongly related to fabric elements (e.g. Gaswirth et al. 2006, Benavente et al. 2007). In addition, water-saturation is also an intrinsic factor because it largely determines the efficiency of frost action on the rock. High water-saturation is given in the Buda Hills as it has been a discharge area of local, intermediate and also regional fluid flow systems since Pliocene-Pleistocene on (e.g. Erőss 2010). Intense tectonics was probably also very important because disintegration of dolomite is initiated by fracturing. In addition, cracks play more important role in disintegration due to freezing of water because cracks and fissures may become filled with water far more quickly than other pores (Prick 1998).

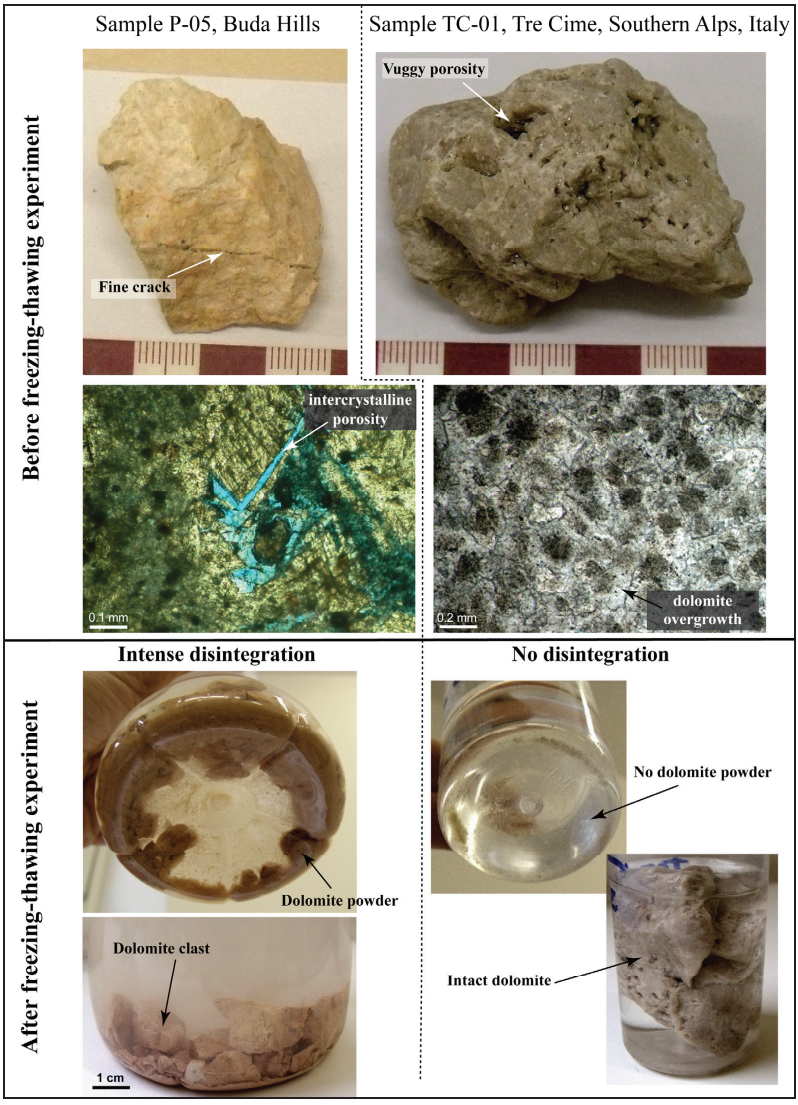

Fig. 28: Samples before and after the freezing experiment

Thus to produce and preserve such high amounts of powdered dolomite under conditions of frost-weathering, demands the coincidence of the following processes and rock properties:

- Significant intercrystalline porosity of the parent dolomite (that was created during the overdolomitization stage in the burial realm).
- Intense tectonics that resulted in highly fractured dolomite and minor amounts of dolomite powder along fractures (i.e. local powderization).
- Subaerial exposure under cold climate conditions resulting in repeated cycles of freeze-and-thaw.
- Higher water-saturation of rocks favours the more pronounced wedging effect of ice.
- No or only gentle erosion after powderization is also necessary because it promotes the preservation of dolomite powder.

At those places where at least one of these factors is missing, powderization of dolomite may be less intense or absent. It is also suggested that powderization of dolomite may have occurred in several other localities, but there are only few places where erosion was so minor that it was preserved because the preservation potential of dolomite powder is obviously very low.

III/4.4 Formation of concretions in disintegrated dolomite

In addition to the above described processes (i.e. dedolomitization in the meteoric phreatic zone, cementation by different hydrothermal minerals and disintegration) the studied dolomite was locally affected by an additional very late meteoric diagenetic event, as well. This late calcite cementation must be younger than the initiation of disintegration of dolomite but it cannot be ruled out that powderization also occurred during or after this process, as well.

The porous, spongy ‘mega-concretion’ is interpreted as being dolomite scree and powder cemented by calcite that precipitated under oxidizing conditions from meteoric waters trickling downwards through the scree. This is suggested by the morphology of the concretionary geobody and also by the stable isotopic composition and luminescent pattern of calcite-III. This particular zone may thus represent a former diffuse discharge zone of a local meteoric fluid circulation system. The morphology of the concretions invokes steep relief at the time of formation. The very same type of concretions, found at the Sorrento Cliffs, is located in the same topographic situation. This is in accordance with the interpretation of

Esteban et al. (2009), namely that this rock is the result of vadose late meteoric diagenesis (i.e. telogenesis) within exposed pulverized dolomite. Although, the presence of phreatic cements instead of vadose cements in the concretion still needs to be explained. It is assumed that the intense downward fluid flow temporarily may have resulted in local water-saturation, i.e. the formation of a 'pseudo-phreatic' zone within the scree. This may explain the lack of vadose features in the cement. However, the exact process of formation of this type of concretions is still unclear.

III/5 Conclusions

Detailed study revealed that platform dolomites of the Buda Hills underwent multiple diagenetic phases from the Triassic on. The most dramatic change in porosity, namely the powderization, was the result of a very late process that was influenced also by the earlier phases of the diagenetic history of the dolomites.

Pervasive, fabric-destructive dolomitization of Triassic platform carbonates most probably occurred in the burial realm, above ca. 60°C, based on textural evidences confirmed by fluid inclusion data (T_h> 62 °C). Replacive dolomitization (dolomite-I) was followed by dolomite overgrowth (dolomite-II) which resulted in a coarser-crystalline dolomite population characterized by significant intercrystalline porosity. This porosity type played a role in the subsequent disintegration process.

It can be stated that disintegration of Triassic dolomites in the Buda Hills was most probably initiated already in Eocene times by mechanical processes. Periods of intense tectonic activity resulting in uplift produced highly fractured dolomite, dolomite breccia and minor amounts of dolomite powder along fractures, represented by the local-type dolomite powder occurrences (Fig. 29a). During this first subaerial period, certain parts of the fractured and brecciated dolomite underwent dedolomitization and calcite cementation, especially at those places where the rock was characterized by elevated permeability and porosity (Fig. 29b). Two types of dedolomite could be distinguished, namely the red and the white calcites. Based on stable isotope data ($\delta^{13}C_{V\text{-}PDB}$= -7.4 to -0.6; $\delta^{18}O_{V\text{-}PDB}$= -10.7 to -6.3 ‰) it is suggested that both calcites are the results of karst related telogenesis. However, petrographical evidence shows that the two types of calcite are of different ages and they probably represent the two separate subaerial exposure periods of the Buda Hills, i.e. Cretaceous to Middle Eocene and Pliocene to recent, respectively.

In addition to dedolomitization, dolomite was locally cemented, mainly along fractures, by quartz, probably due to the Paleogene volcanism related fluid migration. Other

vein-filling minerals (e.g. calcite, barite), related to the Miocene hydrothermal fluid migration event are also found as cementing phases (Poros et al. 2011, and see details in Chapter IV).

Paragenetic relationships suggest that intense powderization is post-Miocene. It is suggested thus, that during the last subaerial exposure period, non-cemented/non-calcitized parts of dolomite have suffered pervasive powderization that resulted in the regional-type dolomite powder (Fig. 29c). Having seen the identical mineralogy and geochemical composition of powdered and intact dolomite samples, disintegration is interpreted as being a physical weathering process. Dissolution related disintegration processes were less likely involved in the powderization. Considering that the Buda Hills were close to the boundary of continuous permafrost during maximum cooling of the last glaciation period (Frenzel et al. 1992), and water-saturation was provided by the hydrogeological position of the area, it is suggested that dolomite disintegration was mainly mechanical, i.e. it was most likely caused by the wedging effect of ice aided by the combination of thermal expansion and contraction during repeated freezing and thawing. The vigorous wedging effect of ice was confirmed by laboratory freezing experiments performed on dolomite samples from the Buda Hills. Subsequent differential erosion resulted in the formation of protruding dolomite pillars, cliff zones and ridges (Fig. 29d). The very last event was the formation of the ‘mega-concretions’ which is the result of cementation by descending meteoric waters within a dolomite scree.

It is concluded thus, that powderization of dolomites in the Buda Hills was triggered by sub-recent, near-surface physical weathering processes. Frost-weathering is one of the adequate explanations for the studied disintegration of dolomite, meanwhile other effects, such as thermal contraction and dilation related disintegration, may also have enhanced the physical-weathering process.

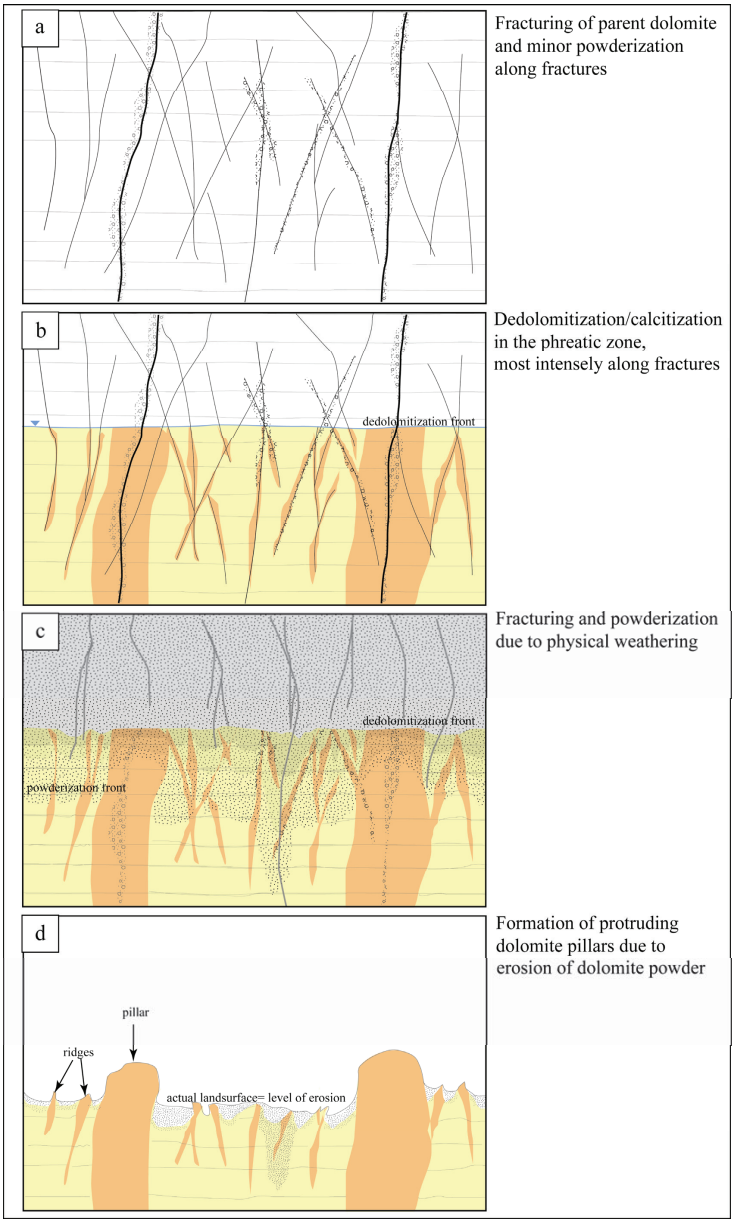

Fig. 29: Stages of disintegration of dolomite in the Buda Hills

Chapter IV – Fluid migration in the Buda Hills: vein-filling paragenesis, hydrocarbon-bearing basinal fluids, and hypogenic caves

IV/1 Introduction

The Buda Hills is famous for its extensive hypogenic cave system (sensu Klimchouk 2007; Goldscheider et al. 2010) and abundant actual thermal springs. There are also abundant mineralized veins recognized in this area. Caves often occur along the mineralized fractures. These phenomena suggest that the contribution of thermal water must have been significant both to the paleo- and the recent fluid systems and also invokes close spatial relationship between the recent- and paleofluid migration events.

Precipitates related to the paleo-thermal-water circulation in the Buda Hills have been studied by several authors since the end of the nineteenth century. Those studies focused on the most common vein-filling minerals, i.e. calcite and barite (e.g. Braun 1889; Brummer 1936).

Schréter (1912) suggested that there were two stages of hydrothermal activity: (1) high-temperature fluid circulation resulting in barite and fluorite precipitation and formation of siliceous veins − from Middle Miocene to Early Pliocene – and that all these were related to the post-volcanic activity of the volcanism in the Visegrád Mts. located to the north of the Buda Hills. (2) low-temperature hydrothermal activity − from the Late Pleistocene to Holocene − resulting in the formation of travertines. He also suggested that the water of recent thermal springs were diluted by vadose water. Schafarzik (1921) claimed that there was an additional hydrothermal phase related to the Paleogene volcanism which produced siliceous cementation.

According to the model of Kovács and Müller (1980), the first fluid circulation event took place under confined conditions. They proposed that the heat source of that fluid flow event was the nearby Neogene volcanism. The second phase ─ from the latest Miocene on ─ occurred already under unconfined conditions. In this stage, they have already assumed a significant karstic contribution to the thermal water system.

Nádor (1991, 1992) claimed that the first high-temperature fluid circulation resulted in the hydrothermal veins. These veins were exposed by younger caves which formed during the subsequent low-temperature fluid circulation event.

Several fluid inclusion studies were carried out on the vein-filling calcite and barite of the Buda Hills (Gatter 1984; Dublyanszky 1991; Molnár and Gatter 1994; Benkovics et al. 1999; Gál et al. 2008). They all showed that the parent fluids were of low salinity (<3 NaCl

wt%) and characterized by a wide range of homogenization temperatures (T_h =50–250°C). Gál et al. (2008) confirmed the suggestion of Báldi and Nagymarosy (1976) regarding the Oligocene age of siliceous cementation of the Oligocene sandstone. They also distinguished a subsequent hydrothermal event of late Early to Middle Miocene age by fitting the orientation of barite veins into the paleostress field model by Márton and Fodor (2003).

Caves of the Buda Karst, hosted mainly by Eocene carbonates, all show fracture-controlled maze-like pattern. Dissolution has been explained by the mixing of ascending hydrothermal water and descending meteoric water (e.g. Kovács and Müller 1980; Takács-Bolner and Kraus 1989; Leél-Őssy 1995; Leél-Őssy and Surányi 2003; Erőss et al. 2008). Most recently, however, it was shown by Erőss (2010) that in the discharge zone of Gellért Hill area no mixing occurs between the meteoric and hydrothermal end members. Alföldi (1979) detected hydrocarbon indications in some of the wells in the basin side. He considered it as an evidence for basinal contribution to the karst system.

My first aim was to decide whether the studied veins from different localities are related to the same regional fluid flow event or not. I also aimed to decide whether the mineralizing fluids had direct volcanic connections indeed, or the fluids are rather sourced from the nearby basin. Also I wanted to prove or disprove the above statements by quantitative analytical data. In addition, my goal was to establish the possible relationship between the paleo- and recent hydrogeology and thus between the veins and the younger cave systems of the Buda Karst on the basis of the reconstruction of the paleofluid migration pathways. I wanted to see also whether this hydrothermal event had any detectable influence on the porosity evolution of the Buda Karst.

IV/2 Applied methods

CL petrography was performed on a MAAS–Nuclide ELM-3 type cold cathode luminoscope on polished thin sections at the Department of Physical and Applied Geology, Eötvös L. University.

Stable carbon and oxygen isotope analyses were carried out in the Institute for Geochemical Research, Hungarian Academy of Sciences. The samples were measured by a Finnigan MAT delta S type mass spectrometer after being pulverised and using the conventional anhydrous phosphoric acid digestion method, under vacuum (McCrea 1950). Isotope compositions are in δ notations as permil deviations from the V-PDB (Vienna Pee Dee Belemnite) carbonate standard. Reproducibility of $\delta^{18}O$ and $\delta^{13}C$ values is better than ±0.2 ‰.

Major, trace and rare earth elements were measured by ICP-AES and ICP-MS by a commercial analytical laboratory.

For the fluid inclusion studies, 100-μm-thick, doubly polished thin sections were prepared. Microthermometry was done on a Linkam FTIR 600 heating-freezing stage at the Department of Mineralogy, Eötvös L. University. Standardisation has been carried out on -56.6, 0 and 385°C temperatures using quartz wafers containing synthetic H_2O and H_2O–CO_2 fluid inclusions. Accuracy of the measurements during freezing experiments and heating up to 150°C was 0.1°C.

Bulk composition of petroleum-bearing inclusions was determined by gas chromatography (GC) at the Department of Analytical Chemistry, Eötvös L. University. GC was done by the Agilent 6890N GC 5973 MS using the HP5-MS column. The process of sample preparation is the following: few grams of the pulverised mineral was submerged in hexane (C_6H_{14}) and put into an ultrasonic bath, so organic compounds from the decrepitated fluid inclusions could dissolve as much as it is possible. The light fraction of the hydrocarbons (<C10) was not detected because it was lost by evaporation during sample preparation.

Raman analysis was done on doubly polished mineral chips at the Budapest University of Technology and Economics, Hungary. Inclusions were analysed using a Jobin Yvon confocal Labram Raman instrument with 532 nm Nd-YAG laser excitation beam, 20 mW laser energy and 50X objective.

UV epifluorescence was acquired on a Nikon Eclipse microscope equipped with 40X and 60X oil immersion objectives and using Hg light illuminator. The block filter (UV-1A) allowed selection of incident radiation at 365 ± 10 nm, and fluorescence was collected above 400 nm. Photomicrographs were recorded using a numerical camera at G2R laboratory (Nancy Université, France).

Fourier transform-infrared (FT-IR) analysis was done at LEM laboratory (Nancy Université, France). A Bruker IFS 55 Fourier transform spectrometer, coupled with a Bruker microscope, collects the infrared beam with cassegrain objectives (15X). Analysis of petroleum inclusions in thin (i.e. less than 300 μm) doubly polished sections was done by transmission, using a circular diaphragm with a variable diameter aperture (<8 μm), adjusted to the size of the inclusions. Spectral resolution is 4 cm^{-1}, and integration time is longer than 2 min and increases as the inclusion size decreases. Spectra were plotted in absorbance units in the mid-infrared range. A reference spectrum was recorded on the host mineral near the inclusion and subtracted from the inclusion spectrum. Contributions of calcite were removed

from the inclusion spectrum when calcite peaks were not oversaturated. The analytical limit was around 1,800 cm^{-1} due to the IR absorption by the host mineral. Spectra of atmospheric CO_2 and H_2O vapours were also subtracted.

Confocal Scanning Laser Microscopy (CSLM) has been applied to petroleum inclusions to record fluorescence images. This is a high resolution imaging technique with an x–y resolution near 0.1 µm and a z resolution near 0.3 µm. CSLM images acquisition has been made on a Biorad Rainbow system adapted to a Nikon inverted microscope at G2R laboratory (Nancy Université, France). A blue diode at 405 nm has been chosen to generate the incident radiation. The fluorescence is collected at wavelengths higher than 420 nm to produce the x-y fluorescence image of 512x512 pixels. The objective (60X, oil immersion) moves along the z-axis in order to obtain a series of x–y 8 bit images. The Igor software (©Wavemetrics) and the ImageJ free software are then applied to threshold the images, reconstruct the voxels and then to calculate the volume of the fluorescent liquid oil inside the inclusion. The volume of the gas bubble is approximated to a sphere, and its diameter is measured from the CSLM image recorded by transmission. The gas percentage at room conditions is calculated.

Modelling of petroleum inclusions is based on Peng-Robinson equation of state. It requires T_h and gas vol% as input data. PIT software (Petroleum Inclusion Thermodynamics) produces a P–T diagram with isopleth and isochores and gives a composition estimate with physical properties of the oil (API gravity, GOR; Thiéry et al. 2000, 2002). It uses both (1) the homogenization temperatures (T_h) measured by microthermometry, and (2) the gas bubble filling degree (Fv) measured by CSLM. It is associated with a two-parameter (α,β) compositional model that describes the wide range of compositions of natural hydrocarbon fluids.

Computer tomographic measurements were carried out in the laboratory of the ENI-E&P Division. For the acquisition of X-Ray tomographic images a fourth-generation medical scanner PICKER PQS with a voxel resolution of about 0.5 x 0.5 x 1 mm was used. The details of the used X-ray CT scanner are listed in the Table 1.

Energy Range	80-140 KV 30-200 mA
Resolution	0,5 x 0,5 mm
Slice Thickness	1-10 mm
Acquisition Time	1-4 sec
Maximum Sample Size	Length:1000 mm Diameter: 165 mm

Table 1: details of the X-ray CT scanner

The CT X-Ray tomography is a non destructive imaging technique that improves the petrophysical characterization of the rocks, particularly in presence of complex porous geometry, allowing a 3D reconstruction of the pore space. So X-ray CT can distinguish between all structures which have a density contrast. The images can be printed on a grey or colour scale, along with a window chosen for the display which corresponds to the interval of the selected density range. While the grey shades immediately display the structures present, the colour scale can provide more information on the details present. It is therefore possible to associate a density value to each colour, or each shade of grey and this value is inversely proportional to porosity.

IV/3 Results

IV/3.1 Field observations

Calcite-barite-sulphide veins, often with brecciated and cemented zones on both sides (Fig. 30a), hosted by Mesozoic-Tertiary sedimentary rocks are common in the Buda Hills. These veins have been recognized and studied at thirteen localities (Fig. 2) in several host rocks of various lithologies and ages, i.e. Triassic dolomites and limestones, Eocene limestones and marls and also Oligocene sandstones. The mineral association varies by host rock types, e.g. calcite forms wide veins in carbonates (Fig. 30b) and hardly occurs in sandstone. Apart from the sandstones, the only omnipresent phase of the paragenesis is calcite. Since I detected changes in the vein-filling paragenesis by host rock types, the field observations are also described according to their different host rocks.

Vein-filling paragenesis hosted by the Triassic (Ladinian–lower Carnian) Budaörs Dolomite Formation

Abundant calcite veins hosted by the Budaörs Dolomite are exposed mainly in the southern part of the Buda Hills at Odvas Hill and at Törökugrató quarry (Fig. 2). The bulk of these hills is made up by the Budaörs Dolomite partly covered by Eocene sediments.

At Odvas Hill, the dolomite is of mosaic breccia texture and more intense brecciation occurs along single fractures and fracture zones. Calcite cementation occurs along these zones, resulting in prominent erosion-carved zones (Fig. 30d). There are also simple calcite veins without any breccia clasts. The strike of both the simple veins and the breccia veins is mainly NNW–SSE. The width of the calcite veins varies between 1 mm and few centimetres, whereas the breccia veins may reach several tens of centimetres in width. In the central part of the calcite veins, there is often some remaining open porosity. In this case the scalenohedral habit of the crystals can be observed. Crystal size is up to 1-2 cm. Barite and 'limonite' were also detected in minor amounts. Barite frequently occurs together with calcite as well, filling thin fractures where barite is the older phase. The white, rarely greenish-coloured barite is of bladed habit (Fig. 30c), of a few mm size.

At Törökugrató quarry, the Budaörs Dolomite and the Upper Eocene–Lower Oligocene Buda Marl are exposed. Both are crosscut by veins mainly filled with calcite. The thickness of the calcite veins may reach 50 cm. Calcite is coarse-crystalline and of scalenohedral habit (Fig. 30e). Small (<few mm), limpid hexahedrons of fluorite (Fig. 30f) were found in association with the scalenohedral calcite. Bladed barite similar to that of the Odvas Hill was found in the Triassic dolomite, precipitated prior to the calcite. In the central part of thick calcite veins, where there is still some remaining porosity, scalenohedra show usually corroded surface and are covered by a younger calcite of cauliflower-like morphology. The cauliflower phase probably precipitated on the walls of a former cave. Calcite veins show uniform NE-SW strike in this quarry.

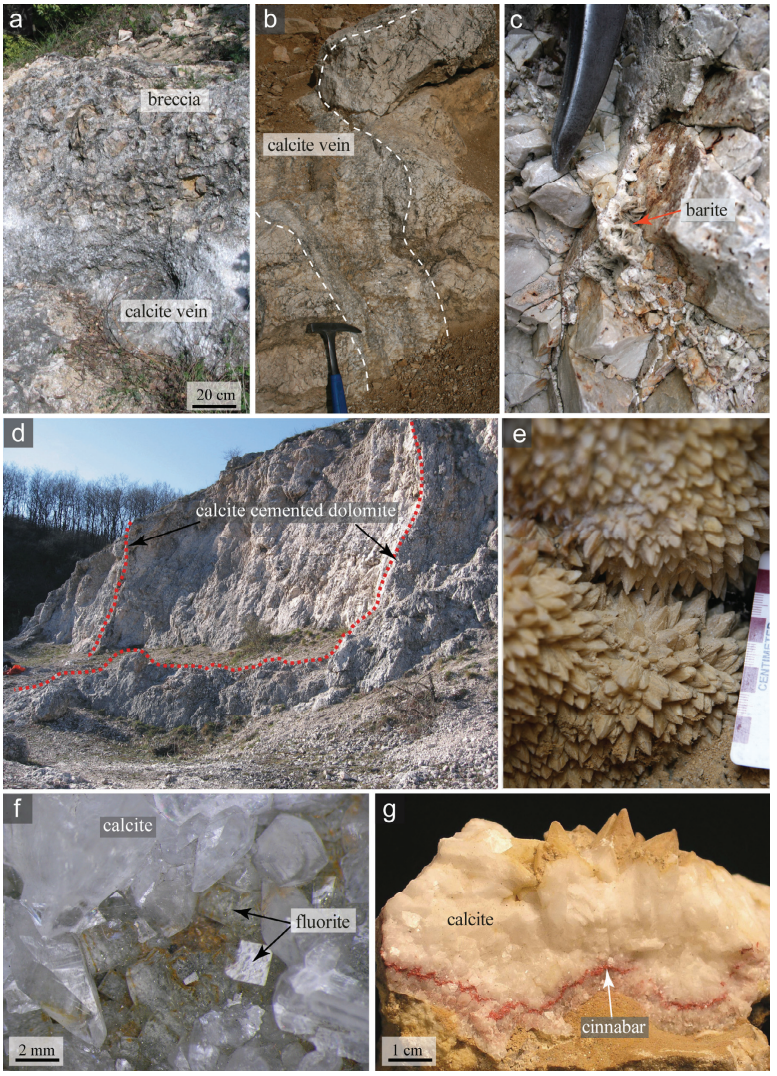

Fig. 30: (a) Calcite vein bordered by calcite-cemented breccia zones, Fenyőgyöngye quarry (b) Half-metre-wide calcite vein hosted by Triassic Dachstein Limestone, Róka Hill (c) Dolomite breccia cemented by bladed barite, Odvas Hill (d) Calcite-cemented breccia zones marked by red dotted lines in the fragmented Budaörs Dolomite, Odvas Hill quarry (e) Scalenohedral calcite at Törökugrató quarry (f) Limpid, euhedral fluorite crystals between calcite scalenohedra, Gellért Hill (g) Calcite with cinnabar from the Róka Hill

Vein-filling paragenesis hosted by the Triassic (Middle (?) Carnian–Norian) Hauptdolomit Formation

The Hauptdolomit is well exposed on Gellért Hill where it is partly covered by Eocene sediments. The hill is bordered by a normal-dextral fault of Pliocene age from the east along the riverside (Fodor et al. 1994). Dolomite is crosscut by calcite veins of a few centimetre width. Minor amounts of fluorite (Fig. 30f) and sulphide minerals (pyrite, marcasite) were also detected in those veins. Moreover, the overlying cherty sandstone is barite-cemented and silicified. The barite has tabular habit and yellowish colour.

Teve Cliff, exposed in an abandoned quarry, is located in the northeastern part of the Buda Hills at the southern foothills of the Kevély range (Fig. 2). Triassic Hauptdolomit is unconformably overlain here by Oligocene Hárshegy Sandstone. Some fractures, filled with barite and 'limonite', occur in the partly disintegrated dolomite. Barite crystals have simple orthorhombic-tabular morphology. These fractures can also be traced in the overlying sandstone which proves their post-Oligocene age. The orientation of the barite-limonite veins is highly variable.

Only a minor amount of calcite was found in the northwesternmost part of the Buda Hills (south of Piliscsaba; Fig. 2), cementing thin fractures of the dolomite between the fitted breccia clasts.

Vein-filling paragenesis hosted by the Triassic (Norian–Rhaetian) Dachstein Limestone Formation

In the Róka Hill quarry (Fig. 2), abundant calcite veins are exposed. They are hosted by the Triassic Dachstein Limestone and by the overlying basal Eocene siliciclastic sediments. In the Triassic limestone, there are some half-metre-wide calcite veins with calcite-cemented breccia zones on both sides. Calcite usually has scalenohedral habit. The orientation of veins is uniformly NNW–SSE. There is a 3-m-wide breccia zone which is bordered by a calcite-cemented fault, towards the Dachstein Limestone. This breccia is oligomictic and consists of clasts of Triassic dolomites and limestones and Eocene limestones and siliciclast fragments. In the breccia zone the cementing calcite is circumgranular. It occurs together with cinnabar, metacinnabar (Nagy and Pelikán 1976) and pyrite. The first phase of the vein-filling calcite is greyish and it is usually followed by milky-white calcite. In some cases, a cinnabar layer also occurs between these two calcite phases (Fig. 30g). Yellowish, tabular barite of 0.5–1 cm size is also present as a post-calcite precipitation.

In the Nagy-Hárs Hill quarry (Fig. 2), the Dachstein Limestone is unconformably overlain by Eocene (only in patches) and Oligocene sediments. The limestone is crosscut by a breccia zone and simple fractures and it is cemented by circumgranular calcite of elongate or scalenohedral habit.

Vein-filling paragenesis hosted by the Eocene–Lower Oligocene carbonates

There are several outcrops of Eocene limestones (Szépvölgy Limestone) and marls (Buda Marl) in the Hármashatár Hill Range (Fig. 2), which is bordered from the east by a normal-dextral fault of Miocene age, representing a part of the western boundary of the Solymár Trough, which is one of the major tectonic features of the Buda Hills (Fodor et al. 1994; Fig. 2). These veins are also exposed within the fracture related hypogenic caves (e.g. Szemlőhegy Cave, Ferenchegy Cave, Józsefhegy Cave). Fracture related caves of the Buda Hills are most commonly hosted by Eocene carbonates. This paragenesis was investigated in more detail in the Szemlőhegy Cave and in several outcrops on the surface within the Hármashatár Hill Range and also in the northern part of the Buda Hills at Lapos quarry (Fig. 2).

Almost identical parageneses and phenomena were observed at the following localities: Mátyás Hill, Pálvölgy, Fenyőgyöngye and Lapos quarries. In these localities, calcite fills up to half-metre-wide veins. Wide breccia zones were often found on both sides of the calcite veins.

Fractures are not always totally occluded by the calcite and the central part is often empty. In these particular cases calcite crystals usually have corroded surfaces. The habit of the calcite crystals is elongate scalenohedral in most cases but other morphological types (short scalenohedral, rombohedral and combination of the two) were also identified (Győri et al. 2011). The greatest morphological variability was observed in Lapos quarry where calcite cemented the brecciated marl. Calcite is accompanied here by tabular barite which is younger than the calcite. A limonitic phase, with few fresh sulphide grains (pyrite/marcasite), was usually observed as a phase preceding the precipitation of calcite (Fig. 31a). These veins exhibit peculiar green-stained patches in the Pálvölgy quarry related to the presence of minor amounts of native copper being oxidized on the actual surface (Lóránth 2000). Few mm wide faded ‘deferrification’-halos were also observed along single calcite veins hosted by reddish-coloured marl at Lapos quarry (Fig. 31b). Calcite-dominated veins uniformly show predominant NNW–SSE and subordinate N–S strike at all the studied localities.

Szemlőhegy Cave exposes a similar vein-filling paragenesis consisting predominantly of calcite. This cave also exposes stylolites filled with either black asphalt-like bitumen (Fig. 31c) or by rusty material. Calcite shows scalenohedral habit with the crystals grown in open space (Fig. 31d). The central part of the fractures is as a rule unfilled. Later corrosion and dissolution commonly occur along these veins, resulting in cavities along former calcite veins (Fig. 31e). Orientation of the veins, and also the orientation of the cave passages, is mainly NE–SW referring to the NE–SW striking right-lateral strike-slip fault (Benkovics et al. 1999). Subordinately, NW–SE striking veins are also present perpendicular to the main strike of the cave. Reactivation of fractures, later cemented by calcite, was also observed, though rarely. Barite veins were also detected following this latter direction. Fractures, alternately filled with calcite and barite, were also observed. Similar phenomenon also occurs in the Kis-Sváb Hill hosted by the Eocene marl. In most cases, the first precipitate is calcite of smaller crystal size followed by a yellowish-coloured barite of tabular habit and then a coarse sparry calcite (Fig. 31f). Simple barite veins are also present, consisting of large (up to 3 cm) yellow orthorhombic crystals.

At Út Hill (Fig. 2) the fractures of the Eocene marl are filled with small bladed barite crystals and a small amount of calcite.

Vein-filling paragenesis hosted by Oligocene sandstone in the northern part of the Buda Hills

Hydrothermal phenomena in the Oligocene Hárshegy Sandstone Formation were investigated in more detail by Gál et al. (2008). They detected minerals related to both the Paleogene and the Neogene hydrothermal systems, the former represented by chalcedony veins. Neogene mineralizing fluids apparently migrated along the NNW–SSE striking fractures. Together with them, significant amounts of barite of various habits (e.g. thin bladed habit, orthorhombic-tabular barite) occur. Small amount of calcite was also observed together with barite at the Ezüst Hill quarry, rarely.

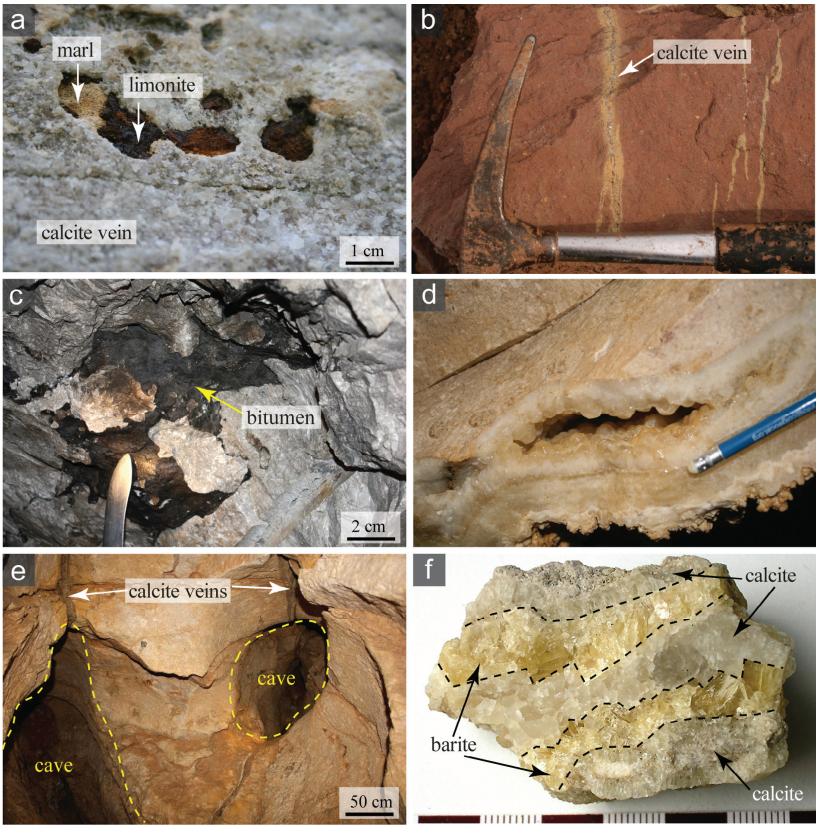

Fig. 31: (a) Limonite predating calcite, hosted by the Buda Marl at Mátyás Hill (b) Calcite veins with faded halo in reddish-coloured Buda Marl at Lapos quarry (c) Stylolite filled with asphalt-like bitumen in the Eocene limestone exposed in the Szemlőhegy Cave (d) Remaining porosity in the central part of a calcite vein in the Eocene limestone exposed in the Szemlőhegy Cave (e) Cave passages formed along fractures formerly filled with calcite, Szemlőhegy Cave (f) Fracture alternately filled with calcite and barite (Kis-Sváb Hill)

On the basis of the field observations, the following general paragenetic order was established in the case of the fracture-filling phases (Fig. 47):

'Limonite' was observed commonly hosted by Eocene carbonates in the central and northern part of the Buda Hills (e.g. Pálvölgy quarry, Lapos quarry). This phase is probably the oxidation product of a former iron sulphide (pyrite/marcasite). Native copper, described by Lóránth (2000), may be related to this first fracture-filling phase.

Barite-I: bladed habit, greenish barite which is mainly present in the Triassic Budaörs Dolomite (and in the Buda Marl) in the Budaörs Hills. Subordinately, barite-I was also found in the northernmost part of the Buda Hills hosted by the Oligocene Hárshegy sandstone. Both 'limonite' and barite-I predate calcite, however, the relative timing of these two phases is ambiguous since they do not occur together.

Fluorite: limpid hexahedrons in between calcite scalenohedra occurring mainly in the southern part of the Buda Hills (e.g. Törökugrató quarry, Gellért Hill).

Calcite: omnipresent phase in each locality and each rock types (excluding the sandstone). It gives the largest proportion of the fracture-filling phases. It usually has scalenohedral habit, however, various morphological types were also observed mainly when cementing in breccia zones.

Cinnabar, metacinnabar and pyrite found intergrown with calcite indicate coprecipitation of these phases. Cinnabar and metacinnabar were found only at Róka Hill.

Barite-II: tabular yellowish barite of various crystal sizes (from 0.5 cm up to 3 cm). This phase occurs mainly in the central and northern part of the Buda Hills, most commonly overgrown on calcite, hosted by Eocene carbonates. Alternation of calcite and barite-II was also observed in a few cases (e.g. Kis-Sváb Hill).

To sum up, at most localities, the strike of extensional fractures filled with the above minerals is predominantly NNW–SSE and subordinately N–S (Fig. 32). However, mineralized veins of clearly different strike were also observed in the case of Törökugrató and at Szemlőhegy Cave (Fig. 32).

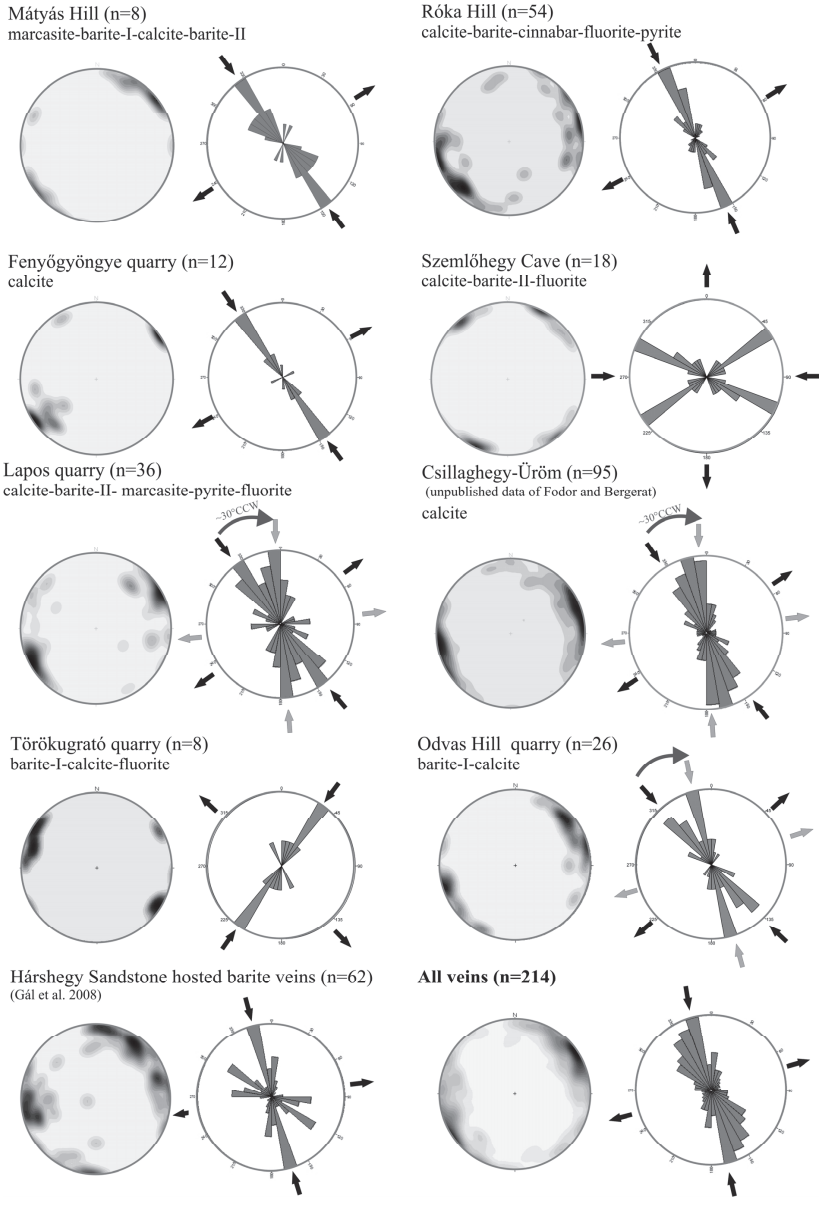

Fig. 32: Orientation of fractures cemented by different minerals illustrated by rose diagram and pole density plot (lower hemisphere projection)

Porosity distribution around caves and veins

It was commonly observed in the case of Szépvölgy Limestone-hosted, fracture related caves and also at Fenyőgyöngye quarry, that cavities are surrounded by a zone of enhanced matrix porosity. At Szemlőhegy Cave, porous zones were observed even in cases where remnants of fracture-filling calcite were still present. The surface of these fracture-filling calcite crystals was significantly corroded. It is important to mention that in the case of those calcite veins which are not associated with subsequent caves, the contact of the veins and the host rock is always sharp and no similar zones of enhanced porosity could be observed along them.

In order to establish the extension of the enhanced-porosity zone, samples were retrieved by diamond coring from the wall of the Szemlőhegy Cave. The borehole was drilled perpendicular to the wall and sub-parallel to the bedding of the host limestone. Remnants of an older calcite vein parallel to the cave wall were still observable as patches on the wall (Fig. 33). The drill core was ~70 cm long and of 2.5 cm in diameter.

Macroscopical observation of the drill core samples showed that there was an obvious gradual porosity increase towards the cave wall (Fig. 34). The width of the zone of enhanced porosity is ~35 cm (from sample-01 to 05). The first 10 cm (sample-01) of the drilling is the corroded calcite vein which discontinuously covers the wall. The coarse-crystalline fracture-filling calcite encloses a few breccia clasts of the host limestone. These clasts are usually porous or even totally dissolved resulting in abundant pore spaces of 2-3 mm up to 1cm in diameter within the calcite vein. Sample-02 is a very porous, white crumbling limestone. Minor amount of the above-mentioned coarse-crystalline calcite is still present in this sample. Sample-03 is also characterized by significant matrix porosity, however, it is much less porous than sample 2. No coarse-crystalline calcite was observed in sample-03. There is a colour change between sample-03 and 04 (i.e. white colour of the host rock turns into light brown) which may be the sign of a redox front. Moreover the porosity also decreases radically at this point. There are some ‘limonite’-coated micro-cracks in sample-04 and 05. From sample-06 towards the host rock the samples are all intact.

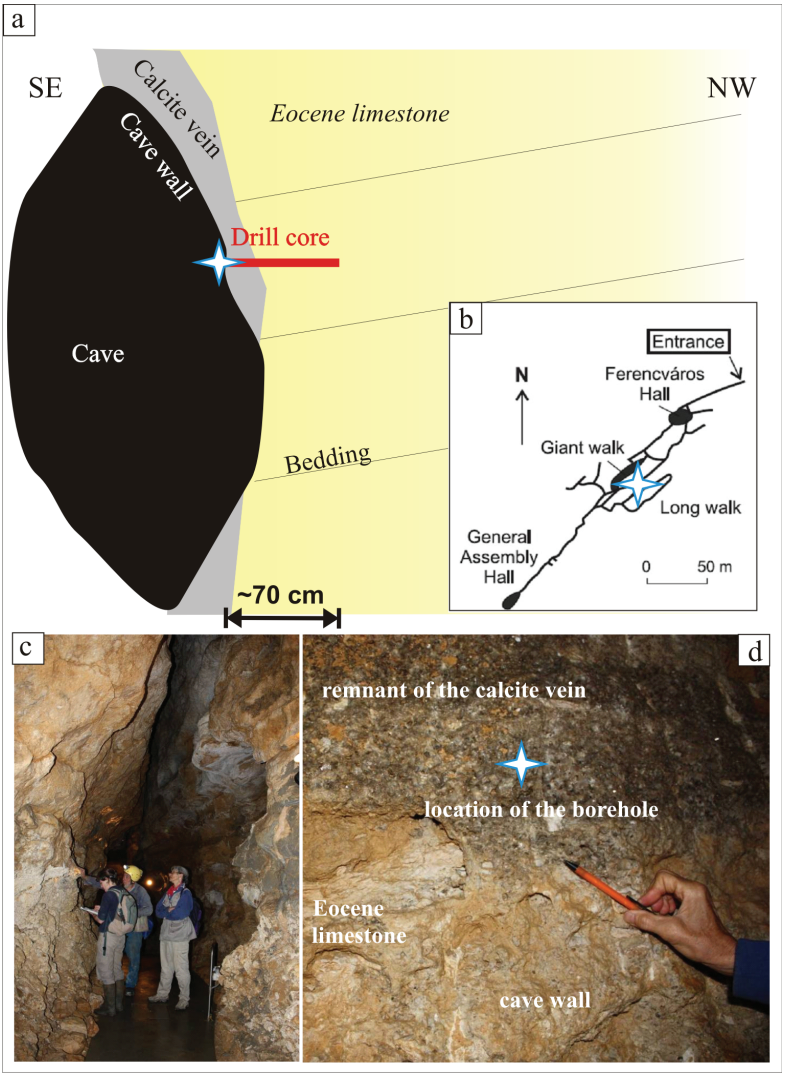

Fig. 33: Location of the borehole indicated on (a) a schematic section (vertically not to scale); (b) on a schematic map (Leél-Őssy and Surányi 2003 after Horváth 1965); (c) and (d) on photographs

The macroscopically-observed gradual porosity change from the cave wall towards the host rock was confirmed by computer tomographic (CT) measurements (Table 2). The following samples were suitable to be measured by CT: sample 01, 03, 04, 06. Only the porosity was determined in the selected samples because the size of the samples did not facilitate permeability measurements. The highest porosity was measured in the case of sample-03 and a radical decrease (from 23.7 down to 3.8 %) was detected towards the host rock (Table 10). It has to be noted that sample-01 representing the vein-calcite, which was taken from closest to the cave wall, is characterized by lower total porosity value than sample-03. Porosity of sample-06 (3.8 %) which is considered as an intact sample falls within the range of the average matrix porosity (3–5 %) of the Szépvölgy limestone (Kleb et al. 1993).

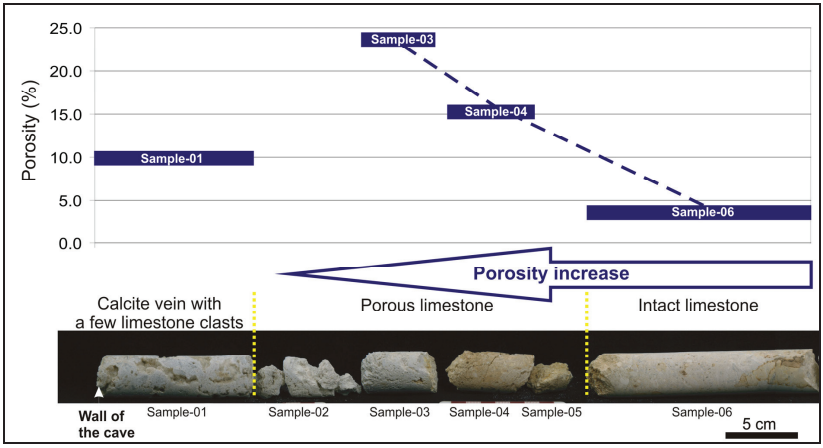

Fig. 34: Porosity values of the core samples

Sample	Porosity	Grain Density	Bulk Density
N.	%	g/cc	g/cc
1	**10.0**	2.657	2.391
3	**23.7**	2.639	2.014
4	**16.4**	2.650	2.214
6	**3.8**	2.646	2.545

Table 2: Result of the Computer Tomography measurements on the drill core samples

IV/3.2 Micropetrography

Fresh *marcasite* was detected along the margins of a calcite vein in the Lapos quarry. Scattered remnants of marcasite were detected in the 'limonite' phase, too, which implies that this phase was originally marcasite.

Bladed barite (*barite-I*) shows growth zoning under stereomicroscope: it has a cloudy, non-transparent central part and a clear rim. This zoning is due to the uneven distribution of abundant fluid inclusions.

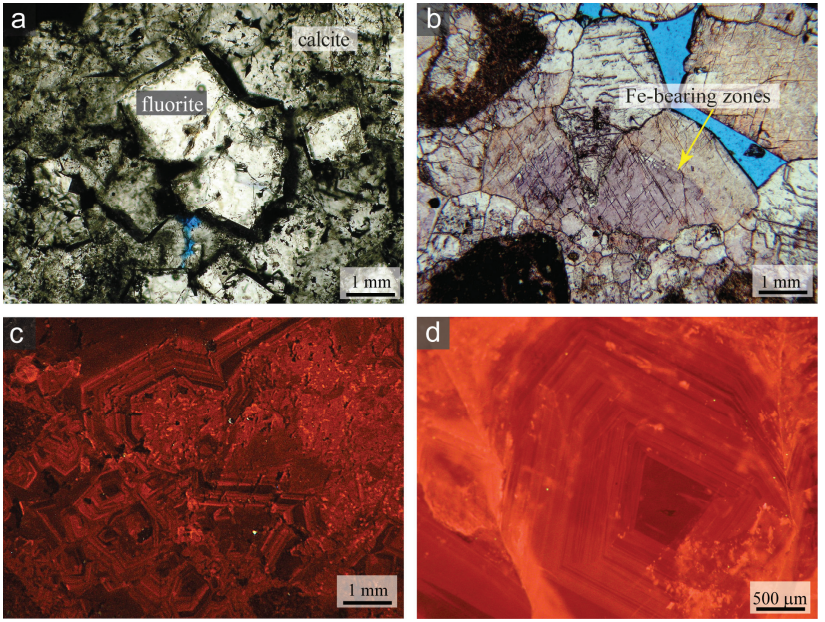

Fig. 35: Micropetrographic observations on vein-calcite (a) Euhedral fluorite crystals with calcite (sample Tug-08) (b) Iron-rich core and zones of breccia-cementing calcite, stained thin section (sample F-40) (a and b prepared with blue epoxy) (c) Cathodoluminescent zonation of vein-calcite (sample Ro-02) (d) Cathodoluminescent pattern of one single crystal of calcite vein (sample M-02)

Fluorite usually occurs together with calcite and commonly forms aggregates (Fig. 35a), consisting of small (~few mm) hexahedral crystals. Fluorite usually contains solid inclusions (supposedly calcite grains) along its growth zones in the outer part of the crystals. Euhedral fluorite was also found in calcite as solid inclusions, mainly along growth zones of calcite (Fig. 37e) or as scattered crystal aggregates (Fig. 36a). The presence of fluorite was confirmed by Raman spectroscopy (Fig. 36). Fluorite inclusions were commonly detected in calcite of several localities (e.g. Róka Hill, Szemlőhegy Cave, Lapos quarry); thus, fluorite is almost omnipresent within this paragenesis.

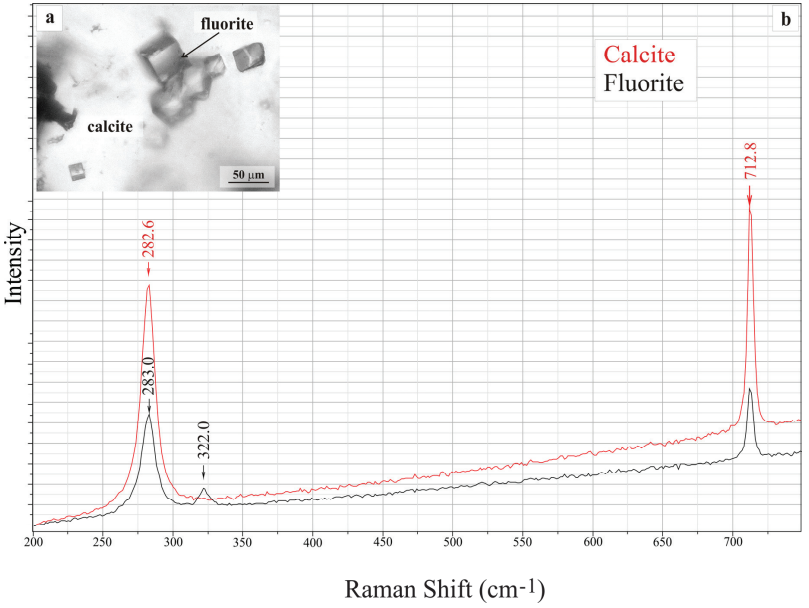

Fig. 36: (a) Fluorite enclosed by calcite (b) Raman spectra of fluorite and calcite (sample Ro-13)

Uniform characteristics were observed in the calcite from different localities: (1) thick 'spongy' growth zones characterized by abundant fluid inclusions and (2) abundant fluorite inclusions. Cathodoluminescent pattern is uniform as well, showing fine zoning by alternation of thin bright and dull-luminescent or non-luminescent zones (Fig. 35c, d). Subordinately, sector zoning (Fig. 37a) was also observed in calcite veins from Róka Hill quarry. Staining of thin sections revealed the elevated iron content in the core of the calcite crystals (Fig. 35b).

Fresh and partly oxidized euhedral *pyrite* grains in zones intergrown with calcite.

In addition to the morphological differences of the two barite phases, micropetrographical differences were also found: *barite-II* shows no zoning; it is uniformly clear and contains only minor amounts of mainly one-phase and rarely two-phase (liquid–vapour) fluid inclusions.

IV/3.3 Fluid inclusion study

Microthermometry was done on primary fluid inclusions of calcite from three different localities, i.e. Róka Hill, Lapos quarry and Fenyőgyöngye quarry. Primary fluid inclusions showed uniform characteristics in all studied samples. At Róka Hill, however, also abundant petroleum inclusions, coeval with aqueous inclusions, were found in the calcite samples. Therefore, detailed description is based on the observations of the samples from this latter locality. Petroleum inclusion-rich calcite samples were all taken from close to the boundary of the host rock (Triassic Dachstein Limestone) and vein (Fig. 30b). Petroleum inclusions also occurred, subordinately, in the central part of the veins. A number of primary, petroleum-bearing inclusions were also found in vein-calcite at the Fenyőgyöngye quarry (hosted by Eocene limestone) and in a quarry near Piliscsaba (hosted by Triassic dolomite).

IV/3.3.1 Fluid inclusion petrography

Based on micropetrography the following three types of primary inclusions were detected: (1) aqueous inclusions, (2) petroleum inclusions and (3) the mixture of the two: aqueous-petroleum-bearing inclusions.

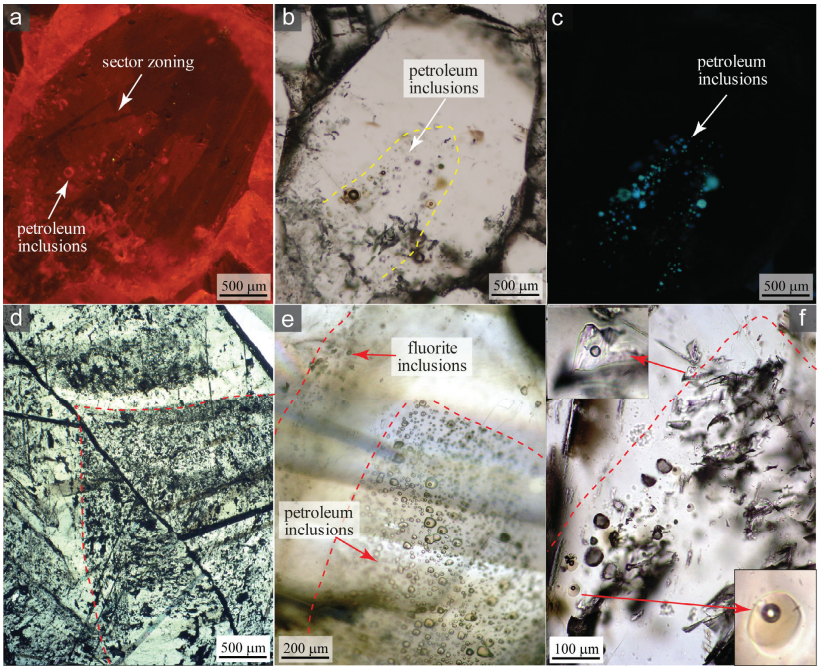

Fig. 37: Fluid inclusions in vein-calcite (sample Ro-13) (a) Sector zoning in calcite that contains petroleum inclusions; cathodoluminescent image (b) Petroleum inclusions along a growth zone of calcite; transmitted light (c) Same picture under UV light (a–c) Same calcite crystal (d) Spongy growth zones consisting of decrepitated and intact aqueous fluid inclusions in calcite (e) Abundant petroleum inclusions in the core of the calcite crystal and fluorite inclusions along the adjoining growth zone (f) Coeval, two-phase (L-V) aqueous and petroleum inclusions within the same growth zone

Aqueous inclusions

Aqueous inclusions commonly occur as thick 'spongy' growth zones (Fig. 37d) in which both intact and decrepitated inclusions can be found. Fluid inclusions generally consist of liquid and vapour phases with visually determined L:V ratios around 80:20. Rarely also some one-phase (L) inclusions occur. Shape of the inclusions is usually elongated. Subordinately also necking-down texture occurs. The outlines of all aqueous inclusions are irregular. The size of the inclusions varies between 10 and 50 µm.

Petroleum inclusions

Two-phase (Liquid HC + Vapour HC) inclusions occur either within the same growth zones with aqueous inclusions (Fig. 37f) or they form thick growth zones without aqueous inclusions. These growth zones are characterized by extraordinary abundance of the petroleum inclusions (Fig. 37e). The contours of petroleum inclusions are generally sharp but the wall of the inclusions is rarely crenulated. It was also observed that the contour of the inclusions is sharp on one side and crenulated on the other side (Fig. 38e). Although petroleum inclusions are commonly rounded, various morphologies were observed by using the CSLM. Fluorescence colour changes as a function of the size of the oil inclusion (Fig. 37c). The most common small (d = 10–20 μm) yellow-coloured inclusions show bright bluish-white fluorescence colour (Fig. 38a, b). Green and red fluorescence colours were also observed in larger dark brown inclusions (~50 μm) characterized by larger vapour phases (Fig. 38c, d). In addition, a non-fluorescent layer was detected between two fluorescent immiscible liquid petroleum phases within certain inclusions. Three-dimensional images, obtained by using CSLM, pointed out that these inclusions do not contain different immiscible liquid phases, only they look like to do so (Fig. 39). This phenomenon is due to the peculiar shape of the inclusions. Using CSLM, it is also possible to measure the L/V ratio. The volume of the vapour phase (Fv) was proved to be around 5 % in the case of the smaller inclusions where leakage is less likely.

Aqueous-petroleum-bearing inclusions

Subordinately, mixed-type inclusions were also found consisting of aqueous and petroleum phases within one and the same inclusion: Liquid HC + Vapour HC + Liquid H_2O ± Vapour H_2O. In this case the proportion of the aqueous and petroleum phases is widely variable. Mixed-type inclusions most commonly consist of a two-phase (L-V) oil-drop with a one-phase (L) 'water-tail' (Fig. 40a). Rarely mixed-type inclusions were observed containing two immiscible vapour phases. Moreover, it was also observed that the 'water-tail' already detached from the oil drop represented by an elongated one-phase inclusion located just near by a two-phase rounded oil-inclusion (Fig. 38f).

Secondary, generally one-phase and rarely two-phase aqueous inclusions were also observed along healed microfractures. They were not the target of investigation since the aim was to establish the physical and chemical properties of the fluid from which the calcite precipitated.

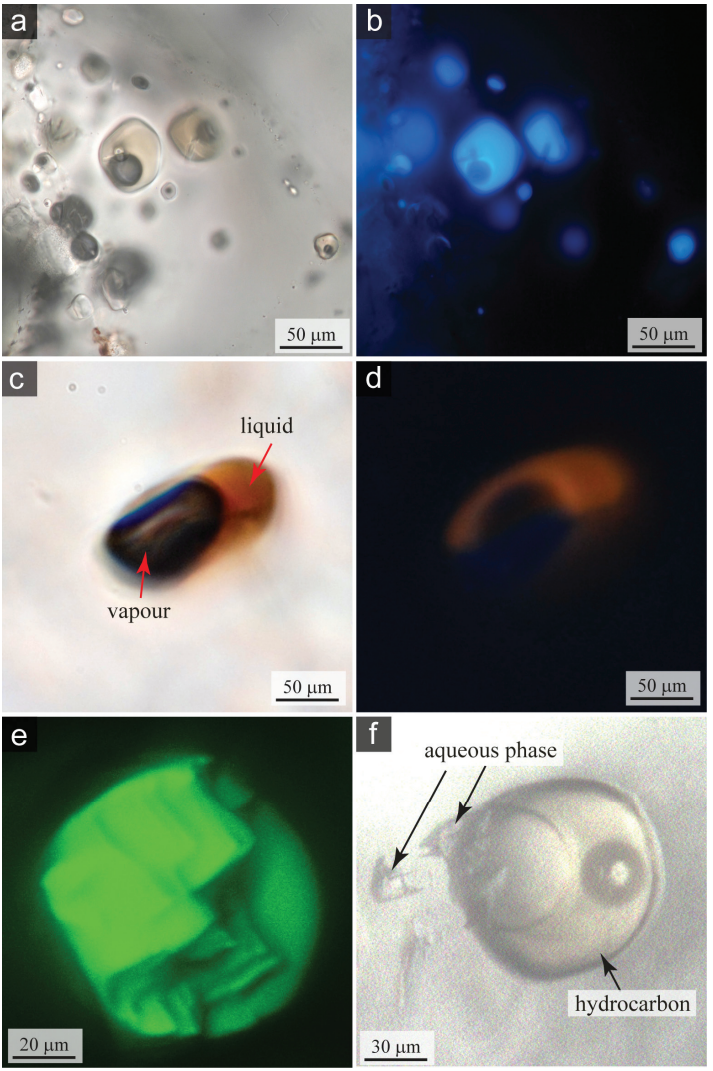

Fig. 38: Petroleum inclusions of vein-calcite: (a) Well-rounded petroleum inclusions in sample Ro-13; transmitted light (b) Same picture under UV light (c) Dark brown hydrocarbon-inclusion containing large vapour phase in sample Ro-02 (d) Same picture under UV light. Note the different fluorescent colour when compared with picture b (e) 3D image obtained by CSLM of a petroleum inclusion with well-rounded contour on one side and crenulated on the other side (f) Hydrocarbon-dominated fluid inclusion next to small, detached aqueous inclusions

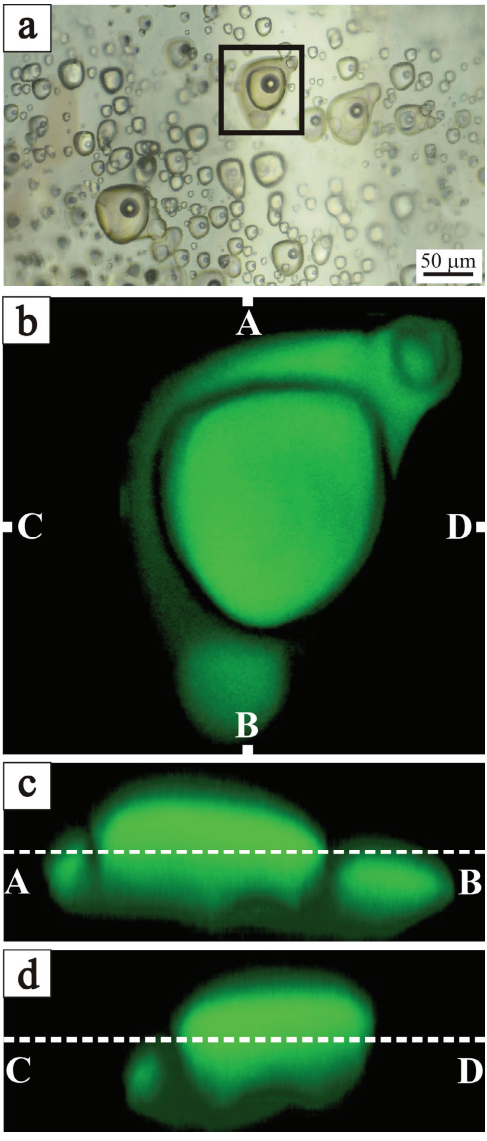

Fig. 39: Petroleum inclusions of peculiar shape. Note that they look like having more than two immiscible phases (a) Transmitted light (b–d) 3D images obtained by using CSLM from three different views

IV/3.3.2 Microthermometry

Microthermometry was done on the coexistent two-phase aqueous and petroleum inclusions. Both aqueous and petroleum inclusions homogenized into the liquid phase in each cases. While homogenization temperature is restricted to a narrow interval, between 78°C and 88°C, in the case of petroleum inclusions, those of the aqueous inclusions fall into a much wider interval from 80°C up to 114°C (Table 1). However, it has to be noted that these intervals overlap and show similar minimum values.

Final melting temperatures of ice were measured in the case of aqueous inclusions. Salinities calculated from the ice-melting temperature values vary between 0.4 and 0.9 NaCl eq. wt%, assuming H_2O–NaCl system, and there is only one outstanding value at 3 NaCl eq. wt%. Final melting temperature was higher than 0°C in two particular cases, probably due to the metastable melting of ice (Table 3). Eutectic temperature could not be detected of the aqueous inclusions in any cases; therefore, a NaCl-bearing fluid is assumed to be enclosed by calcite.

Microthermometry was also done on two-phase aqueous inclusions in calcite devoid of petroleum inclusions. Fluid inclusion petrography of these aqueous inclusions is similar to those accompanied by oil inclusions. Both homogenization temperature (T_h = 70–280°C) and salinity data (0–1.7 NaCl eq. wt%) overlap from the three different localities (Róka Hill, Lapos quarry, Fenyőgyöngye quarry). Nevertheless, there is one outstanding salinity value of 2.6 NaCl eq. wt% from the Róka Hill (Fig. 47).

Phases				
aqueous inclusions	**T_h (°C)**	**T_{melt} (°C)**	**Salinity (NaCl eq. wt%)**	**Remarks**
Liquid-Vapour	99.0			a
Liquid-Vapour	80.1			a
Liquid-Vapour		-0.3	0.5	b
Liquid-Vapour	86.0			a
Liquid-Vapour	92.0	-1.8	3.1	a
Liquid-Vapour		-0.5	0.9	b
Liquid-Vapour	114.0	+0.2		c
Liquid-Vapour	113.0	+0.5		c
Liquid-Vapour	94.0			a
Liquid-Vapour	85.0			a
Liquid-Vapour	85.0	-0.2	0.4	
Liquid-Vapour	85.0	-0.2	0.4	
Liquid-Vapour	93.0	-0.3	0.5	
Liquid-Vapour	87.0	-0.2	0.4	
	T_h (°C) min	**T_h (°C) max**	**T_h (°C) mean**	**Remarks**
aqueous inclusions	80.1	114	92.8	n=12
petroleum inclusions (L-V)	78.0	88.0	83.2	n=27

Table 3: Fluid inclusion data of primary coexistent aqueous and petroleum inclusions occurring in the calcite sample Ro-13. a: The vapour phase of the inclusions disappeared during homogenization and did not reappear during cooling down to room temperature, therefore the final melting temperature was not measured. b: Texture shows necking-down hence only the final melting temperature was measured in this case. c: No final melting temperature data obtained because of the metastable melting of ice above 0°C

IV/3.3.3 FT-IR analysis

FT-IR was used to determine the composition of individual hydrocarbon-bearing inclusions since this method is more efficient in the case of hydrocarbon-bearing inclusions than Raman spectroscopy because it is not affected by fluorescence (Pironon et al. 2000). FT-IR was used instead of Raman analysis also in the case of aqueous components of the inclusions because the host calcite was fluorescent, too. Liquid and vapour phases were measured separately, at room temperature, in the case of large (> 50 μm) petroleum inclusions. Three simple two-phase (L_{HC} + V_{HC}) hydrocarbon-bearing inclusions were investigated by FT-IR. No significant differences were detected in different inclusions. However, CO_2 content varies from 0 to 4 mole% and CH_4 from 3 to 15 mole% (Table 4).

Methane concentration is higher in the vapour phase, while CO_2 is rather associated with the liquid phase in dissolved form. CH_2/CH_3 ratio, calculated from the ratio of the peak areas of the $-CH_2$ and $-CH_3$ functional groups according to the method of Pironon and Barrès (1990), varies from 5 to 8.5 corresponding to equivalent nC_{12} to nC_{19}, respectively. None of the two-phase oil inclusions contain detectable amounts of water. One mixed-type oil inclusion with 'water-tail' was also measured by IR. Although the composition of the hydrocarbon phase shows great similarity with those of the simple two-phase oil inclusions, this inclusion contains large amounts of CO_2 (both in the vapour phase and dissolved in oil). Gas fractions, however, cannot be properly determined because of the saturation of the IR spectrum in the C–H stretching range due to the large size of the inclusion and the thickness of the host mineral (absorption of overtones of carbonate groups superimposed to –CH contributions). Furthermore, the aqueous phase (=water-tail) of this peculiar inclusion also contains CO_2 besides water (Fig. 40b). No high amount of methane was detected in this inclusion. Thus, the aqueous phase may represent the H_2O–NaCl ± CO_2 system. Therefore, the calculated salinity values represent the maximum salinity of the fluid because the invisible amount of CO_2 may reduce the final melting temperature by maximum 1.5°C (Hedenquist and Henley 1985). Thus, the outstanding salinity value (3 NaCl wt%) may be related to an inclusion containing CO_2 because the depression of the final melting temperature is just about 1.5°C higher as compared to the average value (-0.3°C) of all data (Table 3).

Sample	Inclusion	Measured phase	$[CH_4]$ mole%	$[CO_2]$ mole%	[Alk] mole%	CH_2/CH_3
Ro-13/2	1	vapour HC	30.0	0.0	70.0	8.6
Ro-13/2	1	liquid HC	13.8	0.3	85.9	6.4
Ro-13/2	1	liquid HC (margin of the FI)	16.4	0.1	83.5	4.9
Ro-13/2	2	bulk (L+V) HC	3.9	2.6	93.4	6.2
Ro-13/3	4	bulk (L+V) HC	15.4	4.0	80.5	6.0
Ro-13/3	4	vapour HC	22.8	3.1	74.1	5.6
Ro-13/3	4	liquid HC	13.5	4.0	82.6	6.2

Table 4: Composition of individual petroleum-bearing inclusions obtained by IR

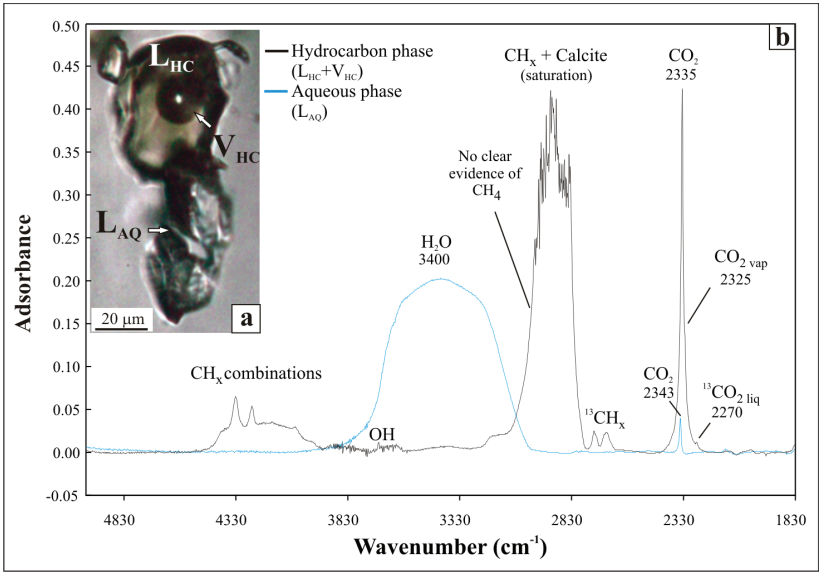

Fig. 40: (a) Mixed-type inclusion in the sample Ro-13/2 (inclusion No. 3) consisting of oil drop and 'water-tail' (b) IR spectrum of the above fluid inclusion

IV/3.3.4 Gas chromatography (GC)

Gas chromatography (GC) was used to establish the bulk composition of petroleum enclosed in the calcite. The most frequent normal alkane compounds are of carbon atomic number between 17 and 24. There is a hump, representing the unresolved complex mixtures, around C_{30} on the gas chromatogram (Fig. 48). Besides the normal alkanes, two isoprenoids were also identified, namely pristane and phytane, by their positions relative to nC_{17} and nC_{18}, respectively. Presence of these isoprenoids was confirmed by GC-MS (Fig. 41).

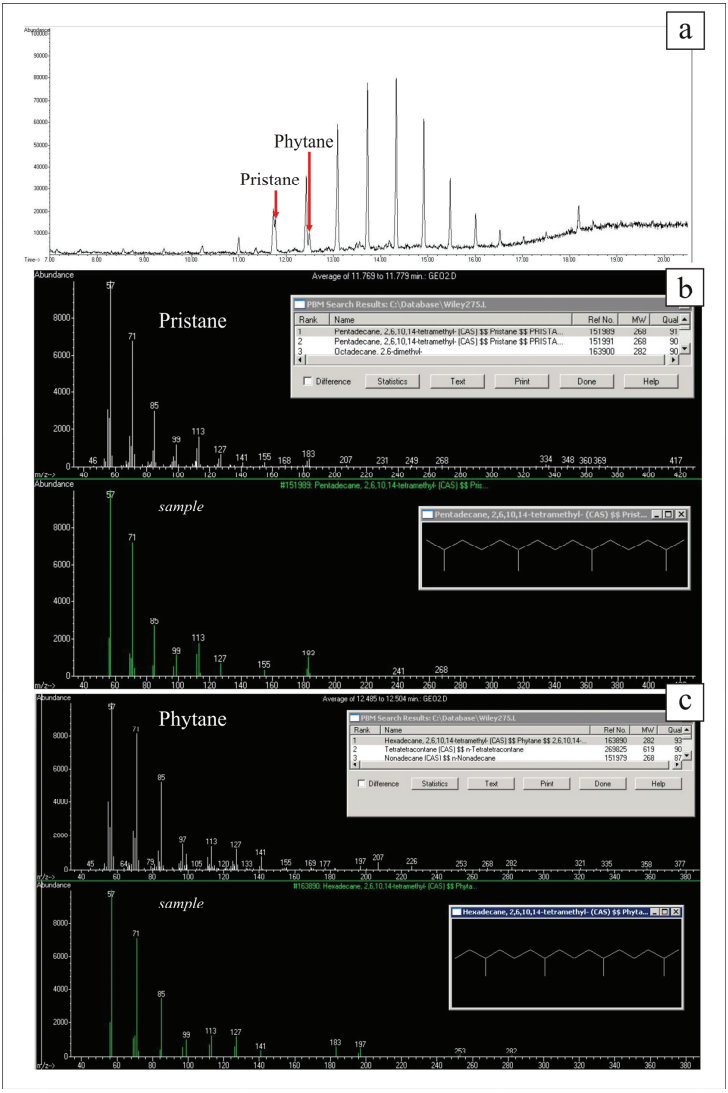

Fig. 41: (a) GC Total Ion Chromatogram of the oil enclosed by calcite (b) MS-spectrum of one component (Retention time: 11.77 min) compared to MS-spectrum of pristane (c) MS-spectrum of one component (Retention time: 12.5 min) compared to MS-spectrum of phytane

Using the PIT software, it is possible to calculate the composition of individual petroleum inclusions from the following input data: homogenization temperature and measured L/V ratio (Thiéry et al. 2000). The result of the calculation by PIT (Table 5) is in accordance with the bulk composition of the oil obtained by GC and corresponds to the range given by FT-IR. All methods pointed to the fact that the hydrocarbons, entrapped in the studied calcite, consist of mainly heavy hydrocarbon molecules. However, the highest frequency of hydrocarbon molecules in individual inclusions is present within the interval of nC_{11} to nC_{19} which is slightly lighter than the bulk composition determined by GC. This may be explained by supposing that when using the GC light fraction of the oil is underestimated the due to evaporation during sample preparation.

T_h	82°C
Fv	5.3%
Tfv	21°C
Alpha	0.93
Beta	0.32
Component	**Mole %**
CO_2	4.0
C_1	19.6
C_2	3.6
C_3	4.5
iC_4	1.2
nC_4	2.6
iC_5	1.9
nC_5	3.1
nC_6	4.5
nC_7	4.8
nC_8	4.6
nC_9	4.4
nC_{10}	4.1
Cn_1	25.6
Cn_2	11.6

Table 5: Composition of a representative petroleum inclusion (same inclusion on Fig. 39) calculated by PIT software using the homogenization temperature (Th) measured by microthermometry and the gas bubble filling degree (Fv) measured by CSLM

GC was also used to investigate the bitumen-like material found along stylolites. It revealed that the black material contains normal alkanes (e.g. dodecane) identified by GC-MS (Fig. 42).

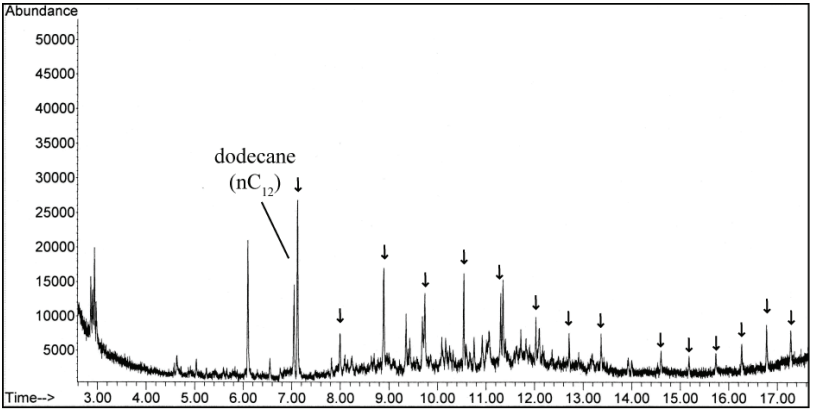

Fig. 42: Gas chromatogram of the asphalt-like bitumen found along a stylolite in the Szemlőhegy Cave. Normal alkanes are marked by arrows

IV/3.4 Geochemistry

IV/3.4.1 Carbon and oxygen isotopes of vein-calcite

Based on field observations, I hypothesised that calcite samples from different localities showing uniform characteristics were of the same origin. Stable oxygen and carbon isotopes were measured from vein-calcite from numerous localities and from different host rocks in order to confirm the above hypothesis.

Stable isotope values of calcite are well separated from those of the host rocks in each case (Fig. 43). Oxygen isotopes of vein-calcite fall into a wide interval (from -9.2 to -18.7% V-PDB) depleted as compared to the host rocks (from 1.3 to -9.8% V-PDB) (Appendix-Table 5). No significant differences in the interval of stable isotope values of different calcite veins could be detected. Ranges are broadly overlapping for different localities. There are only three data-points characterized by negative carbon isotope composition: in two of the three cases, however, significant dissolution was observed on the crystal surfaces.

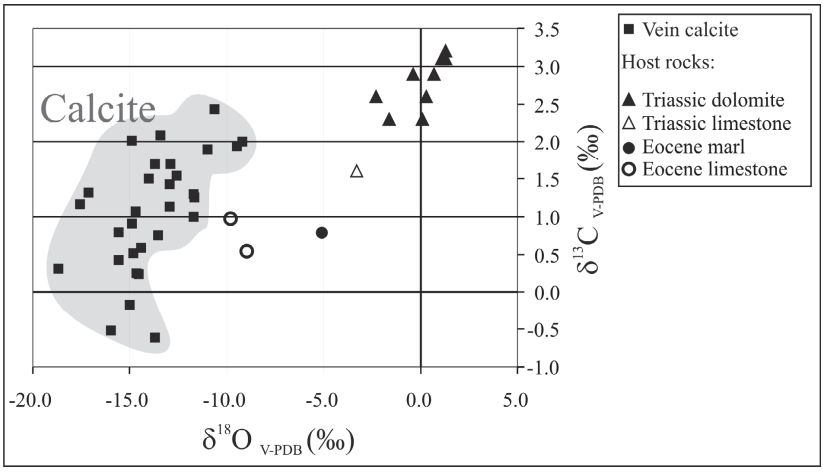

Fig. 43: Stable oxygen and carbon isotope values of calcite veins and of different types of host rocks

IV/3.4.2 Major and trace elements

Calcite

Both major and trace elements were measured from ten vein-calcite samples from seven different localities. Regarding the major elements, no remarkable differences were observed in those calcite samples. Fe_2O_3 content is ranging between 0.1 and 0.3%. Sr concentrations are more variable within the interval from 79.4 to 459 ppm (Appendix-Table 6). All calcite samples have the same flat rare earth element (REE) pattern, and all of them are depleted as compared to the REE concentrations of PAAS (Post-Archean Australian Shale). However, calcite samples containing hydrocarbon inclusions are characterized by the lowest REE concentration values. Most REE were even below detection limit in the case of the sample containing abundant petroleum inclusions (Fig. 44).

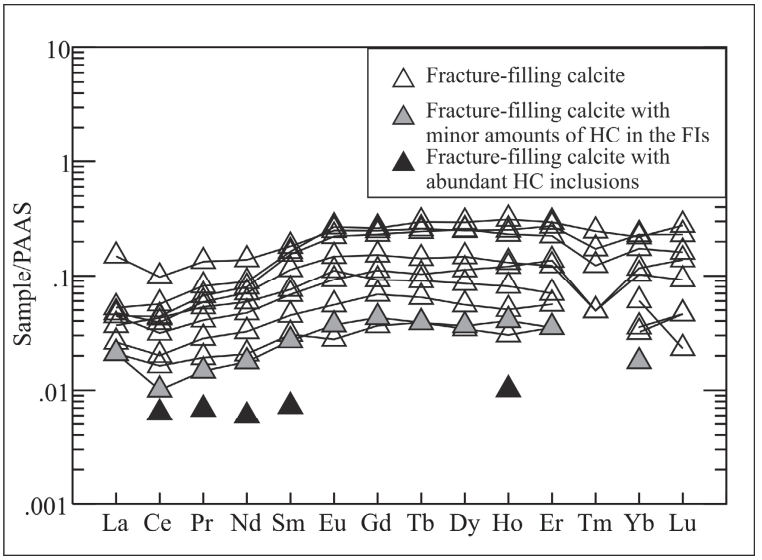

Fig. 44: REE pattern of different vein-calcites from different localities (normalised data for Post-Arch. Aust. Shale (PAAS) REE, Taylor and McLennan (1985)). Missing data points are below the detection limit

Barite

Trace elements, including REE were measured from both types of barite from three different localities in order to see whether the observed differences in crystal morphology are in relationship with the composition or not (Appendix-Table-6). No significant differences were measured in the case of barite-I and II. However, generally barite-I is characterized by slightly higher concentrations of most REE (except for light-REE from La to Nd) and other trace elements (e.g. Cu, Pb and Zn) as compared to the barite-II. No systematic differences were detected in the normalized REE pattern in different types of barite (Fig. 45). All the three samples are depleted in REE, only Eu shows slight enrichment as compared to the PAAS. All the three measured samples are characterized by very high Sr content, i.e. > 5820 ppm.

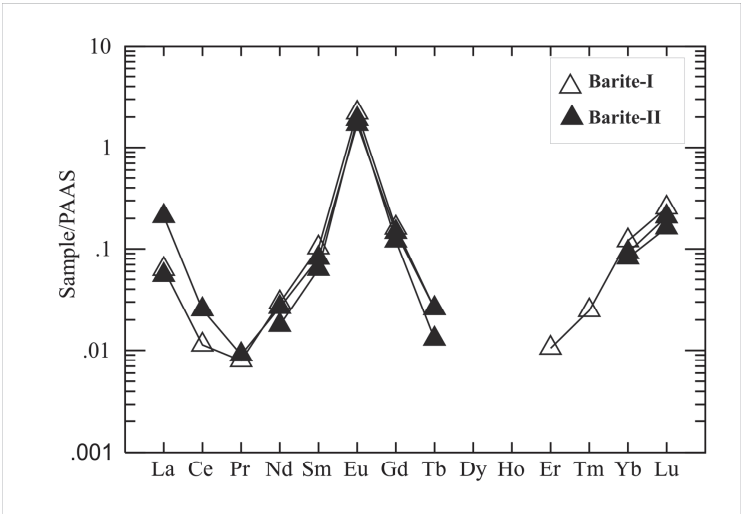

Fig. 45: REE pattern of different types of barite (normalised data for Post-Arch. Aust. Shale (PAAS) REE, Taylor-McLennan (1985)). Missing data points are below the detection limit

IV/4 Discussion

The studied calcite veins and the related parageneses detected at the different localities all belong to the same regional fluid migration event because the following properties of the omnipresent calcite were found to be identical at all localities:

1. Orientation of veins, supposedly extensional in origin, is predominantly NNW–SSE at most studied localities.

2. Appearance of the calcite crystals is also uniform (generally it has scalenohedral habit and milky colour interrupted by growth zones of greyish colour).

3. The vein-filling paragenesis shows great similarities at all localities. For example, calcite is usually accompanied by barite and fluorite. Nevertheless, minor changes of the paragenesis were detected according to the lithology of the host rocks.

4. Geochemical similarities − detected by several analytical methods, i.e. stable isotopes, fluid inclusions, trace elements, and cathodoluminescence − confirm the uniform origin of vein-filling minerals throughout the Buda Hills.

IV/4.1 Physical and chemical properties of mineralizing fluids and related hydrocarbons

Based on the stable isotope values, calcite must have precipitated at relatively high temperature because oxygen isotope values, which vary as a function of the temperature (Craig 1965), are always significantly depleted in vein-calcite samples. Major and trace element concentrations also suggest elevated temperature for the parent fluid. For example, Tullborg et al. (2008) suggest that high-temperature (~150°C) fracture-filling calcites are characterized by elevated Sr-contents (>100 ppm). Fracture-filling calcites from the Buda Hills (with 80–460 ppm Sr) fall within this range. Nevertheless, elevated Sr-content may also be explained by the source of fluids. If the source of this fluid was rich in Sr, more Sr would be incorporated in calcite. Based on the high Sr-content measured (>5820 ppm) in both barite-I and -II it seems that the source was, indeed, rich in Sr. The observed crystal morphological differences of barite-I and -II do not reflect compositional differences. Nevertheless, the question could be still raised whether the high-Sr calcite and the associated minerals are of hydrothermal origin in the sense that the fracture-filling phases precipitated under conditions considerably warmer than the surrounding host rocks at that time.

Fluid inclusion petrography of calcite suggests a heterogeneous parent fluid consisting of dilute water and an immiscible hydrocarbon phase and that both inhomogeneous and homogeneous entrapment occurred. Furthermore, the peculiar well-rounded shape of the oil inclusions occurring together with elongate aqueous inclusions suggests that petroleum and water may have been entrapped together and then they separated and the resulting two different inclusions consist of predominant water and petroleum, respectively. This process can be interpreted as a transcrystalline migration of the enclosed water by dissolution and later recrystallization of the wall of the inclusion triggered by the thermal gradient as it was first described by Lemmlein (1952) in the case of salt crystals. Intense thermal water migration along the veins that were not yet entirely cemented at that stage may have provided the sufficient thermal gradient in this case. While inclusions in salt crystals move towards the heat source, in this case I assume a migration to the opposite direction, namely from the middle part of the vein towards the host rock, because of the retrograde solubility of calcite. Nevertheless, it has to be noted that the separation of water and petroleum was not complete in each cases. The mixed-type inclusions with ‘water-tail’ (Fig. 40a) may represent an intermediate stage of this process. In the case of contemporaneous trapping of two immiscible fluids from a heterogeneous system, the homogenization temperature of the aqueous phase represents the trapping temperature for both fluids (Nedkvitne et al. 1993), so pressure correction must not be undertaken (Burruss 1981). Thus, the minimum value of the

homogenization temperatures of the aqueous inclusions (~80°C) has to be taken into account both for aqueous inclusions occurring together with petroleum inclusions and for those without. Because of the above described transcrystalline fluid migration, reflected by the asymmetric distribution and the wide range of the homogenization temperatures (Fig. 47), it is supposed that the volume of certain inclusions has changed after entrapment. The volume change of inclusions is a common phenomenon in fragile minerals, like calcite. In this particular case, it is possible to specify not only the trapping temperature but also the pressure during entrapment, using the PIT software (Thiéry et al. 2000, 2002). Thus, the temperature and pressure of the fluid at the time of entrapment could be estimated as 80°C and 85 bar, respectively (Fig. 46).

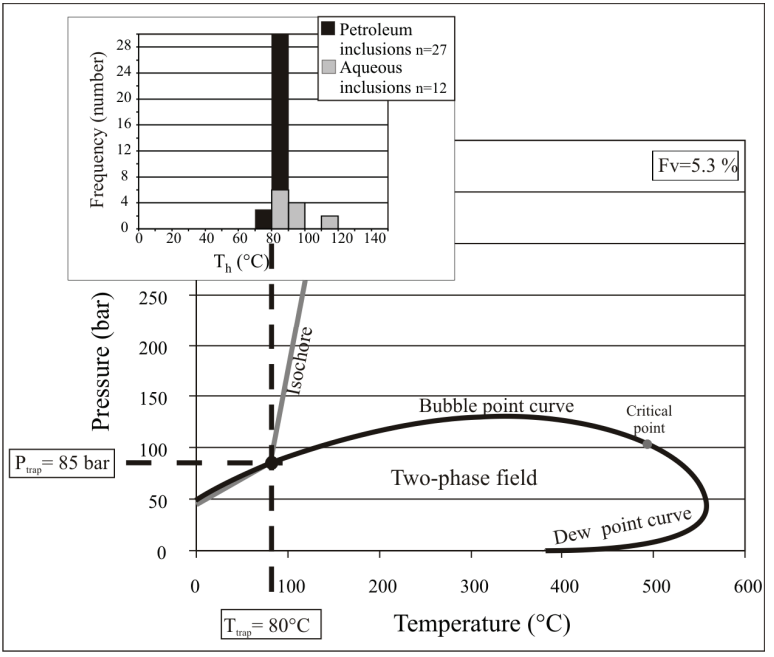

Fig. 46: Pressure and temperature conditions during entrapment of coeval aqueous and petroleum inclusions in calcite calculated by PIT software (Róka Hill, sample Ro-13)

Based on the pressure value obtained from the fluid inclusion study, it is possible to establish the thickness of sediments eroded from above the Upper Triassic limestone at Róka Hill from the latest Early Miocene on. Calculating with hydrostatic pressure conditions, the estimated 85 bar roughly corresponds to 850 m. Therefore, since the real pressure may be slightly higher than the hydrostatic pressure, it can be suggested that the thickness of the eroded sediments was ca. 800 m. The above calculated thickness is in accordance with the 850 m total thickness of the Eocene and Oligocene sediments, known from a borehole (Pm-1) in the Pest side (Alföldi et al. 1968; Fig. 49), where these sediments are not yet stripped by erosion. The mean annual surface temperature in Hungary is ~12°C, and the geothermal gradient measured in the surroundings of Budapest and believed to have been increasing with time from the Miocene on is ranging between 30 and 60°C/km (Dövényi et al. 1983; Dövényi and Horváth 1988). Thus, the maximum temperature of the fluid should have been only around 60°C at the given dept if it was heated only by the geothermal gradient (calculating with 60°C/km and 800 m depth). Since fluid inclusion data point to higher temperatures (80°C), an external heating agent or origin of fluids from the deeper part of the crust is required. Therefore, the fluid inclusion data can be considered as confirming the hydrothermal origin of calcite.

Based on the observed mineral paragenesis, the hydrothermal fluid certainly carried elevated concentrations of the following elements: Ca, Ba, F, S (both in oxidized and reduced form), Fe, Sr and very minor amounts of Hg and Cu. The source of Ca and CO_3^{2-} may have been both the groundwater stored in the carbonate rocks and the hydrothermal fluids. Moreover, hydrocarbons must have migrated together with the hydrothermal fluids based on the coexistence of water and petroleum in the studied fluid inclusions of calcite. CO_2 was detected in the aqueous phase trapped together with petroleum within one and the same inclusion. No other gas, not even methane, was detected by IR in the aqueous phase in spite of the fact that methane is the hydrocarbon most soluble in water (Guillaume et al. 2003). Therefore, in the case of contemporaneous trapping of petroleum and aqueous inclusions, methane saturation is assumed for the aqueous inclusions (Munz 2001). Even though oil always contains some water when they are trapped together (Pironon et al. 2000), I could not detect any water in the petroleum phase. Therefore, it is very likely that the water in the petroleum and the methane in the aqueous phase are present but remain below detection limit. Thus, the aqueous phase, enclosed by the calcite, may represent the H_2O–NaCl–CH_4 ± CO_2–system.

Fig. 47: Paragenetic order of fracture-filling minerals and the related fluid inclusion data. Fluid inclusion data of barite-II is from Gál et al. (2008)

Comparing the results of this study with the fluid inclusion data from barite-II (Gál et al. 2008), a change in the salinity of the hydrothermal fluid can be detected from the calcite towards barite-II (Fig. 47). Calcite is of 0–1.7 wt% salinity which slightly rises in the case of barite-II up to 0.9–2.9 wt%. The very low salinity of the inclusions in calcite may refer to significant karst water contribution to the mineralizing fluids. In the case of barite precipitation, the proportion of the mineralizing fluids (which are supposed to be more saline than the karst water) might have slightly increased at the expense of the karst water. It has to be emphasized that the very low salinity values suggest that these hydrothermal fluids are the mixture of large amounts of warm, regional karst water and small amounts of hydrocarbon-bearing fluids.

Hydrocarbons accompanying the hydrothermal fluids can be interpreted as black oil because of their yellow (rarely brown) colour in thin section and the high liquid/vapour ratio of individual inclusions at room temperature (Munz 2001). Homogenization temperature values (around 80°C), the relatively low CH_4-content (<30%) and the high CH_2/CH_3 ratio (~6) are also characteristic to black oils (Grimmer et al. 2003) and point to the presence of long hydrocarbon chains. The often observed, visually-determined bright bluish-white fluorescence of the petroleum inclusions is not in agreement with the previous statements since this colour is rather characteristic of relatively mature, volatile oils. Although the fluorescence colour of the oil is not only the function of the degree of maturity but it is also affected by the type and origin of source-rock and of course the choice of barrier filters used for fluorescence microscopy. In addition, fluorescence and API gravity variation may reflect maturity, indeed, but spectrometric colour determination is needed (Oxtoby 2002).

It has been already described that a mixture of petroleum and water provides for a reducing micro-environment in siliciclastic host rocks (Surdam et al. 1993). Therefore, it can be supposed that the studied hydrocarbon-bearing hydrothermal fluid was reducing supported by the following observations: (1) redox front along calcite veins (Fig. 31b) in the reddish marl (2) presence of sulphides besides the sulphate phases in the petroleum-bearing paragenesis. Petrographic observations showed that growth zones containing abundant petroleum inclusions exhibit the brightest cathodoluminescence. Moreover, sector zoning was also observed, showing brighter luminescence where hydrocarbon-bearing inclusions occurred (Fig. 37a). Recrystallization of calcite during the movement of aqueous inclusions may explain this luminescent pattern. Not only the CL pattern of calcites with hydrocarbon inclusions is different from that of the inclusion-free crystals, but there is a difference in the REE concentrations, as well. Those calcite samples, containing petroleum inclusions, are

more depleted in REE as compared to those calcite samples without any hydrocarbons (Fig. 44). This trend is in accordance with the strong sensitivity of the behaviour of REEs to the variation in redox state which might have changed significantly due to the presence of the hydrocarbons. Alternative explanation is that organic complexation of REE (e.g. Landström and Tullborg 1995) may have resulted in the depletion of REE in the aqueous phase of the fluid. REE could have been incorporated, however, into calcite in the immediate vicinity of the oil inclusions resulting in the observed more intense luminescence in such places. Thus, the calcite, being precipitated from the aqueous phase migrating together with oil drops, is characterized by overall lower REE content. Although I cannot give the precise explanation for this trend, it seems to be possible to predict whether the calcite likely contains petroleum-bearing inclusions or not, based on its REE content.

Physical and chemical properties of the hydrothermal fluids may have changed due to the fluid–rock interaction in different host rocks. For example, the absence of the otherwise omnipresent calcite and fluorite in the sandstone may be explained either by the changes in the pH of the fluid when entering the pore space of the sandstone or by the lack of the Ca-source.

IV/4.2 Source of the mineralizing fluids and the related hydrocarbons

To produce such an extensive hydrothermal mineralization, it demands a large volume of circulating fluids supposedly driven by the elevated heat flux. The question could be raised whether these fluids need a direct volcanic heat source—as it was previously supposed—or not. When accepting the idea of direct volcanic connections, the Visegrád Mts., the closest Neogene volcanic area, north to the Buda Hills, could be − and has been for long − considered as the fluid source. However, when I abandon the hypothesis of direct volcanic heat source, hydrocarbon indications may help to reconstruct the migration pathway by localising the source of the hydrocarbons. In this case there are two possible source rocks in the Buda Hills, namely the Upper Triassic bituminous limestone and dolomite called Mátyáshegy Formation (Vető 1999) and the Lower Oligocene Tard Clay (Csíky 1956).

Both possible source rocks were investigated with GC by previous authors (i.e. Brukner-Wein et al. 1990; Vető 1999; Hetényi et al. 2004). In the case of the Triassic source rock, there is always a prominent hump between C_{15} and C_{20} on the gas chromatogram (Vető 1999; Hetényi et al. 2004), while the extract of the Tard Clay has always a hump in the C_{27}–C_{32} interval (Brukner-Wein et al. 1990), even though this latter may be also present in the case of the Triassic carbonate. The gas chromatogram of my sample (bulk sample of the

petroleum inclusions enclosed in the calcite from Róka Hill) shows greater similarities with that of the Tard Clay compared to the other candidate based on the position of the hump occurring between the C_{27} and C_{32} intervals, confirmed by the lack of the hump between C_{15} and C_{20} characteristic to the Triassic rocks (Fig. 48). Moreover, the extremely low pristane/phytane ratio of the Triassic source significantly differs from that observed in my sample. Nevertheless, some differences do occur between the Oligocene rock and my sample, too, e.g. the normal alkane distribution: (1) the most frequent normal alkane fraction (nC_{27} to nC_{31}) of the Tard Clay extract is of very low concentration in my sample. (2) Tard Clay is characterized by odd-predominance which is not obvious in my case. The latter can be explained by the differences in the state of maturity since the odd-predominance is an immature character. The lack of high amounts of heavy normal alkanes in my petroleum inclusions may refer to the changes in composition of hydrocarbons while being transported by aqueous media. Therefore, I assume that Tard Clay is more likely to be the source rock in my case than the Triassic bituminous carbonate. Nevertheless, Tard Clay is immature in the whole area of the Buda Hills, based on vitrinite reflectance data (Ro = 0.3–0.5%; Korpás et al. 1993). In addition, Tard Clay is immature even at 600–700 depths below ground surface in borehole Ad-3 (Fig. 1b) southwest to Buda Hills (T_{max} < 430°C; Brukner-Wein et al. 1990). Therefore, hydrocarbons found as fluid inclusions in the Buda Hills must have been generated from the Tard Clay somewhere else, east to Buda Hills, e.g. under the Pest Plain (Fig. 49) where several known hydrocarbon accumulations have been reported (e.g. at borehole Gomba-6 where Tard Clay is known from more than 2,000 m depth). Therefore, it can be stated that the mineralizing fluids and thus also the associated elements, i.e. Ba, F, S, Fe, Sr, Hg, Cu and hydrocarbons with CO_2 all originated in the basin which borders the Buda Hills to the east. The supposed source of the Ca^{2+} and CO_3^{2-} to precipitate calcite may be the already mentioned karst water contribution. Therefore, it may be assumed that the vein-filling minerals precipitated from a mixture of two fluids, i.e. karst water and basinal water.

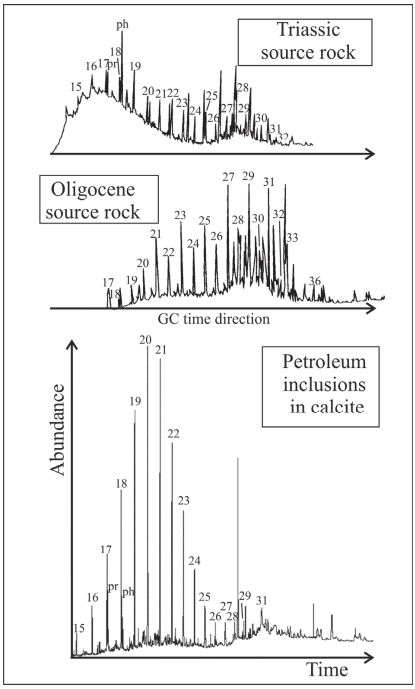

Fig. 48: Gas chromatograms of the extracts of the possible source rocks (Triassic exposed by borehole Zs-14– according to Vető (1999); Oligocene exposed by borehole Ad-3 – according to Brukner-Wein et al. (1990)) and of the bulk sample of the petroleum inclusions enclosed in calcite. Carbon atomic numbers of identified normal-alkanes are indicated. pr: pristane; ph: phytane

IV/4.3 Structural control of hydrocarbon-bearing basinal fluid migration

General strike of the above-described hydrothermal veins (NNW–SSE) is parallel to one of the major structural elements in the Buda Hills, the so-called Solymár Trough (Fig. 2) which is bordered by two normal fault zones formed in the Miocene–Pliocene, due to the predominantly extensional stress field (Fodor et al. 1994). Integrated paleomagnetic and structural studies in the TR revealed several counterclockwise rotation events during Tertiary times (Márton and Fodor 2003). Counterclockwise rotation of the TR resulted in clockwise rotation in the observed stress field. Thus, the strike of the extensional fractures gradually changed from ESE–WNW to NNE–SSW from the Early to Late Miocene (between 19 and 10 Ma; Fig. 5). This model thus permits to roughly estimate the age of the different sets of veins based on their strike directions. Based on the predominantly NNW–SSE strike of the studied

veins, the maximum age of the fracturing must be latest Early Miocene (17–16 Ma), so the age of the first phase of fracture-filling minerals is either coeval with or slightly younger than that. It is suggested that those veins that are characterized by clearly different strike (Törökugrató, Szemlőhegy Cave) are coeval with those ones showing NNW-SSE direction – based on great similarities e.g. in mineralogy – but they probably formed by reactivation of former fractures or were affected by local stress field variations.

Hydrocarbon indications are all related to these major Miocene–Pliocene faults, indicating that hydrocarbons, just as the hydrothermal fluids, must have migrated mainly along these very faults (Fig. 49a). In addition, the unconformity between Triassic and Eocene carbonates might have also acted as a migration pathway (Milota et al. 1995; Fig. 49b). Hydrocarbon indications in recent groundwater, detected by GC (Alföldi 1979), were found also along or near those faults where the Miocene hydrocarbon indications were found (Fig. 49a, b). This implies that basinal fluids, transporting also the hydrocarbons, must have been migrating upward and northwestward to the Buda Karst, using the same migration pathways from the Miocene up to the Holocene and even at present. Evidence for the basinal contribution to the karst system having been active also in post-Miocene times is the presence of barite and fluorite in Pleistocene travertines (Kovács-Pálffy and Földvári 2004) located along the same Miocene–Pliocene faults (Fig. 2). In addition, a less than ca. 1.5 million years old barite-calcite vein is exposed by the Molnár János Cave (Leél-Őssy 2004). Nevertheless, the driving force of the basinal contribution might have changed since the latest Early Miocene. Initially, in the Miocene, due to extension and general subsidence of the Pannonian Basin, a predominantly compaction-driven upward flow can be hypothesised, whereas from the Pliocene on, due to the inversion of the Pannonian Basin (Bada et al. 2007), compaction-driven flow must have been converted into a compressional flow (Tóth and Almási 2001).

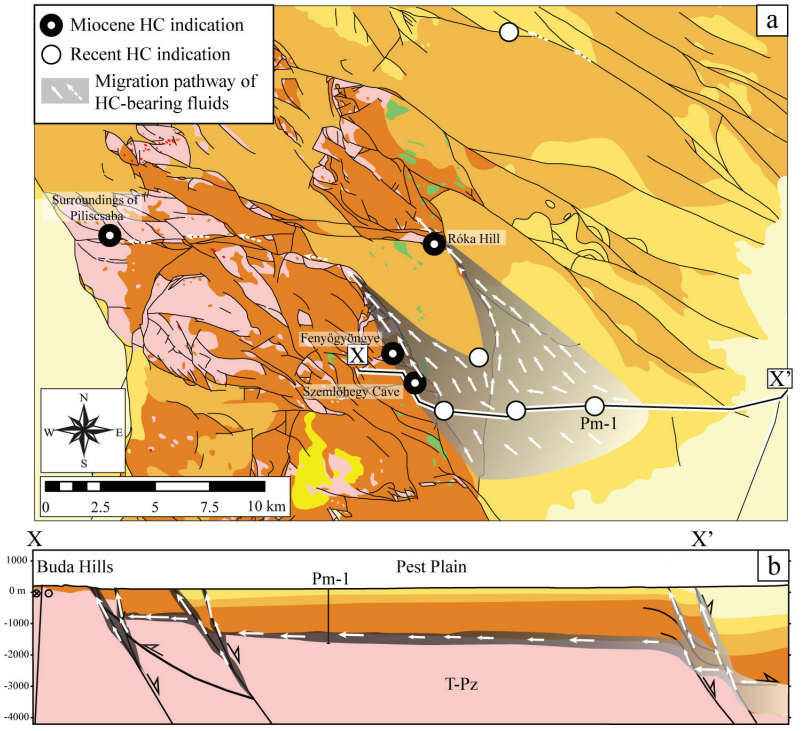

Fig. 49: (a) Miocene and recent HC indications and the reconstructed migration pathway of HC-bearing basinal fluids indicated on the map modified after Fodor (unpublished) (detail of Fig. 2). Miocene HC indications include both petroleum inclusions in calcite and stylolite filled by asphalt-like bitumen. Recent HC indications found in groundwater from wells according to Alföldi (1979) (b) Migration pathway indicated on the cross section modified after Fodor (unpublished). Legend is identical to that of Fig. 2 in the case of both (a) and (b) figures

IV/4.4 Hydrocarbon maturation

The source rock of the hydrocarbons is probably the Oligocene Tard Clay. Based on the established age of the petroleum inclusion bearing calcite veins, it is assumed that this source rock begun to generate hydrocarbons in latest Early–Middle Miocene times (~17–11 M years ago). This contradicts to previous estimates of some authors (e.g. Milota et al. 1995) who suggested that the earliest date when this source rock began to generate hydrocarbons was about 6 million years ago. Therefore, it is very likely that the hydrocarbons occurring as fluid

inclusions in the calcite were generated by forced maturation (sensu Davis and Smith 2006) due to the locally increased heat flux on the margins of the uplifted block of the Buda Hills where upward migration of hydrothermal basinal fluids has been continuous during the uplift. This explains that hydrocarbons were generated as early as the latest Early–Middle Miocene here. Heat transported by advection and conduction was reported to result in non-burial organic maturation by Anderson (1991). Undoubtedly, this forced maturation must have been followed by burial maturation in the subsiding basin, so recent hydrocarbon indications known from the wells represent hydrocarbons generated already during burial maturation. Accordingly, the elevated methane content of recent hydrocarbon indications points to the more advanced state of the maturity as compared to Miocene hydrocarbons.

IV/4.5 MVT characteristics of the studied vein-filling paragenesis

The paragenesis (i.e. barite, calcite, fluorite and associated sulphides), the geological setting (i.e. thick uplifted carbonate succession bordered by down-to-the-basin extensional faults), the source of the fluids (i.e. basinal fluid contribution to a karst system), and their genetic association with hydrocarbons can be interpreted as a Mississippi Valley-type (MVT) association since these are considered as the most evident MVT attributes (e.g. Anderson and Macqueen, 1982; Leach and Sangster, 1993). The heat source in this case is the elevated heat flow of the Pannonian Basin due to its attenuated lithosphere and there is no need to suppose direct volcanic connections. The vein-filling paragenesis consists mainly of carbonate and sulphate minerals and only minor amounts of sulphide indications were found. This observation is in accordance with the measured low-salinity of the hydrothermal fluids since low-salinity fluids are of low metal-transporting capacity. It may explain the lack of economy-grade ores associated with the Miocene Mississippi Valley-type fluid migration in the Buda Hills.

IV/4.6 Evolution of the karst system and the effect of the basinal contribution to the porosity

Close spatial relationship between the Miocene hydrothermal veins and the young caves suggests that the Miocene hydrothermal fluids were migrating along the same fractures as the younger cave-forming fluids. Since the observed gradual increase in porosity of core samples from the host rock towards the cave wall was the combined result of two fluid migration events, it would be important to distinguish these two processes. The first fluid migration event resulted in the precipitation of calcite in the original fracture. This must have

been an oversaturated fluid which was able to penetrate into the host rock within a distance of about 15 cm. This is shown by the distribution of the coarse crystalline, hydrothermal calcite in the drill core samples. The second solution, which used the same fluid migration pathways as the former oversaturated fluid, must have been undersaturated since it resulted in partial dissolution of both the vein-calcite and the host limestone. Fluid-rock interaction in this case can be traced in a wider, i.e. 35 cm thick zone, by the distribution of the resulted porosity increase. This means that the detected gradual porosity decrease beyond the 15th cm of the core towards the host rock is exclusively due to the second fluid migration event. Since the enhanced porosity zone was observed only around those calcite veins along which also the younger caves were formed it can be stated that only the second fluid was responsible for significant dissolution and formation of matrix porosity in the host rock. The second fluid may have used either the remaining porosity in the middle part of the veins and/or the original matrix porosity of the host carbonate. The measured low porosity value of the calcite vein (core sample No. 1) shows also that coarse crystalline calcite is less prone to dissolution than the micritic limestone.

Nevertheless, calcite precipitation and cave-formation cannot be considered as completely independent events and the effect of basinal fluids on the formation of hypogenic caves should also be discussed. Recalling the previous results of Alföldi (1979), in accordance with the results of Erőss (2010) it is suggested that the thermal component of the recent karst is a mixture of regional karst water and hydrocarbon-bearing basinal fluids similarly to the Miocene hydrothermal fluids. In both cases, together with the liquid hydrocarbons, aggressive gases (CO_2 and H_2S) may have been migrating up to the karst system possibly enhancing the dissolution of carbonates. Methane may also contribute to carbonate dissolution when it is oxidized to CO_2 and H_2O by reaching shallower depths of the aquifer (Forti et al. 2002). However, the proportion of the basinal fluids and also the amount of aggressive gases must have diminished with time in favour of karst water due to the accelerating uplift and erosion, as it was suggested already by Schréter (1912). Therefore, with time, mixing corrosion may have played more and more important role in dissolution and cave-formation as it was previously suggested also by numerous authors

Imprints of the superimposed hydrothermal and meteoric events on the carbonates of the Buda Hills were possible to recognize also by the different stable isotopic compositions of hydrothermal and meteoric precipitates. The ‘mixing-karst’ signal is very pronounced as shown by Figure No. 50, where oxygen and carbon stable isotope data from the Buda Hills are summarized. Stable isotopic composition of travertines, which precipitated as a result of

carbonate dissolution, reflects the mixing of these fluids, i.e. composition of travertines overlaps both with the hydrothermal and the meteoric fields and falls also in between the two fields as well (Fig. 50).

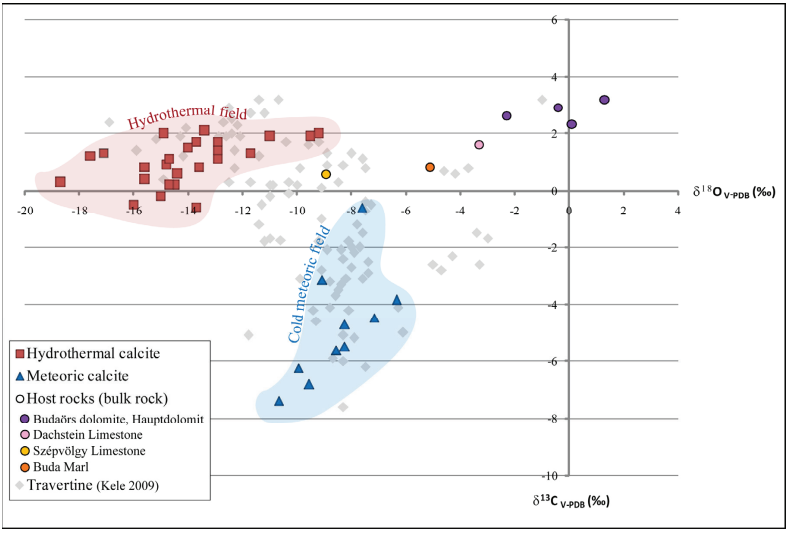

Fig. 50: $\delta^{18}O$ vs $\delta^{13}C$ values of the different calcite phases and carbonate host rocks (different colours refer to different host rocks) measured during this study, supplemented with the data of travertines (Kele 2009) of the Buda Hills. Data of meteoric calcite cements from Chapter III/3.4.1.

IV/5 Conclusions

Based on detailed mineralogical and fluid inclusion studies, the contribution of hydrocarbon-bearing basinal fluids was proved in the Buda Karst. This research revealed that from the Miocene on the fluids have been sourced in the siliciclastic sediment fill of the nearby basin, just like in the case of the actual groundwater system, as it was already suggested for recent thermal waters by Alföldi (1979).

Direct volcanic contribution to the hydrothermal fluids could not be confirmed. Instead, it is suggested that the elevated heat flux related to the attenuated lithosphere of the Pannonian Basin should be considered as the heat source of the hydrothermal fluids.

Migration pathways reconstructed for basinal fluids in Miocene times proved to be identical to those of the recent groundwater flow system. It is suggested that basinal contribution has been continuous from the Miocene on. Therefore, hydrothermal events

having resulted in the formation of the studied vein-filling minerals, travertines and hypogenic caves should be treated as different stages of the evolution of one single hydrothermal system.

Coexistence of aqueous and petroleum inclusions allowed to establish the thickness of sediments having been eroded since the latest Early Miocene (800 m) calculated from the entrapment pressure value (85 bar). These data confirm that basinal fluid circulation started under confined conditions as it was suggested by Kovács and Müller (1980). Entrapment temperature (80°C) was also determined and falls within the lower interval of those homogenization temperature ranges presented in several previous studies from the Buda Hills. It shows that fluid inclusions characterized by extremely high homogenization temperature values (up to 250°C) should be reconsidered and treated as stretched inclusions.

Extreme low salinity of the fluid inclusions (<1.7 NaCl eq. wt%) implies that basinal fluids were diluted by large amounts of regional karst water already in the basin side.

Detailed fluid inclusion studies revealed that significant amounts of CO_2 and minor CH_4 are associated with the black oil-type hydrocarbons migrating upwards from the basin dispersed in an aqueous medium. Unique shape of the petroleum inclusions reconstructed by using CSLM may be the result of separation of water from the inclusion after entrapment, a process known as transcrystalline fluid migration.

Geochemistry of the vein-filling calcite reflects the relatively high temperature origin of the basinal fluids by its significantly depleted oxygen isotopic composition (from −9.2 to −18.7%). REE concentration of calcite seems to reflect the variable amounts of hydrocarbons present in different samples since those calcites containing abundant petroleum inclusions are depleted in REE as compared to the hydrocarbon-free samples.

In the case of hypogenic caves a gradual decrease in porosity from the cave walls towards the host rock was observed and considered to be the result of interaction with fluids of basinal and karstic origin.

Chapter V – Implications for hydrocarbon exploration

Based on detailed study of the detected hydrocarbon indications, it is possible to delineate a hypothetical, actual petroleum system in the Buda Hills. Components of the petroleum system are as follows: source rock is probably the Oligocene Tard Clay; migration pathway is predominantly the Miocene-Pliocene extensional fault system and the regional pre-Mid-Eocene unconformity; potential reservoir: Eocene and Triassic carbonates characterized by cavernous and fracture porosity (Szépvölgy Limestone, Buda Marl, Dachstein Limestone, Hauptdolomit, Budaörs Dolomite); potential seals are the Oligocene clays (Tard Clay, Kiscell Clay); critical moment: Pliocene to recent uplift and erosion.

Even if it is assumed that there were significant amounts of hydrocarbons migrating upward from the basin, it is evident that hydrocarbons could not have been preserved in the Buda Hills because the appropriate seal was eroded. It is important to mention, however, that fluid inclusion study proved that the initial stage of hydrocarbon migration began under confined conditions. This means that the seal was not yet completely removed at that time. Nevertheless, it has to be kept in mind, too, that initially cavernous porosity of the studied carbonates was less significant. Groundwater circulation and thus dissolution became more and more pronounced as the system gradually changed from confined to unconfined due to the accelerating uplift and erosion. Thus, the same process was responsible for porosity increase and the removal of the seal. This change is reflected also by the simultaneous intensification of travertine formation. This usually happens when erosion opens the system and results in vigorous discharge from the confined aquifer (Klimchouk 2007). Thus, the conditions were appropriate for hydrocarbon accumulation in the Buda Hills, only for a very short period, sometimes in Pliocene to Pleistocene times, namely when the seal was still present and the porosity and permeability of the carbonates were already sufficient.

Despite the lack of commercial-grade hydrocarbon accumulations, the properties of carbonate rocks of the Buda Hills can be taken for surface analogues of reservoir rocks. When looking at the diagenetic history of these carbonate rocks, two major factors were identified which considerably improved the reservoir qualities: formation of the *hypogenic cave system* and the intense *powderization of Triassic dolomites.*

V/1 Hypogenic cave-system

Hypogenic caves, and also later collapse breccias, are considered to be potential hydrocarbon reservoirs in the literature; that is why it is important to understand the controls of their formation.

On the large scale (>km) to find analogous situations one may have to look for areas with the following characteristics:

1) Tectonic setting: margins of uplifted carbonate blocks within a former extensional basin

2) Geodynamic evolution: basin inversion

3) Indicator paragenesis: as shown by this study the presence of barite-fluorite-calcite-sulphide veins with petroleum inclusions can be taken for a strong indication for hydrocarbon-bearing basinal contribution in karst water flow systems.

On the small scale it is literally impossible to predict the position of large karstic cavities when we have borehole information only, because the observed gradual porosity-increase from the host carbonate towards cave passages affects only a very narrow zone (~0.5 meter). Even though this zone probably cannot be used as an efficient indicator of nearby open cavities, it provides some additional secondary pore volume which may be significant in the case of large-scale caves. Therefore the zone of elevated porosity surrounding the caves should be also considered when calculating the total pore volume of karstified carbonates. Interestingly, gradual porosity decrease is only present in the case of hypogenic caves while meteoric water-table caves are characterized by abrupt transition from host rock to cavity in the very same Eocene carbonates of the Buda Hills (Győri et al. 2011). Thus, the style of porosity distribution around caves might be used as a criterion to distinguishing between caves of different origins.

V/2 Powdered dolomite

Because of their inherent porosity, also powdered dolomites must be considered as potential reservoir-analogues. As outlined in the previous chapters, powderization of dolomite in the Buda Hills might be the result of a sub-recent, near-surface process, therefore including powdered dolomite bodies in the above theoretical ‘petroleum system’ of the Buda Hills seems to be difficult. However, in other more favourable situations powdered dolomites may, all the same, serve as reservoirs, e.g. as mentioned before, dolomite powder was found to host large amounts of heavy oil in the Canadian Grosmont Formation. Therefore it is worth to discuss the reservoir properties of powdered dolomites, too.

It is obvious that reservoir properties of powdered dolomite differ significantly from those of the parent dolomite rock. Since dolomite powder of the Buda Hills has formed at shallow depth the question arises whether it would be possible to preserve this porosity and permeability at all during burial. It is very likely that the porosity will be reduced dramatically during burial due to diagenesis (e.g. compaction and cementation). Therefore it can be stated that this type of dolomite powder may act as reservoir only in the case of hydrocarbon charge prior to significant porosity reduction. Nevertheless, the question still remains unanswered whether it is possible to bury a dolomite powder before erosion since its resistance against erosion and therefore its preservation potential are obviously very low.

It is suggested that the best candidates to be preserved even after burial are the 'concretionary geobodies'. This rock type exhibits apparently one of the best reservoir properties throughout the Buda Karst, however, it is important to mention that the volume of these 'mega-concretions' is insignificant compared to that of the powdered dolomite.

Chapter VI – Final conclusions

Superimposed hydrothermal and meteoric events and multiple subaerial exposure periods resulted in two major porosity-creating processes in the carbonates of the Buda Hills, i.e. 1) surface related powderization of Triassic dolomites 2) hypogenic cave formation in the Triassic and Paleogene carbonates.

Stages of porosity evolution

The oldest exposed carbonates, namely the Middle and Upper Triassic dolomites, were affected by both processes. Therefore, the stages of the porosity evolution of carbonates are summarized as follows, based on the paragenetic sequence established for the Triassic dolomites, according to the stages of Alpine tectogenesis (Fig. 51).

- Middle Triassic to Jurassic extension and subsidence: During this period pervasive dolomitization of platform carbonates resulted in replacive dolomitization (dolomite-I), followed by dolomite-cementation (dolomite-II).
- Cretaceous/Early Tertiary deformation (thrusting, strike-slip faulting, uplift and exposure): Time of the pre-Mid-Eocene subaerial exposure is characterized by intense tectonically controlled fracturing and thus creation of fracture porosity. Along fractures, brecciation and also minor powderization occurred (i.e. local powderization). Besides the formation of karstic cavities, which subsequently became filled by Eocene bauxite, karst related dedolomitization (red calcite) was also detected. Dedolomitization and calcite cementation of fractured and brecciated dolomite resulted in porosity destruction. Subsequent to the subaerial exposure period, during Late Eocene-Early Oligocene times, local quartz cementation of brecciated dolomite by Paleogene volcanism related fluids also resulted in minor porosity destruction.
- Neogene extension and subsidence: During latest Early Miocene, normal-faulting increased fracture porosity. However, it was immediately and almost completely destroyed by precipitation of calcite, barite, fluorite, and sulphide minerals due to compaction-driven upward migration of basinal fluids along the fractures. Besides the obvious porosity destruction by fracture-filling minerals, this process resulted in minor dissolution as well, due to the presence of hydrocarbon related aggressive gases (e.g. CO_2 and H_2S), transported upwards from the basin side along the remaining porosity of the mineralized fractures and also in the matrix porosity of the host carbonates.

Fig. 51: Diagram summarizing the detected diagenetic phases in the Triassic platform dolomites of the Buda Hills.

- Plio/Pleistocene inversion (uplift and exposure): Pliocene to recent inversion of the Pannonian Basin caused uplift and erosion of the Buda Hills. This led to increased mixing of hydrothermal and cold meteoric fluids and thus to the formation of the hypogenic cave-system. Therefore this process accounts for significant large-scale porosity creation. During the second major subaerial exposure period, due to the interaction of dolomite with meteoric fluids, a second dedolomitization event (white calcite) took place in the upper part of the meteoric phreatic realm. The most dramatic porosity change, namely the powderization of dolomite due to physical weathering, is a sub-recent process that resulted in creation of significant micro-porosity. Within the volumes of disintegrated dolomite 'mega-concretions' were formed locally, due to precipitation from descending meteoric waters.

Origins of the actual porosity of the studied formations

It can be stated, thus that the establishment of the actual porosity of the Buda Karst initiated in Miocene times. Detailed diagenetic studies revealed that the earlier history of the carbonates did not substantially affect the formation of the hypogenic cave system. In the case of powderization of dolomite, however, the diagenetic history of the rock influenced the degree and extent of disintegration. As opposed to previous studies, present study revealed, that powderization of dolomite is very likely a process independent from the Neogene hydrothermal system. It is rather the result of physical weathering as it was not accompanied by either chemical or mineralogical changes. Considering that the Buda Hills were close to the boundary of continuous permafrost during the maximum cooling of the last glaciation, one plausible explanation may be that dolomite disintegration was caused by the wedging effect of ice aided by the combination of thermal expansion and contraction during repeated freezing and thawing. Intercrystalline porosity of dolomite-II population may have played some role in enhancing the wedging effect of ice, while dedolomitization events, during both the first and the second subaerial periods, made the rock more resistant against later disintegration.

Porosity evolution of dolomites, and also of the Paleogene carbonates, was affected by interaction with both meteoric and hydrothermal fluids. Meteoric diagenesis occurred during both the pre-Mid-Eocene and the sub-recent/recent subaerial exposure periods. Since these unconformities often overlap in the Buda Hills, it is difficult to sort out the effects of the separate subaerial exposure periods. The effect of Paleogene volcanism related fluids had minor importance in the porosity evolution of carbonates while Neogene hydrothermal fluids have played important role since the Miocene on. Based on fluid inclusion data, Neogene hydrothermal fluids can be considered as the mixture of warm regional karst water and minor

amounts of hydrocarbon-bearing basinal fluids. This research first revealed the presence of hydrocarbon-bearing fluid inclusions in the Buda Hills. Hydrocarbon related gases may have played role in the initiation of dissolution of carbonates. Due to the accelerating uplift and erosion groundwater circulation has been intensified and colder meteoric fluids began to admix to the hydrothermal ones. With time the proportion of hydrothermal fluids gradually diminished in favour of cold meteoric fluids. It has to be emphasized that all the Neogene hydrothermal events, namely the formation of the calcite-barite veins, travertines and hypogenic caves should be treated as a continuum, i.e. as different stages of one and the same hydrothermal system.

As final conclusion, it can be stated that basinal contribution, even if represented by very small amounts, may have detectable imprints and effects on karst systems. In the case of the Buda Thermal Karst the following effects of basinal fluids were recognized:

1. Formation of a regional vein-filling paragenesis consisting of calcite, barite, fluorite and sulphide phases.

2. Elevated advective heat flow, along the margins of the basin possibly resulting in early forced maturation of organic-rich sediments. Hydrocarbon inclusions are pointing to maturation of Oligocene source rocks preceding overall burial related maturation in the basin.

3. Formation of hypogenic caves, not only due to the mixing of different fluids but also due to the dissolution-enhancing effect of aggressive gases (e.g. CO_2 and H_2S), transported upwards from the basin side.

A calcite-barite-fluorite paragenesis, containing hydrocarbon inclusions, associated with sulphides can be considered as a strong indication for basinal contribution in karst water flow systems. In addition, this study provides a clue to estimate the duration of similar flow systems: basinal contribution towards an uplifted block may be maintained for more than 10 M years.

Abstract

Porosity evolution of carbonates in the Buda Hills was the subject of this research. The aim was to provide an analogue for carbonate reservoirs that underwent multiphase diagenesis. Two major porosity types were recognized: 1) micro-porosity of powdered Triassic dolomites 2) cavernous and fracture porosity represented by the famous hypogenic cave system, hosted by Triassic and Paleogene carbonates.

Powderization of dolomite is a general phenomenon in the Buda Hills, where its areal extent is exceptionally large compared to similar occurrences elsewhere in the world. Geochemistry and mineralogy of the dolomite remained constant throughout the disintegration. Powderization is absent at places where the Triassic dolomites are partially calcitized as a result of karst related dedolomitization. Since powderization was controlled by surface related processes and no geochemical changes were associated with it, disintegration of dolomite is interpreted as the result of sub-recent physical weathering, supposedly related to frost action.

Hypogenic caves are found along older calcite-barite-fluorite-sulphide veins, pointing to the fact that young cave-forming fluids migrated along the same fractures as the older mineralizing fluids did. Predominantly NNW–SSE strike of fractures concludes a latest Early Miocene maximum age for the fracture-filling minerals. Vein-calcite contains coeval primary, HC-bearing- and aqueous inclusions indicating that also HCs have migrated together with the mineralizing fluids. The coexistence of aqueous and HC inclusions permitted to establish the entrapment temperature (80°C) and pressure (85 bar) of the fluid and thus also the thickness of sediments, having been eroded since latest Early Miocene times, was calculated (800 m). Low salinity of the fluids (<1.7 NaCl eq. wt%) implies that HC-bearing fluids were diluted by regional karst water. Fluid inclusion studies also revealed that aggressive gases (e.g. CO_2, H_2S) were associated with HCs and that these gases may have played a role in dissolution of the carbonates. Based on the location of the paleo- and recent HC indications, identical migration pathways were reconstructed for both systems. It was proved that HC-bearing fluids have migrated northwestward from the basin east to the Buda Hills from the Miocene on. Due to the uplift related intensification of groundwater circulation, the proportion of hydrothermal fluids has diminished in favour of cold meteoric fluids.

Establishment of the actual porosity of the Buda Karst initiated in Miocene times and earlier diagenetic history of the carbonates affected only the powderization of dolomite, and it had no direct effect on the localization of hypogenic caves.

Magyar nyelvű összefoglaló

Munkám során a Budai-hegység karbonátos képződményeinek porozitás fejlődését vizsgáltam. Két jelentős kiterjedésű, másodlagos porozitás-típus fordul elő a Budai Karsztban: 1) a porlódó triász dolomitok mikro-porozitása; 2) a hipogén barlangokhoz kötődő kavernás és repedéses porozitás, mely a triász és eocén karbonátokra jellemző.

1) A dolomit porlódása gyakori jelenség a Budai-hegységben és területi kiterjedése jelentősen meghaladja a világon ismert egyéb porló dolomit előfordulásokét. Az elvégzett vizsgálatok alapján kijelenthető, hogy a porlódás során a budai-hegységi dolomitok geokémiai és ásványtani összetétele változatlan maradt. Az is kiderült, hogy ahol a kőzet porlódása alárendelt, ott legtöbb esetben kalcittal van átitatva, mely a karsztosodáshoz kapcsolódó dedolomitosodás eredménye. Elterjedése alapján a porlódást egyértelműen felszíni folyamat okozta, amely a szub-recens, feltehetőleg fagyhatással összefüggő, fizikai mállás lehetett.

2) A budai-hegységi hipogén barlangok túlnyomó része korábbi kalcit-barit-fluorit-szulfid telérek mentén jött létre, mely arra utal, hogy a barlangképző fluidumok ugyanazon repedésrendszer mentén migrálhattak, mint a korábbi ásványkiválásért felelős oldatok. A döntően ÉÉNy-DDK-i csapású telérek iránya alapján az ásványkitöltő fázisok legkésőbbi kora-miocén korúak. A kalcitban talált elsődleges, szénhidrogén-tartalmú és vizes zárványok azt bizonyítják, hogy a kalcit anyaoldatával együtt szénhidrogének is migráltak. A csapdázódási hőmérséklet (80°C) és nyomás (85 bar) meghatározását a szénhidrogén-tartalmú és vizes zárványok együttes jelenléte tette lehetővé, amiből egyúttal a kora-miocén óta lepusztult üledékek vastagsága is kiszámítható volt (800 m). A fluidum kis sótartalma (<1.7 NaCl ekv. súly%) azt bizonyítja, hogy a szénhidrogén-tartalmú oldatokat jelentősen felhígította a regionális karsztvíz. A szénhidrogénekkel együtt 'agresszív' gázok (pl. CO_2, H_2S) is jelen voltak, melyek a befogadó kőzettel kölcsönhatásba lépve annak oldódásához vezethettek. A miocén korú illetve jelenleg észlelhető szénhidrogénnyomok elhelyezkedése alapján az alábbi áramlási útvonal rekonstruálható: a szénhidrogén-tartalmú oldatok a Budai-hegységtől keletre található medencéből migrálhattak ÉNY felé a miocéntől egészen máig. A kiemelkedésnek köszönhetően a kisebb hőmérsékletű meteorikus vizek fokozatosan túlsúlyba kerültek és a medence-eredetű fluidumok relatív mennyisége csökkent.

Megállapítható továbbá, hogy a Budai Karszt jelenlegi porozitásának kialakulását a miocén óta zajló folyamatok határozzák meg, és azt csak a dolomit porlódás esetében befolyásolták a karbonátok korábbi diagenetikus bélyegei.

References

Alföldi, L., 1979: Budapesti hévizek (Thermal waters of Budapest), VITUKI Közlemények, v. 20, 102 p. [in Hungarian]

Alföldi, L., Bélteky, L., Böcker, T., Horváth, J., Korim, K., Liebe, P., Rémi, R., 1968: Budapest hévizei (Thermal waters of Budapest), VITUKI, Budapest, 365 p. [in Hungarian]

Anderson, G.M., 1991: Organic maturation and ore precipitation in Southeast Missouri, Economic Geology, v. 86, pp. 909–926.

Anderson, G.M. and Macqueen, R.W., 1982: Ore deposit models-6. Mississippi Valley-type lead-zinc deposits, Geoscience Canada, v. 9, pp. 107-117.

Bada, G., Horváth, F., Dövényi, P., Szafián, P., Windhoffer, G., Cloetingh, S., 2007: Present-day stress field and tectonic inversion in the Pannonian basin. Global and Planetary Change, v. 58, pp. 65-180.

Balog, A., Read, J.F., Haas, J., 1999: Climate-controlled early dolomite, Late Triassic cyclic platform carbonates, Hungary, Journal of Sedimentary Research, v. 69/1, pp. 267-282.

Báldi, T., 1983: Magyarországi oligocén és alsó-miocén formációk (Oligocene and Lower Miocene formations in Hungary), Akadémia Kiadó, Budapest, 293 p. [in Hungarian]

Báldi, T. and Nagymarosy, A., 1976: A Hárshegyi Homokkő kovásodása és annak hidrotermális eredete (Hydrothermal origin of the silicification of the Hárshegy Sandstone), Földtani Közlöny, v. 106, pp. 257-275. [in Hungarian with English abstract]

Báldi, T. and Báldi-Beke, M., 1986: A Magyar Paleogén Medencék fejlődése (Evolution of the Hungarian Paleogene basins), Őslénytani Viták, v. 33, pp. 95–145. [in Hungarian with English abstract]

Bárdossy, Gy., 1977: Karsztbauxitok (Karst Bauxites), Akadémiai Kiadó, Budapest, 413 p. [in Hungarian]

Benavente, D., Martínez-Martínez, J., García-del-Cura, M.A., Canaveras, J.C., 2007: Salt weathering in dual-porosity building dolostones, Engineering Geology, v. 94, pp. 215-226.

Benkovics, L, Obert, D., Bergerat, F., Mansyc, J.L., Dubois, M., 1999: Brittle tectonics and major dextral strike-slip zone in the Buda karst (Budapest, Hungary), Geodinamica Acta (Paris), v. 12, pp. 201-211.

Braun, G., 1889: A Budai hegyek ásványai különös tekintettel a calcitra (Minerals of the Buda Hills, focusing on the calcite), Pallas Részvénytársaság Nyomdája, Budapest, 23 p. [in Hungarian]

Brugger, F., 1940: A Buda környéki dolomitok kőzetkémiai vizsgálata (Petrochemical investigations of the dolomite in the surroundings of Buda), Matematikai és Természetudományi Értesítő, v. 59, pp. 619-641. [in Hungarian]

Brukner-Wein, A., Hetényi, M., Vető, I., 1990: Organic geochemistry of an anoxic cycle: a case history from the Oligocene section, Hungary, Organic Geochemistry, v. 15/2, pp. 123-130.

Brummer, E., 1936: Mátyás-hegyi kőfejtők ásványairól (Minerals from the quarries of Mátyás-hegy), Földtani Értesítő, v. 1, pp. 52-58. [in Hungarian]

Budai, J.M., Lohmann, K.C., Owen, R.M., 1984: Burial dedolomite in the Mississipian Madison limestone, Wyoming and Utah thrust belt, Journal of Sedimentary Petrology, v. 54, pp. 276–288.

Burruss, R.C., 1981: Hydrocarbon fluid inclusions in studies of sedimentary diagenesis *in* Hollister LS, Crawford ML (eds): Short Course in Fluid Inclusions: Applications to Petrology, Min Assoc Can, Calgary, pp. 138-156.

Craig, H., 1965: The measurements of oxygen isotope paleotemperatures *in* Tongiorgi, E., (ed): Stable Isotopes in Oceanographic Studies and Paleotemperatures, Spoleto, Cons Naz Rech, Lab Geol Nucl, Pisa, pp. 161-182.

Cueto, N., Benavente, D., Martínez-Martínez, J., García-del-Cura, M.A., 2009: Rock fabric, pore geometry and mineralogy effects on water transport in fractured dolostones, Engineering Geology, v. 107, pp. 1–15.

Csíky, G., 1956: A Budapest környéki újabb szénhidrogénkutatások és azok földtani eredményei (Results of the hydrocarbon exploration in the surroundings of Budapest), Földtani Közlöny, v. 86, pp. 373-389. [in Hungarian]

Csontos, L., 1995: Tertiary tectonic evolution in the Intra-Carpathian Area: a review, Acta Vulcanologica, v. 7, pp. 1-13.

Csontos, L., Nagymarosy, A., Horváth, E., Kovác, M., 1992: Tertiary evolution of the Intra-Carpathian area: a model, Tectonophysics, v. 208, pp. 221-241.

Davis, G.R. and Smith, L.B., 2006: Structurally controlled hydrothermal dolomite reservoir facies: An overview, AAPG Bulletin, v. 90/11, pp.1641–1690.

de Groot, K, 1967: Experimental dedolomitization, Journal of Sedimentary Petrology, v. 37/4, pp. 1216-1220.

Dickson, J.A.D., 1966: Carbonate identification and genesis as revealed by staining, Journal of Sedimentary Petrology, v. 36, pp. 491-505.

Dövényi, P., Horváth, F., 1988: A review of temperature, thermal conductivity, and heat flow data from the Pannonian Basin *in* Royden, L.H., Horváth, F. (eds): The Pannonian basin – A study in basin evolution, AAPG Memoir 45, Tulsa, Okl, pp. 195-233.

Dövényi, P., Horváth, F., Liebe, P., Gálfi, J., Erki, I., 1983: Geothermal conditions of Hungary. Geophysical Transactions, v. 29, pp. 3-114.

Dublyansky, Y.V., 1991: A Budai-hegység hidrotermális paleokarsztja. A folyadékzárvány vizsgálatok első eredményei (Hydrothermal paleokarst of the Buda Hills. First results of the fluid inclusion studies), Karszt és Barlang, v. 1991/I-I, pp.19-24.

Erőss, A., 2010: Characterization of fluids and evaluation of their effects on karst development at the Rózsadomb and Gellért Hill, Buda Thermal Karst, Hungary, Ph.D. Dissertation, Eötvös Loránd University, Budapest, 171 p.

Erőss, A., Mádl-Szőnyi, J., Csoma, É.A., 2008: Characteristics of discharge at Rose and Gellért Hills, Budapest, Hungary. Central European Geology, v. 51, pp. 267-281.

Esteban, M. and Wilson, J.L., 1993: Introduction to karst systems and paleokarst reservoirs *in* Fritz, R.D., Wilson, J.L., Yurewicz, D.A. (eds).: Paleokarst related hydrocarbon reservoirs, SEPM Core Workshop No. 18, New Orleans, pp. 1-10.

Esteban, M., Budai, T., Juhász, E., Lapointe, P., 2009: Alteration of Triassic carbonates in the Budai Mountains — a hydrothermal model, Central European Geology, v. 52/1, pp. 1-29.

Evamy, B.D., 1967: Dedolomitization and the development of rhombohedral pores in limestone, Journal of Sedimentary Petrology, v. 37/4, pp. 1204-1215.

Fodor, L., Magyari, Á., Kázmér, M., Fogarasi, A., 1992: Gravity-flow dominated sedimentation on the Buda paleoslope (Hungary) record of Late Eocene continental escape of the Bakony unit, Geologische Rundschau, v. 81/3, pp. 695-716.

Fodor, L., Magyari, Á, Fogarasi, A., Palotás, K., 1994: Tercier szerkezetfejlődés és késő paleogén üledékképződés a Budai-hegységben. A Budai-vonal új értelmezése (Tertiary tectonics and Late Paleogene sedimentation in the Buda Hills, Hungary. A new interpretation of the Buda Line), Földtani Közlöny, v. 124/2, 305 p.

Fodor, L., Jelen, B., Márton, E., Skaberne, D., Čar, J., Vrabec. M., 1998: Miocene-Pliocene tectonic evolution of the Slovenian Periadriatic fault: Implications for Alpine-Carpathian extrusion models, Tectonics, v. 17/5, pp. 690-709.

Folkman, Y., 1969: Diagenetic dedolomitization in the Albian-Cenoman Yagur dolomite on Mount Carmal (Northern Israel), Journal of Sedimentary Petrology, v. 39/1, pp. 380-385.

Forti, P., Galdenzi, S., Sarbu, S.M., 2002: The hypogenic caves: a powerful tool for the study of seeps and their environmental effects, Continental Shelf Research, v. 22, pp. 2373-2386.

Földvári, A., 1933: A Dunántúli-középhegység eocén előtti karsztja (Pre-Eocene karts of the Transdanubian Range), Földtani Közlöny, v. 63, pp. 49-55. [in Hungarian]

Frenzel, B., Pécsi, M., Velichko, A.A. (eds.) 1992: Atlas of Paleoclimates and Paleoenvironments of the Northern Hemisphere. Late Pleistocene- Holocene, Geographical Research Institute, Hungarian Academy of Sciences, Gustav Fischer Verlag, Budapest, Stuttgart, 153 p.

Fritz, P., 1967: Oxygen and carbon isotopic composition of carbonates from the Jura of Southern Germany, Canadian Journal of Earth Sciences, v. 4, pp. 1247-1267.

Fritz, R.D., Wilson, J.L., Yurewicz, D.A., 1993: Paleokarst related hydrocarbon reservoirs, SEPM Core Workshop No. 18, New Orleans, 269 p.

Fu, Q., Qing, H., Bergman, K.M., Yang, C., 2008: Dedolomitization and calcite cementation in the Middle Devonian Winnipegosis Formation in Central Saskatchewan, Canada, Sedimentology, v. 55, pp. 1623–1642.

Gaswirth, S.B., Budd, D.A, Crawford, B.R., 2006: Textural and stratigraphic controls on fractured dolomite in a carbonate aquifer system, Ocala limestone, west-central Florida, Sedimentary Geology, v. 184, pp. 241–254.

Gatter, I., 1984: A karbonátos kőzetek érkitöltéseinek és a barlangok hévizes kiválásainak folyadekzárvány-vizsgálata (Fluid inclusion investitigatition of vein-fillings of carbonate rocks and the hydrothermal precipitations of the caves), Karszt és Barlang, v. 1980/2, pp. 93-98. [in Hungarian]

Gál, B., Poros, Zs., Molnár, F., 2008: A Hárshegyi Homokkő Formáció hidrotermális kifejlődései és azok kapcsolatai regionális földtani eseményekhez (Hydrothermal events in the Hárshegy Sandstone Formation and their relationships to regional processes, Buda Hills, Hungary), Földtani Közlöny, v. 138/1, pp. 49-60. [in Hungarian with English abstract]

Goldscheider, N., Mádl-Szőnyi, J., Erőss, A., Schill, E., 2010: Review: Thermal water resources in carbonate rock aquifers, Hydrogeology Journal, v. 18, pp. 1303-1318.

Goldstein, R.H., 2001: Fluid inclusions in sedimentary and diagenetic systems, Lithos, v. 51, pp. 159-193.

Goldstein, R.H. and Reynolds, T.J., 1994: Systematics of Fluid Inclusions in Diagenetic Minerals, SEPM Short Course, v. 31, 199 p.

Gregg, J.M. and Sibley, D.F., 1984. Epigenetic dolomitization and the origin of xenotopic dolomite texture, Journal of Sedimentary Petrology, v. 54, pp. 908–931.

Grimmer, J.O.W., Pironon, J., Teinturier, S., Mutterer, J., 2003: Recognition and differentiation of gas condensates and other oil types using microthermometry of petroleum inclusions. Abstract. Journal of Geochemical Exploration, v. 78-79, pp. 367-371.

Guillaume, D., Teinturier, S., Dubessy, J., Pironon, J., 2003: Calibration of methane analysis by Raman spectroscopy in H_2O–NaCl–CH_4 fluid inclusions, Chemical Geology, v. 194, pp. 41-49.

Győri, O., Poros, Zs., Mindszenty, A., Molnár, F., Fodor, L., Szabó, R., 2011: Budai-hegységi paleogén karbonátos kőzetek diagenezistörténete (Diagenetic history of the Paleogene carbonates, Buda Hills, Hungary), Földtani Közlöny, *in press* [in Hungarian with English abstract]

Haas, J., 1989: Felső-Triász karbonátos táblafejlődés a Dunántúli középhegységben (Late Triassic platform evolution in the Transdanubian Range), D.Sc. Theses, Budapest, 220 p. [in Hungarian]

Haas, J. and Budai, T., 1995: Upper Permian-Triassic facies zones in the Transdanubian Range – Riv. Ital.di Paleont.e.Strat, v. 101/3, pp. 249-266.

Haas, J. and Demény, A., 2002: Early dolomitisation of Late Triassic platform carbonates in the Transdanubian Range (Hungary), Sedimentary Geology, v. 151, pp. 225–242.

Haas, J., Kovács, S., Krystyn, L., Lein, R., 1995: Significance of Late Permian–Triassic facies zones in terrain reconstruction in the Alpine–North Pannonian domain, Tectonophysics, v. 242, pp. 19-40.

Haas, J., Korpás, L., Török, Á., Dosztály, L., Góczán, F., Hámor-Vidó, M., Oravecz-Scheffer, A., Tradi-Filácz, E., 2000: Felső-triász medence- és lejtőfáciesek a Budai-hegységben – a Vérhalom téri fúrás vizsgálatának tükrében (Upper Triassic basin and slope facies in the Buda Mts. – based on study of core drilling Vérhalom tér, Budapest), Földtani Közlöny, v. 130/3, pp. 371–421. [in Hungarian with English abstract]

Haas, J., Hámor, G., Jámbor, Á., Kovács, S., Nagymarosy, A., Szeredkényi. T, 2001: Geology of Hungary, ed. Haas, J., Eötvös University Press, Budapest, 317 p.

Haas, J., Budai, T., Csontos, L., Fodor, L., Konrád, Gy., 2010: Magyarország pre-kainozoos földtani térképe. 1: 500 000 (Pre-Cenozioc geological map of Hungary), Földtani Intézet Kiadványa (Publication of the Geological Institute of Hungary)

Hanshaw, B.B. and William, B., 1985: Deciphering hydrological systems by means of geochemical processes, Hydrological Sciences Journal, v. 30/2, pp. 257-271.

Hedenquist, J.W. and Henley, R.W., 1985: The importance of CO_2 on freezing point measurements of fluid inclusions: Evidence from active geothermal systems and implications for epithermal ore deposition, Economic Geology, v. 80, pp. 1379-1406.

Hetényi, M., Sajgó, Cs., Vető, I., Brukner-Wein, A., Szántó, Zs., 2004: Organic matter in a low productivity anoxic intraplatform basin in the Triassic Tethys, Organic Geochemistry, v. 35, pp. 1201-1219.

Hofmann, K., 1871: A Buda-Kovácsi hegység földtani viszonyai (Geology of the Buda-Kovácsi Mts.), Annual Report, Geological Institute of Hungary, v. 1, pp. 199-276. [in Hungarian]

Horváth, J., 1965: A Szemlőhegyi-barlang 1961-62. évi felérése (Mapping of Szemlőhegy Cave in 1961-62), Karszt és Barlang, v. I, pp. 21–30. [in Hungarian]

Jakucs, L., 1950: A dolomitporlódás kérdése a Budai-hegységben (Powderization of dolomite in the Buda Hills), Földtani Közlöny, v. 80/10-12., pp. 361-380. [in Hungarian]

James, N. P. and Choquette, P. W., 1989: Palaeokarst, New York / Berlin / Heidelberg / London / Paris / Tokyo, Springer-Verlag, 416 p.

Jaskó, S., 1979: Az infraoligocén denudáció nyomai a Budai-hegységben, Földtani Közlöny, v. 109/2, pp. 199–210. [in Hungarian with German abstract]

Ji, H., Wang, S., Ouyang, Z., Zhang, S., Sun, C., Liu, X., Zhou, D., 2004: Geochemistry of red residua underlying dolomites in karst terrains of Yunnan-Guizhou Plateau II. The mobility of rare earth elements during weathering, Chemical Geology, v. 203, pp. 29-50.

Kázmér, M. and Kovács, S., 1985: Permian-Palaegene paleogeography along the eastern part of the Insubric-Periadriatic lineament system: Evidence for continental escape of the Bakony-Drauzug unit, Acta Geologica Hungarica, v. 28, pp. 71-84.

Kele, S., 2009: Édesvízi mészkövek vizsgálata a Kárpát-medencéből: paleoklimatológiai és szedimentológiai elemzések (Travertines of the Carpathian Basin), Ph.D. Thesis, Eötvös Loránd University, Budapest, 176 p. [in Hungarian with English abstract]

Kleb, B., Benkovics, L., Dudko A., Gálos, M., Juhász, E., Kertész, P., Korpás, L., Marek, I., Nádos, A., Török, Á., 1993: Komplex földtani vizsgálatok és fúrások a Rózsadomb

térségében (Complex geological investigations and drillings in the Rózsadomb Area) PHARE Project, Report, v. 1, 249 p. [in Hungarian]

Klimchouk, A.B., 2007: Hypogene speleogenesis: hydrogeological and morphogenetic perspective, Special Paper No. 1, National Cave and Karst Research Institute, Carlsbad, NM, 106 p.

Koch, A., 1871: Szentendre-Visegrádi és a Pilis-hegység földtani leírása (Geological description of Szentendre-Visegrád and Pilis Mts.), Földtani Évkönyv, v. I, pp. 141-199. [in Hungarian]

Korpás, L., Dosztály, L., Dudko, A., Góczán, F., Gyuricza, Gy., Hámor-Vidó, M., Hertelendi, E., Horváth-Kollányi, K., Lantos, M., Lelkes Gy., Nagymarosy, A., Oravecz-Scheffer, A., Piros, O., Rákosi. L., 1993: A Budai-hegység complex paleokarszt rendszere (The composite palaeokarst systems of the Buda Hills), Research Report, Geological Institute of Hungary, [in Hungarian]

Korte, C., Kozur, H.W., Veizer, J., 2005: $\delta^{13}C$ and $\delta^{18}O$ values of Triassic brachiopods and carbonate rocks as proxies for coeval seawater and palaeotemperature, Palaeogeography, Palaeoclimatology, Palaeoecology, v. 226, pp. 287– 306.

Kósa, G., Mindszenty, A., Mohai, R., 2003: Roncskarszt térszínre progradáló eocén törmelékkúp Budakeszin (Eocene alluvial fan prograding over a high dissected palaeokarst surface built up by Upper Triassic dolomites. New details on the early Paleogene evolution of the Buda Hills), Földtani Közlöny, v. 133/2, pp. 271-285. [in Hungarian with English abstract]

Kovács, J. and Müller, P., 1980: A budai-hegyek hévizes tevékenységének kialakulása és nyomai (Evolution and evidence of the thermal water activity in the Buda Hills), Karszt és Barlang, v. II, pp. 93-98. [in Hungarian]

Kovács, I., Csontos, L., Szabó, Cs., Bali, E., Falus, G., Benedek, K., Zajacz, Z., 2007: Paleogene-early Miocene igneous rocks and geodynamics of the Alpine- Carpathian-Pannonian-Dinaric region: an integrated approach. In: Beccaluva, L., Bianchini, G., Wilson, M. (Eds.), Cenozoic Volcanism in the Mediterranean Area, v. 418., Geological Society of America Special Paper, pp. 93–112.

Kovács-Pálffy, P. and Földvári, M., 2004: Mineralogy of the travertines in NE Transdanubia (Hungary) (Északkelet-dunántúli édesvízi mészkövek ásványtana), Földtani Közlöny, v. 134/4, pp. 563-587.

Land, L.S., 1983: The application of stable isotopes to studies of the origin of dolomite and to problems of diagenesis of clastic sediments *in* Arthur, M.A., Anderson, T.F., Kaplan,

I.R., Veizer, J., Land, L.S. (eds.): Stable Isotopes in Sedimentary Geology, Society of Sedimentary Geology, Short Course, v. 10, pp. 4.1–4.22.

Landström, O. and Tullborg, E.L., 1995: Interactions of trace elements with fracture filling minerals from the Äspö Hars Rock laboratory, SKB Technical Report, TR 95-13, Swed Nucl Fuel and Waste Management Co. (SKB), Stockholm, Sweden

Leach, D.L. and Sangster, D.F., 1993: Mississippi Valley-type lead-zinc deposits *in* Kirkham, R.V., Sinclair, W.D., Thorp, R.I., Duke, J.M. (eds.): Mineral Deposit Modeling, Geological Association of Canada, Special Paper, v. 40, pp. 289-314.

Leél-Őssy, Sz., 1995: A Rózsadomb és környékének különleges barlangjai (Particular caves of the Rózsadomb Area), Földtani Közlöny, v. 125/3-4, pp. 363-432. [in Hungarian]

Leél-Őssy, Sz., 2004: A Budai termálkarsztos barlangok genetikája és értékei (Genesis and values of hydrothermal caves in the Buda Hills) *in* Hazslinszky, T. (ed): Genesis and Formations of hydrothermal caves. Proceedings of the International Conference on the occasion of the 100th anniversary of the discovery of the Pál-völgy Cave, Budapest, Hungarian Speleological Society, pp. 45-53. [in Hungarian]

Leél-Őssy, Sz. and Surányi, G., 2003: Peculiar hydrothermal caves in Budapest, Hungary, Acta Geologica Hungarica, v. 46/ 4, pp. 407-436.

Lemmlein, G.G., 1952: Migration of liquid fluid inclusions in a crystal towards a source of heat. Dokl. Akad. Nauk. SSSR, v. 85, pp. 325-328.

Lenkey, L., Dövényi, P., Horváth, F., Cloetingh, S.A.P.L., 2002: Geothermics of the Pannonian basin and its bearing on the neotectonics, EGU Stephan Mueller Special Publication, ser. 3, pp. 29-40.

Lóránth, Cs., 2000: Réz előfordulás a Budai-hegységben (Copper in the Buda Hills), AuXit, v. 2, pp. 28-29. [in Hungarian]

Lucia, F.J., 1961: Dedolomitization in the Tansill (Permian) Formation, Geological Society of American Bulletin, v. 72, pp. 1107-1110.

Machel, H.G., 1997: Recrystallization versus neomorphism, and the concept of 'significant recrystallization' in dolomite research, Sedimentary Geology, v. 113, pp. 161-168.

Machel, H.G., 2004: Concepts and models of dolomitization: a critical reappraisal *in* Braithwaite, C.J.R., Rizzi, G., Darke, G. (eds): The Geometry and Petrogenesis of Dolomite Hydrocarbon Reservoirs. Geological Society, London, Special Publications, v. 235, pp. 7–63.

Mackay, J. R., 1999: Cold-Climate Shattering (1974 to 1993) of 200 Glacial Erratics on the Exposed Bottom of a Recently Drained Arctic Lake, Western Arctic Coast, Canada, Permafrost and Periglacial Processes, v. 10, pp. 125-136.

Magyari, Á., 1991: Késő-eocén üledékképződés és tektonika kapcsolata a Budaörsi-hegyekben (Relations between Late Eocene tectonics and sedimentation in the Budaörs Hills), Msc. Thesis, Eötvös Loránd University, Budapest, 95 p. [in Hungarian with English abstract]

Márton, E. and Fodor, L., 2003: Tertiary paleomagnetic results and structural analysis form the Transdanubian Range (Hungary): rotational disintegration of the Alcapa unit, Tectonophysics, v. 363, pp. 201-224.

McCrea, J.M., 1950: On the isotopic chemistry of carbonates and a paleotemperature scale, The Journal of Chemical Physics, v. 18, pp. 849-857.

Milota, K., Kovács, A., Galicz, Zs., 1995: Petroleum potential of the North Hungarian Oligocene sediments, Petroleum Geoscience, v. 1, pp. 81-87.

Mindszenty, A., Gál-Sólymos, K., Csordás-Tóth, A., Imre, I., Felvári, Gy., Ruttner, A., Böröczky, T., 1991: Extraclasts from Cretaceous/Tertiary bauxites of the Transdanubian Central Range and the Northern Calcareous Alps. Preliminary results and tentative geological interpretation, Jubliäumsschrift 20 jahre Geol. Zusammenarbeit Österreich-Ungarn Teil I., pp. 309-345.

Mindszenty, A., Csoma, A., Török, Á., Hips, K., Hertelendi, E., 2001: Flexura jellegű előtéri deformációhoz köthető karsztbauxitszintek a Dunántúli-középhegységben (Rudistid limestones, bauxites, paleokarst and geodynamics. The case of the Cretaceous of the Transdanubian Range), Földtani Közlöny, v. 131/1-2, pp. 107-152. [in Hungarian with English abstract]

Molnár, F. and Gatter, I., 1994: Magyarországi üledékes és hidrotermás baritkristályok összehasonlító ásványtani-genetitikai vizsgálata (Comparative mineralogic-genetic studies of sedimentary and hydrothermal barite crystals from Hungary), Földtani Közlöny, v. 124/1, pp. 43-57.

Munz, I.A., 2001: Petroleum inclusions in sedimentary basins: systematics, analytical methods and applications, Lithos, v. 55, pp. 195-212.

Müller, P. and Magyar, I., 2008: A budai pannóniai képződmények (The Pannonian deposits of the Buda Mountains), Földtani Közlöny, v. 138/4, pp. 345-356. [in Hungarian with English abstract]

Nader, F.H., Swennen, R., Ottenburgs, R., 2003: Karst-meteoric dedolomitization in Jurassic carbonates, Lebanon, Geologica Belgica, v. 6/1-2, pp. 3-23.

Nádor, A., 1991: A Budai-hegység paleokarszt jelenségei és fejlődéstörténetük (Palaeokarst of the Buda Hills and their evolution), Ph.D. Thesis, Eötvös Loránd University, Budapest, 171 p. [in Hungarian]

Nádor, A., 1992: Paleokarstic features in Triassic-Eocene carbonates, Zentralblatt für Geologie und Palentologie, v. 1, pp. 1317-1329.

Nagy, B., 1979: A budai-hegységi porlott dolomitok ásvány-kőzettani, geokémiai és genetikai vizsgálata (Mineralogical, petrological, geochemical investigations of pulverulent dolomite in the Buda Hills), Földtani Közlöny, v. 109, pp. 46-74, [in Hungarian with English abstract]

Nagy, B. and Pelikán, P., 1976: Metacinnabarit és cinnabarit a csillaghegyi Róka-hegyen (Metacinnabar and cinnabar from the Róka Hill), Annual Report, Geological Institute of Hungary of 1973, pp. 51-55. [in Hungarian]

Nedkvitne, T., Karlsen, D.A., Bjørlykke, K., Larter, S., 1993: Relationship between reservoir diagenetic evolution and petroleum emplacement in the Ula field, North Sea, Marine and Petroleum Geology, v. 10, pp. 255-270.

Nendtvich, K., 1859: Buda vidékének dolomitjai (Dolomites of Buda), Magyar Akadémiai Értesítő, pp. 112-127. [in Hungarian]

Oxtoby, N.H., 2002: Comments on: Assessing the maturity of oil trapped in fluid inclusions using molecular geochemistry data and visually-determined fluorescence colours, Critical comment, Applied Geochemistry, v. 17, pp. 1371-1374.

Pappone, G. and Ferranti L., 1995: Thrust tectonics in the Picentini Mountains, Southern Appennines, Italy, Tectonophysics, v. 252, pp. 331-348.

Piane, C.D., Burlini, L., Kunze, K., Brack, P., Burg, J.P., 2008: Rheology of dolomite: Large strain torsion experiments and natural examples, Journal of Structural Geology, v. 30, pp. 767–776.

Pironon, J. and Barrès, O., 1990: Semi-quantitative FT-IR microscopy limits: Evidence from synthetic hydrocarbon fluid inclusions in sylvite, Geochimica et Cosmochimica Acta, v. 54, pp. 509–518.

Pironon, J., Thiéry, R., Teinturier, S., Walgenwitz, F., 2000: Water in petroleum inclusions: evidence from Raman and FT-IR measurements, PVT consequences. Journal of Geochemical Exploration, v. 69-70, pp. 663-668.

Poros, Zs., Mindszenty, A., Molnár, F., Pironon, J., Győri, O., Ronchi, P., Szekeres, Z., 2011: Imprints of hydrocarbon-bearing basinal fluids on a karst system: mineralogical and fluid inclusion studies from the Buda Hills, Hungary, International Journal of Earth Sciences, published online, DOI 10.1007/s00531-011-0677-8

Prick, A., 1998: Frost-weathering in a mountain permafrost area (Plateau Mountain, Alberta, Canada), Permafrost−Seventh International Conference (Proceedings), Yellowknife (Canada), Collection Nordicana No. 55, pp. 915-920.

Ronchi, P., Jadoul, F., Savino, R., 2004: Quarternary dedolomitization along fracture systems in a Late Triassic dolomitized platform (Western Southern Alps, Italy), Carbonates and Evaporites, v. 19/1, pp. 51-66.

Royden, L.H. and Horváth, F., 1988: The Pannonian basin – A study in basin evolution, AAPG Memoir 45, Tulsa, Okl, 394 p.

Rozlozsnik, P., 1935: Adatok a Buda-kovácsi hegység óharmadkori rétegeinek ismeretéhez (Tertiary formations of the Buda-kovácsi Hills), Annual Report of 1925–1928, Geological Institute of Hungary, pp. 65–86. [in Hungarian]

Ruszkiczay-Rüdiger, Zs., Fodor, L., Bada, G., Leeél-Őssy, Sz., Horváth, E., Dunai, T.J., 2005: Quantification of Quaternary vertical movements in the central Pannonian Basin: A review of chronologic data along the Danube River, Hungary, Tectonophysics, v. 410, pp. 157–172.

Schafarzik, F., 1884: Jelentés az 1883 év nyarán a Pilis hegységben eszközölt részletes felvételről (Report on the field observations in the Pilis Mts. in the summer of the year 1883), Földtani Közlöny, v. 14, pp. 249-272. [in Hungarian]

Schafarzik, F., 1902: Budapest és Szentendre vidéke (Surroundings of Budapest and Szentendre), 15. zóna, XX. Rov. Jelű lap 1:75000. Magyarázatok a magyar kor. országainak részletes földtani térképéhez, pp. 1-61. [in Hungarian]

Schafarzik, F., 1921: Visszapillantás a budai hévforrások fejlődéstörténetére (Retrospection to the evolution of the thermal springs in Buda), Hidrológiai Közlöny, v. 1, pp. 9-14. [in Hungarian]

Schafarzik, F. & Vendl, A., 1929: Geológiai kirándulások Budapest környékén (Geological excursions in the surroundings of Budapest) Stadium Sajtóvállalat Rt. Budapest, 341 p. [in Hungarian]

Scherf, E., 1922: Hévforrások okozta kőzetváltozások (hidrotermális kőzetmetamorfózis) a Budai és Pilisi-hegységben (Alteration of rocks (hydrothermal metamorphism) in the Buda Hills and Pilis), Hidrológiai Közlöny, v. 2, pp.19-75. [in Hungarian]

Scheuer, Gy. and Schweitzer, F., 1988: A Gerecse és a Budai-hegység édesvizi mészkőösszletei (Travertines of the Gerecse and Buda Mountains), Földrajzi Tanulmányok, Akadémai Kiadó, Budapest, v. 20, 123 p.

Schréter, Z., 1912: A budapesti hévforrások földtani fejlődéstörténete (Evolution of the thermal springs in Budapest), Magyar Balneológiai Értesítő, v. 1 /5, pp. 2-4. [in Hungarian]

Sibley, D.F., 1990: Unstable to stable transformations during dolomitization, Journal of Geology, v. 98, pp. 739–748.

Spötl, C., Vennemann, T.W., 2003: Continuous-flow isotope ratio mass spectrometric analysis of carbonate minerals, Rapid Communications in Mass Spectrometry, v. 17, pp. 1004-1006.

Suppe, J., 1983: Geometry and kinematics of fault-bend folding, American Journal of Science, v. 283, pp. 684-721.

Surdam, R.C., Jiao, Z.S., MacGowan, D.B., 1993: Redox reactions involving hydrocarbons and mineral oxidants, a mechanism for significant porosity enhancement in sandstones, AAPG Bulletin, v. 77, pp. 1509-1518.

Szabó, J., 1858: Pest-Buda környékének földtani leírása (Geology of the surroundings of Pest-Buda), Special Publication of the Hungarian Academy of Sciences, Természettudományi pályamunkák. vol. 4, 58 p. [in Hungarian]

Szantner, F., Knauer, J., Mindszenty, A., 1986: Bauxitprognózis. MTA Veszprémi Akad. Biz. Kiadása, p. 467. [in Hungarian]

Szanyi, Gy., Bada, G., Surányi, G., Leél-Őssy, Sz., Varga, Zs., 2009: A Budai-hegység pleisztocén kiemelkedétörténete barlangi lemezes kalcitkiválások uránsoros kormeghatározása alapján (Pleistocene uplift history of the Buda Hills (Hungary), using uranium-series dating of cave rafts), Földtani Közlöny, v. 139/4, pp. 353-366. [in Hungarian with English abstract]

Szőts, E., 1948: Jelentés a nagykovácsi és pilisvörösvári medence eocén képződményeinek rétegtani viszonyairól (Stratigraphy of Eocene formations in the Nagykovácsi and Pilisvörösvár Basins), Annual Report of 1948, Geological Institute of Hungary, pp. 39-46. [in Hungarian]

Takács-Bolner, K. and Kraus, S., 1989: A melegvizes eredetű barlangok kutatásának eredményei (Results of research of the thermal water caves), Karszt és Barlang, v. I-II, pp. 61-66. [in Hungarian]

Tari, G., 1994: Alpine Tectonics of the Pannonian Basin, PhD. Thesis, Rice University, Texas, USA, 489 p.

Taylor, S.R. and McLennan, S.M., 1985: The continental crust: its composition and evolution: Blackwell, Oxford, 312 p.

Telegdi-Roth, K., 1927: Infraoligocén denudáció nyomai a Dunántúli-középhegység északnyugati peremén (Infraoligocene denudation in the NW margin of the Transdanubian Range), Földtani Közlöny, pp. 32–41. [in Hungarian]

Thiéry, R., Pironon, J., Walgenwitz, F., Montel, F., 2000: PIT (Petroleum Inclusion Thermodynamic): a new modelling tool for the characterization of hydrocarbon fluid inclusions from volumetric and microthermometric measurements. Journal of Geochemical Exploration, v. 69–70, pp. 701–704.

Thiéry, R., Pironon, J., Walgenwitz, F., Montel, F., 2002: Individual characterization of petroleum inclusions (composition and P-T trapping conditions) by microthermometry and confocal scanning laser microscopy: inferences from applied thermodynamics of oils, Marine and Petroleum Geology, v. 19, pp. 847-859.

Timkó, J., 1909: Budapest dunajobbparti környékének, továbbá Gödöllő-Isaszeg vidékének agrogeológiai vizsonyai (Agrogeologic properties of the surroundings of Budapest and Gödöllő-Isaszeg), Geological report of 1907, pp. 172-184. [in Hungarian]

Tóth, Á. and T. Gecse, É., 1981: Dedolomitosodott telérszerű kőzettestek a Nagyegyházi-medence felső-triász dolomitaljzatában (Dedolomitized vein-like bodies in the Upper Triassic basement dolomite of the Nagyegyház Basin), Annual Report of 1979, Geological Institute of Hungary, pp. 181-199. [in Hungarian]

Tóth, J. and Almási, I., 2001: Interpretation of observed fluid potential patterns in a deep sedimentary basin under tectonic compression: Hungarian Great Plain, Pannonian Basin, Geofluids, v. 1, pp. 11-36.

Tullborg, E-L., Drake, H., Sandström, B., 2008: Palaeohydrogeology: A methodology based on fracture mineral studies, Applied Geochemistry, v. 23, pp. 1881–1897.

Vető, I., 1999: Triassic sourced oil shows near Budapest, Annual Report of 1992-1993, Geological Institute of Hungary, v. II, pp. 111-115.

Wein, Gy., 1977: A Budai-hegység tektonikája (Tectonics of the Buda Hills), Special Publication, Geological Institute of Hungary, Budapest, 76 p. [in Hungarian]

White, D.E., 1957: Thermal waters of volcanic origin, Geological Society of America Bulletin, v. 68, p. 1637– 1658.

Woronick, R.E. and Land, L.S., 1985: Late burial diagenesis, Lower Cretaceous Pearsall and Lower Glen Rose formations, South Texas *in* Schneidermann, N. and Harris, P.M. (eds): Carbonate Cements, Special Publication, Soc. econ. Paleont. Miner., v. 36, pp. 265-275.

Appendix

Sample codes and sample locations:

1. Piliscsaba quarry: P-02 to P-08
2. Zajnát Hills: Z-01 to Z-07
3. Ördögoltár: P-01
4. Kis-Kevély quarry: Kk-01 to Kk-02
5. Teve Cliff: T-01 to T-07
6. Solymár Wall: Kk-03
7. Lapos quarry: L-01 to L-36
8. Róka Hill: Ro-01 to Ro-17
9. Surroundings of Piliscsaba: P-09 P-23
10. Zsíros Hill, Nagykovácsi, Nk-01 to Nk-07
11. Kopasz Hill, Telki: K-01 to K-09
12. Nagy-Hárs Hill: H-01 to H-05
13. Budakeszi quarry: Bu-01 to Bu-05
14. János Hill/Tündér Hill quarry: J-01 to J-14
15. Tündér cliff and surroundings: Tu-01 to Tu-07
16. Fenyőgyöngye quarry: F-01 to F-40
17. Mátyás Hill and Pálvölgy quarry: M-01 to M-07; Pv-01
18. Szemlőhegy Cave: Szb-01 to Szb-22; drillcore samples: Szf-01 to Szf-09
19. Kis-Sváb Hill: Ksv-01 to Ksv-02
20. Gellért Hill: G-01 to G-07; samples from underground: Gt-01 to Gt-08
21. Kecske Hill quarry, Csík Hills: Cs-14 to Cs-16
22. Sorrento Cliffs, Csík Hills: Cs-04 to Cs-13
23. Ló Hill: Cs-01 to Cs-03
24. Törökugrató quarry: Tug-01 to Tug-10
25. Út Hill: Ut-01 to Ut-02
26. Odvas Hill: O-01 to O-20

Sample locations 1-3

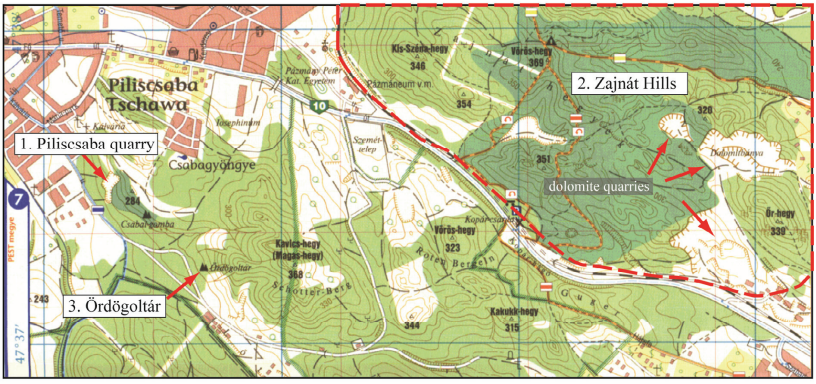

Sample locations 4-6

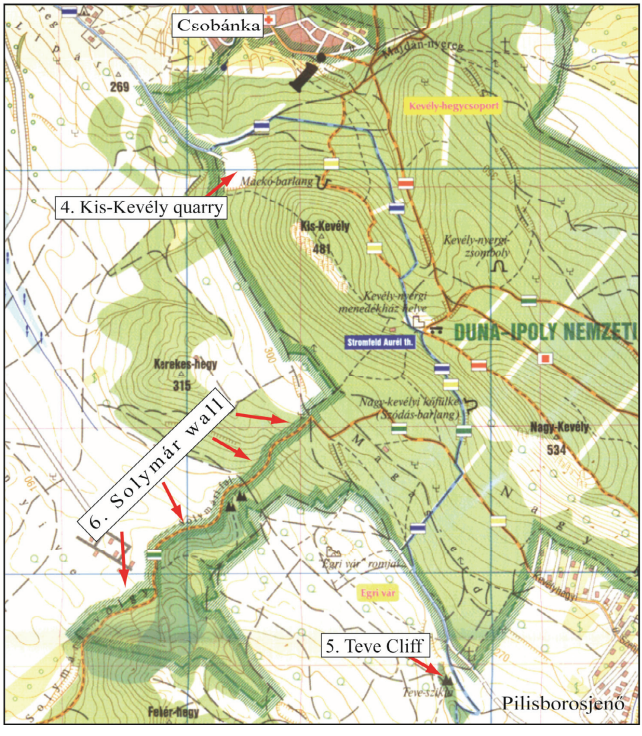

Sample locations 7-8

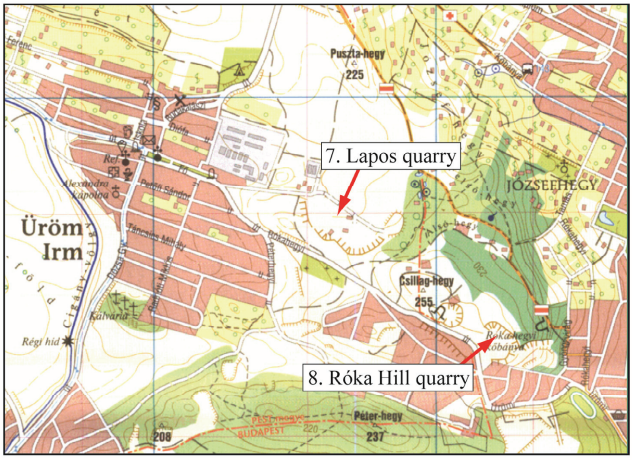

Sample locations 9. - Surroundings of Piliscsaba

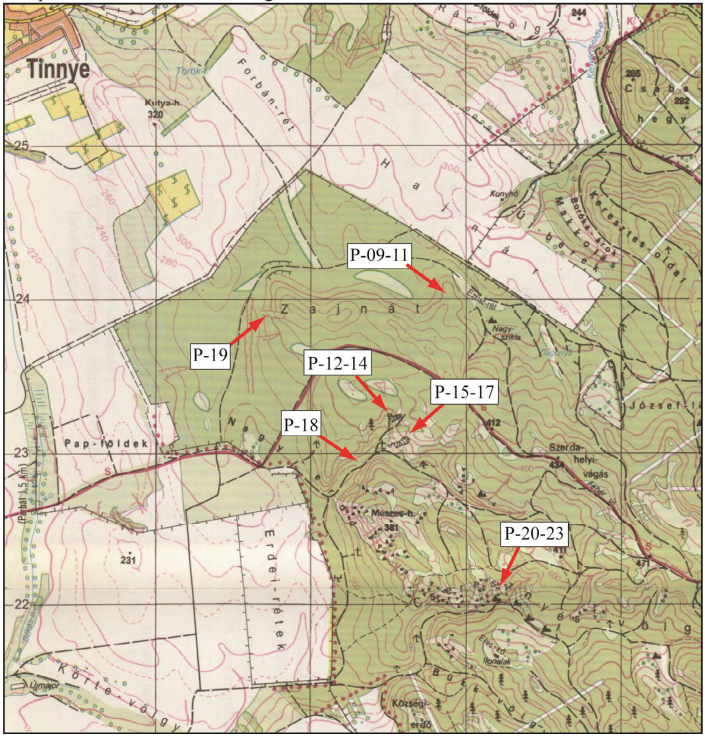

Sample location 10.

Sample location 11. - Kopasz Hill and surroundings

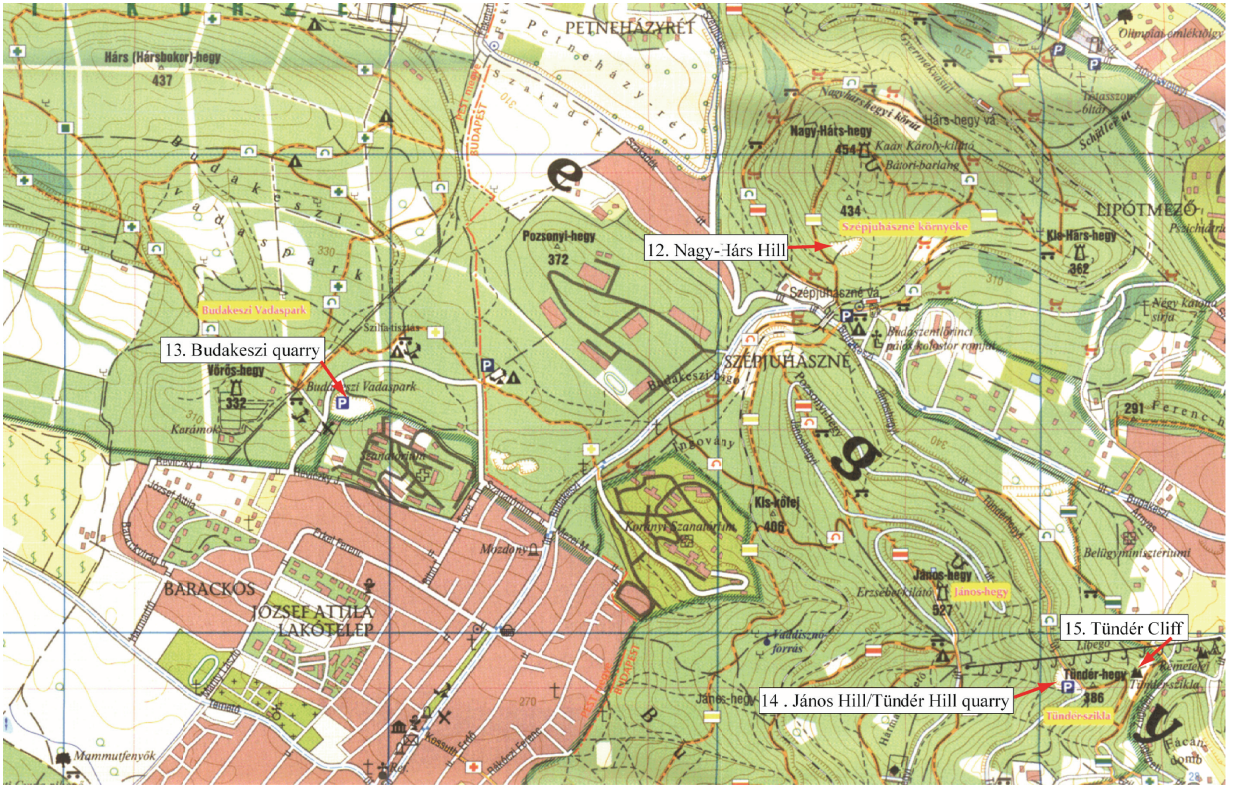

Sample locations 12-15.

Sample locations 16-18.

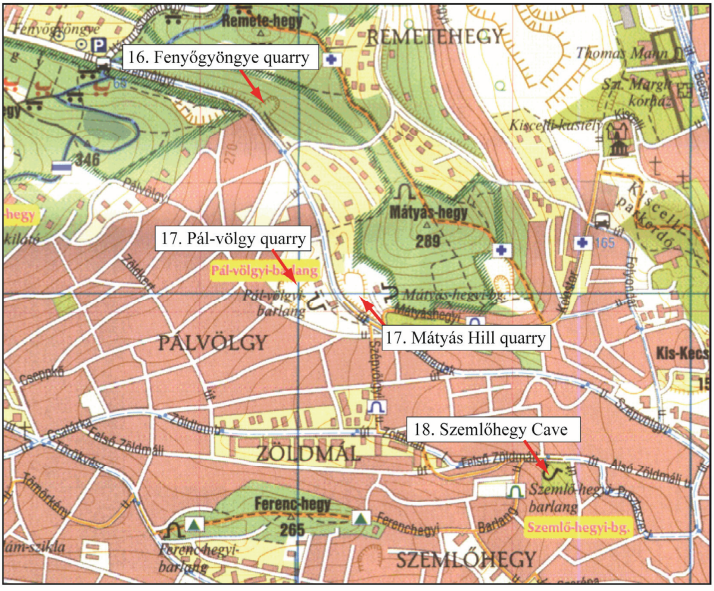

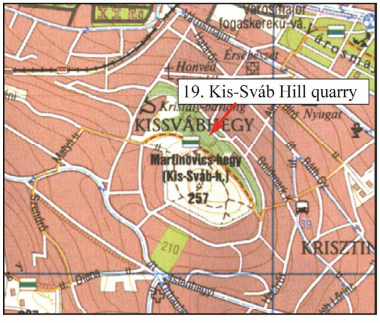

Sample location 19.

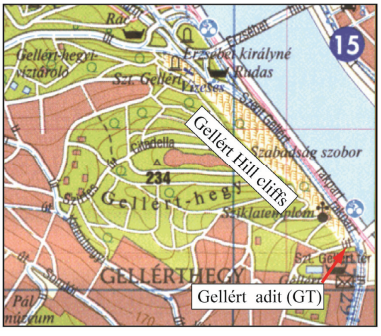

Sample location 20. - Gellért Hill

Sample locations 21-26.

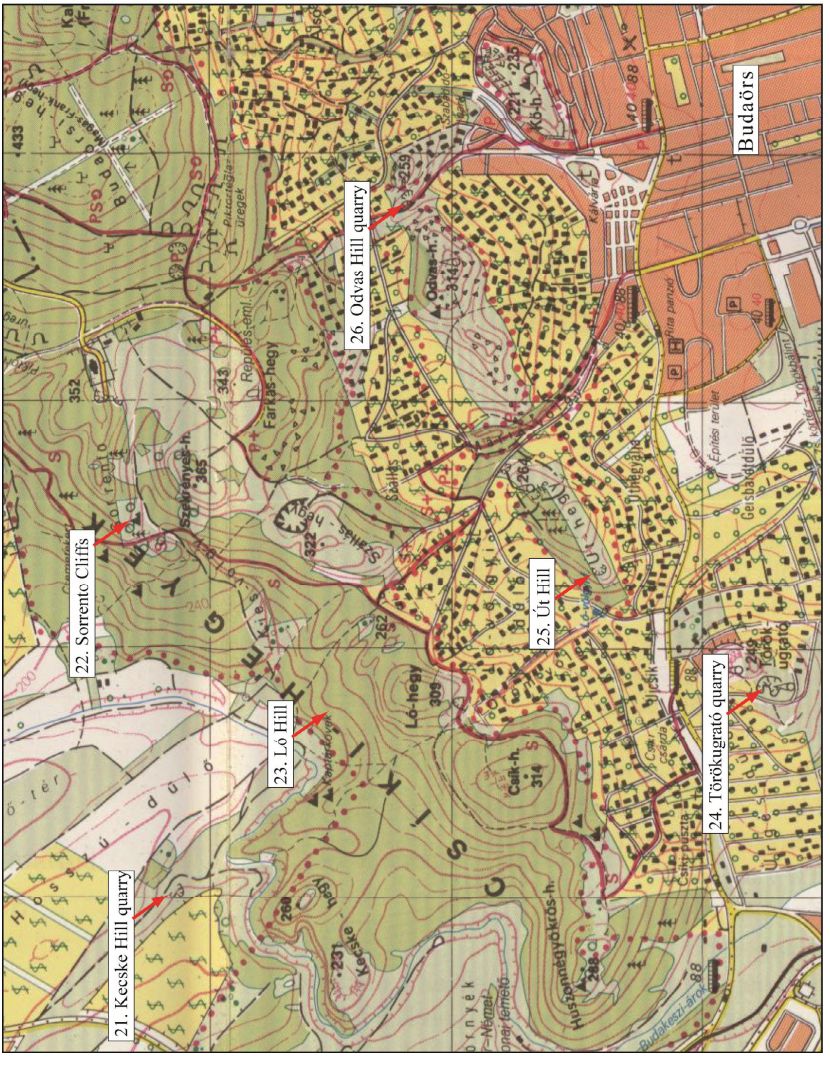

Sample	T-04 (D-01)	O-13 (D-02)	Tu-05 (D-03)	Bu-02 (DP-01)	T-07 (DP-02)	P-08 (DP-03)	J-09 (DP-04)	Z-03 (DP-05)	K-02 (DP-06)	Cs-03 (DP-07)	Cs-12 (DP-08)	Cs-14 (DP-09)	T-05 (DC-01)	Tu-07 (DC-02)	J-02 (DC-03)
SiO_2 (wt%)	0.18	0.06	0.06	<0.01	0.01	0.07	0.36	0.1	0.51	0.17	0.25	0.31	0.1	0.03	0.12
Al_2O_3	0.03	0.04	0.01	<0.01	0.01	0.06	0.27	0.04	0.32	0.06	0.03	0.05	0.03	0.01	0.08
Fe_2O_3	0.1	0.03	0.02	<0.01	0.07	0.15	0.23	0.09	0.14	0.20	0.82	0.16	0.09	0.08	0.07
CaO	29.4	29.8	29.6	29.2	30.1	30.4	29	29.9	30.5	30.9	30.2	30.8	37.7	30.3	48.8
MgO	20.5	20.4	20.6	20.4	19.9	22.3	20.9	21	22.2	22.5	22.4	22.5	16.9	22.5	6.28
LOI	47.8	47.7	47.6	48.3	47.8	47.2	47.4	47.7	46.4	47.2	46.7	47.3	45.2	46.9	44.5
Total	98.1	98.1	98	98	98	100	98.2	98.9	100	101	100.5	101	100	99.9	100.5
La (ppm)	0.7	0.6	0.5	<0.5	1.2	0.8	1.6	<0.5	0.5	<0.5	<0.5	<0.5	0.6	1.1	0.8
Ce	1.2	0.7	0.6	0.5	1.7	1	2.1	<0.5	1	0.7	0.7	<0.5	1.4	1.8	0.8
Pr	0.13	0.07	0.07	0.06	0.2	0.13	0.23	0.03	0.13	0.1	0.11	0.04	0.19	0.23	0.12
Nd	0.6	0.3	0.3	0.3	0.8	0.5	0.9	0.1	0.6	0.4	0.5	0.2	0.9	0.9	0.5
Sm	0.11	0.04	0.05	0.07	0.2	0.12	0.14	<0.03	0.21	0.09	0.12	0.07	0.15	0.19	0.09
Eu	<0.03	<0.03	<0.03	<0.03	0.04	<0.03	0.05	<0.03	0.07	0.03	0.03	<0.03	0.05	0.04	<0.03
Gd	0.09	<0.05	0.06	0.06	0.15	0.1	0.14	<0.05	0.31	0.1	0.13	0.06	0.21	0.17	0.09
Tb	0.01	<0.01	<0.01	0.01	0.02	0.01	0.02	<0.01	0.05	0.01	0.02	0.01	0.02	0.02	0.02
Dy	0.07	<0.05	0.06	0.05	0.08	0.05	0.15	<0.05	0.25	0.08	0.11	0.05	0.15	0.12	0.11
Ho	0.02	0.01	0.01	0.02	0.01	0.02	0.04	0.01	0.04	0.02	0.02	0.01	0.03	0.02	0.03
Er	0.05	<0.03	0.03	0.06	0.04	0.03	0.11	<0.03	0.11	0.06	0.05	0.03	0.07	0.07	0.08
Tm	0.02	0.03	0.03	0.04	0.04	0.03	0.05	<0.01	0.05	<0.01	<0.01	<0.01	0.04	0.03	0.04
Yb	0.05	0.03	<0.03	0.04	0.03	0.04	0.08	<0.03	0.11	0.03	0.05	0.03	0.06	0.06	0.08
Lu	0.01	<0.01	<0.01	<0.01	<0.01	<0.01	0.02	<0.01	0.02	<0.01	0.01	<0.01	0.01	0.01	0.01
Ba	66.2	2.3	2	2.4	30.5	1.7	5.1	1.6	8.1	193	5	8.9	14	3.2	3590
Cu	3	4	<1	<1	2	4	1	<5	<5	<5	<5	<5	1	<1	<1
Hg	0.05	0.07	0.01	<0.01	0.73	0.01	0.01						0.23	0.01	0.12
Mn	11	14	6	9	6	31	46						6	21	7
Mo	1	<1	1	<1	1	1	<1	<2	<2	3	<2	<2	1	<1	<1
Ni	1	2	1	1	2	1	2	<5	36	<5	8	6	1	2	2
P	20	10	20	20	30	40	40						40	40	50
Pb	10	3	2	2	<2	<2	<2	<5	14	<5	<5	<5	2	2	<2
S	500	200	200	1000	300	100	200						8800	600	<100
Sr	72.1	78.3	74.6	74.7	98.5	80	83	80.3	81.9	81.6	65.5	75.6	113	73.2	119.5
Zn	9	17	5	4	6	8	11	<5	22	21	62	23	9	6	6

Appendix-Table 1: Geochemical data (major and trace elements including REE) of the following rock types: D= fresh/intact dolomite; DP= powdered dolomite (regional type: DP-01 and from DP-04 to DP-08; local type: DP-02, DP-03, DP-09); DC= dolomite associated with calcite (DC-01: red calcite, DC-02 and 03: white calcite). All samples belong to Hauptdolomit Fm expect O-13 which represents Budaörs Fm.

Sample Tu-01				
Texture	**Phase proportions**	**T_h (°C)**	**T_{melt} (°C)**	**NaCl equ. wt%**
nonplanar-anhedral	L-V: 95-5	73		
planar-euhedral	L-V: 95-5	85		
planar-euhedral	L-V:80-20		-2.3	3.9
planar-euhedral	L-V:97-3	69		
planar-euhedral	L-V:99-1	70		
planar-euhedral	L-V:99-1	79		
planar-euhedral	L-V:80-20		-2.7	4.5
planar-euhedral	L-V:80-20		-2	3.4
nonplanar-anhedral	L-V:97-3	67		
planar-euhedral	L-V: 95-5	75		
planar-euhedral	L-V: 95-5	75		
planar-euhedral	L-V:90-10	77		
planar-e/nonplanar-a boundary	L-V:90-10	124		
planar-euhedral	L-V: 95-5	72		
planar-e/nonplanar-a boundary	L-V:70-30		-3	5
nonplanar-anhedral	L-V:97-3	65		
planar-euhedral	L-V:97-3	88		
planar-euhedral	L-V:99-1	62		
planar-subhedral	L-V:99-1	92		
nonplanar-anhedral	L-V:97-3	67		
planar-e/nonplanar-a boundary	L-V:99-1	77		
planar-e/nonplanar-a boundary	L-V:99-1	77		
planar-e/nonplanar-a boundary	L-V:99-1	77		
planar-e/nonplanar-a boundary	L-V:97-3	75		

Appendix-Table 2: Microthermometric data of primary, two-phase aqueous inclusions of sample Tu-01, Hauptdolomit, Tündér Cliff

Sample O-02				
Texture	**Vapour vol%**	**T_h (°C)**	**T_{melt} (°C)**	**NaCl equ. wt%**
nonplanar-anhedral	5		-4.5	7.2
planar-euhedral	1-2	81		
planar-euhedral	1-2	82		
planar-euhedral	2	89		
planar-euhedral	2	80		
planar-euhedral	2	80		
planar-euhedral	1-3	70-72		
planar-euhedral	1-3	70-72		
planar-euhedral	1-3	70-72		
planar-euhedral	1-3	70-72		
planar-euhedral	1-3	70-72		
planar-euhedral	1-3	70-72		
nonplanar-anhedral	5	105		
planar-euhedral	3	82		
planar-subhedral	1-3	78		
planar-subhedral	1-3	79		
planar-subhedral	1-3	84		
planar-subhedral	1-3	84		
planar-euhedral	2-4	75		
planar-euhedral	2-4	78		
planar-euhedral	2-4	75		
planar-euhedral	1	75		
planar-euhedral	1	75		
planar-euhedral	1	75		
nonplanar-anhedral	1	86		
nonplanar-anhedral	1	72		
nonplanar-anhedral	1	78		
nonplanar-anhedral	1	75		
nonplanar-anhedral	1	82		
nonplanar-anhedral	1	80		
nonplanar-anhedral	1	78		
nonplanar-anhedral	1	89		
nonplanar-anhedral	3	72		
nonplanar-anhedral	3	72		
nonplanar-anhedral	1	79		
nonplanar-anhedral	1	85		
nonplanar-anhedral	15		-3	5
nonplanar-anhedral	20		-2.6	4.3
nonplanar-anhedral	3-5	85		
nonplanar-anhedral	1	82		
nonplanar-anhedral	1	75		
planar-euhedral	15		-0.5	7.9-7.2
planar-euhedral	10		-0.5	7.9-7.2
nonplanar-anhedral	15-20		-2	3.4
planar-euhedral	5	80		
planar-euhedral	5	78		
planar-euhedral	5	78		

Appendix-Table 3: Microthermometric data of primary, two-phase aqueous inclusions of sample O-02, Budaörs Dolomite, Odvas Hill

Sample	Sample description	Measured phase	$\delta^{13}C_{V\text{-}PDB}$ (‰)	$\delta^{18}O_{V\text{-}PDB}$ (‰)	Treatment for separation	Formation
O-02	planar-e dolomite	dolomite	2.6	0.3	micro-drilling	Budaörs Fm
T-04 (D-01)	nonplanar-a and planar-e	dolomite	3.2	1.3	micro-drilling	Hauptdolomit Fm
T-05 (DC-01)	nonplanar-a dolomite	dolomite	3.1	1.1	etching	Hauptdolomit Fm
T-04 (D-01)	planar-e dolomite	dolomite	2.9	0.7	micro-drilling	Hauptdolomit Fm
T-04 (D-01)	nonplanar-a dolomite	dolomite	3.1	1.3	micro-drilling	Hauptdolomit Fm
O-02	planar-e dolomite	dolomite	2.3	-1.6	micro-drilling	Budaörs Fm
O-02	nonplanar-a dolomite	dolomite	2.3	0.1	micro-drilling	Budaörs Fm
O-04	nonplanar-a and planar-e	dolomite	2.9	-0.4	micro-drilling	Budaörs Fm
O-04	nonplanar-a and planar-e	dolomite	2.6	-2.3	micro-drilling	Budaörs Fm
G-05	nonplanar-a and planar-e	dolomite	2.2	-4.8	micro-drilling	Hauptdolomit Fm
NK-05	planar-e dolomite	dolomite	2.24	-4.03	micro-drilling	Budaörs Fm
NK-05	nonplanar-a dolomite	dolomite	2.33	-0.38	micro-drilling	Budaörs Fm
Tug-07	nonplanar-a and planar-e	dolomite	2.2	-3.8	micro-drilling	Budaörs Fm
	Dolomite associated with calcite or quartz:					
Kk-03	dolomite breccia and red calcite	dolomite	3.7	-0.5	etching	Hauptdolomit Fm
Tu-04	white calcite along vein	calcite	-7.4	-10.7	micro-drilling	Hauptdolomit Fm
Tu-06	white calcite in vug	calcite	-6.2	-10	micro-drilling	Hauptdolomit Fm
J-06	white calcite veinlet	calcite	-6.8	-9.6	micro-drilling	Hauptdolomit Fm
J-02 (DC-03)	dolomite and white calcite	calcite	-5.6	-8.6	etching	Hauptdolomit Fm
K-07	dolomite breccia and white calcite	calcite	-5.5	-8.3	etching	Hauptdolomit Fm
J-04	fine-crystalline white calcite along veinlet	calcite	-4.5	-7.2	micro-drilling	Hauptdolomit Fm
J-04	coarse-crystalline white calcite along veinlet	calcite	-3.8	-6.3	micro-drilling	Hauptdolomit Fm
J-05	calcite from the concretion (calcite-III)	calcite	-4.7	-8.3	micro-drilling	Hauptdolomit Fm
J-13	white calcite	calcite	-3.2	-9.1	micro-drilling	Hauptdolomit Fm
Kk-03	dolomite breccia and red calcite	calcite	-0.6	-7.6	etching	Hauptdolomit Fm
T-05/1	dolomite and red calcite	calcite+dolomite	-2.5	-4.7	etching	Hauptdolomit Fm
T-05/2	dolomite and red calcite	calcite+dolomite	-1.8	-2.5	etching	Hauptdolomit Fm
T-05	dolomite and small amount of red calcite	calcite+dolomite	-1.3	-2.8	micro-drilling	Hauptdolomit Fm
T-05	red calcite and small amount of dolomite	calcite+dolomite	-2.1	-3.8	micro-drilling	Hauptdolomit Fm
NK-06	dolomite and red calcite	calcite+dolomite	-0.1	-3.7	micro-drilling	Hauptdolomit Fm
K-07	dolomite breccia and white calcite	calcite+dolomite	-1.8	-5.8	etching	Hauptdolomit Fm
J-02 (DC-03)	dolomite and white calcite	calcite+dolomite	-0.6	-2.1	etching	Hauptdolomit Fm
Tu-08	red calcite and small amount of dolomite	calcite+dolomite	-3.52	-5.47	micro-drilling	Hauptdolomit Fm
O-20	dolomite and very minor red calcite	dolomite	2.95	-1.18	micro-drilling	Budaörs Fm
Cs-05	boxwork of quartz and powdered dolomite clasts	dolomite	3.13	1.15	micro-drilling	Budaörs Fm
Cs-10	powdered dolomite next to siliceous vein	dolomite	3.03	0.34	micro-drilling	Budaörs Fm

Appendix-Table 4: $\delta^{13}C_{V\text{-}PDB}$ (‰) and $\delta^{18}O_{V\text{-}PDB}$ (‰) values of different types of dolomite samples

Sample	Sample description	Measured phase	$\delta^{13}C_{V\text{-}PDB}$ (‰)	$\delta^{18}O_{V\text{-}PDB}$ (‰)	Treatment for separation	Formation
	Disintegrated dolomite samples:					
P-06	dolomite of fitted breccia texture	dolomite	3.15	0.93	bulk sample	Hauptdolomit Fm
Bu-02 (DP-01)	powdered dolomite from below bauxite	dolomite	3	0.3	bulk sample	Hauptdolomit Fm
Cs-03	texture-preserving powdered dolomite	dolomite	3.7	0.1	bulk sample	Budaörs Fm
Cs-07	local-type powdered dolomite	dolomite	2.72	-0.18	bulk sample	Budaörs Fm
Cs-11	powdered dolomite with reddish stain	dolomite	3.03	0.67	bulk sample	Budaörs Fm
Cs-14	thin powdered dolomite layer	dolomite	3.41	0.52	bulk sample	Budaörs Fm
K-02A	powdered dolomite from below bauxite	dolomite	2.91	-0.57	bulk sample	Hauptdolomit Fm
Nk-01	local-type powdered dolomite	dolomite	2.91	-0.28	bulk sample	Budaörs Fm
Nk-02	mosaic breccia blocks floating in powdered dolomite	dolomite	2.44	-0.6	bulk sample	Budaörs Fm
Nk-03	dolomite of mosaic breccia texture	dolomite	2.52	-0.3	bulk sample	Budaörs Fm
P-05	disintegrated dolomite bed	dolomite	2.47	-0.52	bulk sample	Hauptdolomit Fm
P-07A	dolomite clasts from a sample that is a mixture of breccia and powdered dolomite	dolomite	2.59	0.07	bulk sample	Hauptdolomit Fm
P-07B	dolomite powder from a sample that is a mixture of breccia and powdered dolomite	dolomite	2.67	-0.57	bulk sample	Hauptdolomit Fm
P-08A	dolomite powder from a layer of thin powdered dolomite with a few dolomite clasts	dolomite	2.72	-0.51	bulk sample	Hauptdolomit Fm
P-08B	dolomite clast from a layer of thin powdered dolomite with a few dolomite clasts	dolomite	2.81	-0.21	bulk sample	Hauptdolomit Fm
P-14	powdered dolomite along a fracture	dolomite	2.6	-1.1	bulk sample	Hauptdolomit Fm
Z-03	reddish-coloured dolomite powder from below bauxite	dolomite	2.84	-0.41	bulk sample	Hauptdolomit Fm

Appendix-Table 4 continued: $\delta^{13}C_{V\text{-}PDB}$ (‰) and $\delta^{18}O_{V\text{-}PDB}$ (‰) values of different types of dolomite samples

Sample-code	Sample location and host rock type	measured phase	$\delta^{13}C_{V\text{-}PDB}$ (‰)	$\delta^{18}O_{V\text{-}PDB}$ (‰)
O-02	Odvas Hill, Budaörs Dolomite	dolomite cement	2.3	-1.6
O-02	Odvas Hill, Budaörs Dolomite	replacive dolomite	2.3	0.1
O-02	Odvas Hill, Budaörs Dolomite	dolomite cement	2.6	0.3
O-04	Odvas Hill, Budaörs Dolomite	bulk rock	2.6	-2.3
O-04	Odvas Hill, Budaörs Dolomite	bulk rock	2.9	-0.4
T-04	Teve Cliff, Hauptdolomit	dolomite cement	2.9	0.7
T-04	Teve Cliff, Hauptdolomit	replacive dolomite	3.1	1.3
T-04	Teve Cliff, Hauptdolomit	bulk rock	3.2	1.3
T-05	Teve Cliff, Hauptdolomit	replacive dolomite	3.1	1.1
Ro-42	Róka Hill, Dachsten Limestone	bulk rock	1.6	-3.3
L-17	Lapos quarry, Buda Marl	bulk rock	0.8	-5.1
F-24	Fenyőgyöngye quarry, Szépvölgy Limestone	bulk rock	0.56	-8.96
M-14	Mátyás Hill, Szépvölgy Limestone	bulk rock	0.98	-9.8
L-11	Lapos quarry, Buda Marl	vein-calcite	1	-11.7
L-11	Lapos quarry, Buda Marl	vein-calcite	1.3	-11.7
L-05	Lapos quarry, Buda Marl	vein-calcite	2.4	-10.6
L-28	Lapos quarry, Buda Marl	vein-calcite	0.5	-14.8
L-31	Lapos quarry, Buda Marl	vein-calcite	1.5	-12.6
Ro-33	Róka Hill, boundary of breccia and Dachstein Limestone	vein-calcite	1.9	-11
Ro-34	Róka Hill, boundary of breccia and Dachstein Limestone	vein-calcite	2	-9.2
Ro-35	Róka Hill, breccia	vein-calcite	1.7	-13.7
Ro-24	Róka Hill, Dachstein Limestone	vein-calcite	2.1	-13.4
Ro-46	Róka Hill, breccia	vein-calcite	0.8	-13.6
Ro-20	Róka Hill, breccia	vein-calcite	0.8	-15.6
Ro-61	Róka Hill, breccia	vein-calcite	0.4	-15.6
F-11	Fenyőgyöngye quarry, Szépvölgy Limestone	vein-calcite	1.7	-12.9
F-12	Fenyőgyöngye quarry, Szépvölgy Limestone	vein-calcite	1.5	-14
F-05	Fenyőgyöngye quarry, Szépvölgy Limestone	vein-calcite	2	-14.9
O-16	Odvas Hill, Budaörs Dolomite	vein-calcite	-0.2	-15
O-04	Odvas Hill, Budaörs Dolomite	vein-calcite	0.9	-14.8
Tug-06	Törökugrató, Budaörs Dolomite	vein-calcite	0.6	-14.4
Tug-08	Törökugrató, Budaörs Dolomite	vein-calcite	1.1	-14.7
Tug-08	Törökugrató, Budaörs Dolomite	vein-calcite	1.3	-11.7
Tug-09	Törökugrató, Szépvölgy Limestone	vein-calcite	1.4	-12.9
Tug-03	Törökugrató, Budaörs Dolomite	vein-calcite	0.3	-18.7
Tug-01	Törökugrató, Budaörs Dolomite	vein-calcite (corroded)	-0.5	-16
Szb-02	Szemlőhegy Cave, Szépvölgy Limestone	vein-calcite	1.3	-17.1
Szb-11	Szemlőhegy Cave, Szépvölgy Limestone	vein-calcite	1.1	-12.9
Sz-f 1a	Szemlőhegy Cave, Szépvölgy Limestone	vein-calcite (corroded)	-0.6	-13.7
Sz-f 1b	Szemlőhegy Cave, Szépvölgy Limestone	vein-calcite (corroded)	1.2	-17.6
Sz-f 1c	Szemlőhegy Cave, Szépvölgy Limestone	vein-calcite (corroded)	0.2	-14.5
Szb-18	Szemlőhegy Cave, Szépvölgy Limestone	vein-calcite (corroded)	0.2	-14.7
P-15	Piliscsaba, Hauptdolomit	vein-calcite	1.9	-9.5

Appendix-Table 5: Stable oxygen and carbon isotope values of vein-calcite and different host rocks

Sample	O-16	Tug-01	Tug-03	Szb-11	Szb-18	L-18	Ro-12	M-05	M-03	F-16	O-01	Ksv-02	L-01
Mineral	calcite	calcite	calcite	calcite	calcite	calcite	calcite	calcite	calcite	calcite	barite-I	barite-II	barite-II
SiO_2 (wt%)	0.09	0.09	0.06	0.13	1.25	0.08	0.12	0.11	0.23	0.03			
Al_2O_3	0.02	0.02	0.01	0.03	0.22	0.03	0.02	0.03	0.06	0.02			
Fe_2O_3	0.02	0.02	0.01	0.03	0.02	0.03	0.01	0.02	0.02	0.01			
CaO	54.3	55.3	55.4	54.7	53.9	55	54.2	53.6	53.5	54.6			
MgO	0.82	0.21	0.22	0.21	0.36	0.13	0.5	0.15	0.89	0.39			
Na_2O	0.02	0.01	0.01	0.02	0.03	0.02	0.03	0.02	0.01	0.01			
K_2O	0.02	0.02	0.02	0.02	0.03	0.02	0.02	0.01	0.02	0.01			
TiO_2	<0.01	<0.01	<0.01	<0.01	0.01	<0.01	<0.01	<0.01	<0.01	<0.01			
MnO	0.08	0.06	0.05	0.02	0.03	0.02	0.01	0.02	0.04	0.02			
P_2O_5	0.01	0.01	0.01	0.01	0.01	0.01	0.01	0.01	0.01	0.01			
LOI	43.1	42.8	42.5	43.2	42.4	43.2	43.3	45.2	43.2	43.2			
Total	98.5	98.6	98.3	98.4	98.5	98.5	98.3	99.2	98	98.4			
La (ppm)	1.4	2.1	1.7	1	5.7	0.8	<0.5	1.8	1.7	0.8	2.4	2.1	8
Ce	3.4	4.5	3.5	1.6	7.8	1.3	0.5	3.1	2.5	0.8	0.9	<0.5	2
Pr	0.47	0.72	0.59	0.25	1.18	0.17	0.06	0.52	0.36	0.13	0.07	<0.03	0.08
Nd	2	3	2.7	1.1	4.7	0.7	0.2	2.4	1.6	0.6	1	0.6	0.9
Sm	0.42	0.91	0.86	0.25	1.01	0.17	0.04	0.63	0.38	0.15	0.57	0.35	0.45
Eu	0.12	0.29	0.24	0.06	0.27	0.03	<0.03	0.16	0.1	0.04	2.37	2.05	1.83
Gd	0.43	1.22	1.08	0.32	1.16	0.17	<0.05	0.71	0.52	0.2	0.75	0.56	0.68
Tb	0.07	0.23	0.19	0.05	0.2	0.03	<0.01	0.11	0.08	0.03	0.02	0.01	0.02
Dy	0.4	1.38	1.19	0.26	1.17	0.16	<0.05	0.69	0.53	0.17	<0.05	<0.05	<0.05
Ho	0.08	0.31	0.23	0.05	0.25	0.03	0.01	0.13	0.12	0.04	<0.01	<0.01	<0.01
Er	0.2	0.84	0.64	0.16	0.78	0.1	<0.03	0.35	0.39	0.1	0.03	<0.03	<0.03
Tm	<0.01	0.1	0.05	<0.01	0.07	<0.01	<0.01	0.02	0.02	<0.01	0.01	<0.01	<0.01
Yb	0.17	0.62	0.49	0.1	0.65	0.09	<0.03	0.29	0.33	0.05	0.34	0.23	0.26
Lu	0.01	0.12	0.07	0.02	0.1	0.02	<0.01	0.04	0.06	<0.01	0.11	0.07	0.09
Ba	54.4	7.2	1.9	61.6	2390	2.7	1.5	45.3	21.1	6	>10000	>10000	>10000
Co	0.6	1.2	0.7	1.1	6.4	0.8	0.8	1.8	<0.5	2	1.5	<0.5	<0.5
Cs	<0.01	0.13	<0.01	0.02	0.09	0.02	<0.01	0.01	0.06	<0.01	<0.01	<0.01	0.01
Cu	<5	<5	<5	<5	<5	<5	<5	<5	<5	<5	23	<5	<5
Ga	0.1	0.3	0.1	0.1	0.2	0.1	<0.1	0.1	0.2	0.1	0.2	0.1	0.1
Hf	<0.2	<0.2	<0.2	<0.2	<0.2	<0.2	<0.2	<0.2	<0.2	<0.2	0.2	<0.2	<0.2
Ni	<5	<5	<5	<5	<5	<5	<5	<5	<5	<5	<5	<5	<5
Nb	<0.2	0.2	<0.2	<0.2	<0.2	<0.2	<0.2	<0.2	<0.2	<0.2	<0.2	<0.2	<0.2
Pb	<5	<5	<5	<5	<5	<5	<5	5	6	<5	17	<5	<5
Rb	0.4	0.3	<0.2	0.2	0.6	0.2	0.2	<0.2	0.3	<0.2	<0.2	<0.2	0.3
Sr	243	194	164	108.5	231	79.4	288	86.9	459	429	>10000	>10000	5820
Ta	<0.1	0.1	<0.1	<0.1	<0.1	<0.1	<0.1	<0.1	<0.1	<0.1	0.1	0.1	0.1
Th	0.46	0.37	0.12	0.12	0.4	0.08	0.07	0.14	0.08	<0.05	<0.05	<0.05	0.1
U	0.4	1.67	0.58	0.13	0.19	0.29	<0.05	0.32	0.07	<0.05	0.15	<0.05	<0.05
V	5	15	14	<5	11	<5	<5	<5	9	<5	<5	<5	<5
W	3	3	3	2	4	4	7	2	2	3	<1	<1	<1
Y	2.8	10.1	9.6	2.2	11.7	1.8	<0.5	5.1	5.1	2	1.8	1.3	1.5
Zn	<5	12	<5	<5	18	<5	<5	<5	<5	<5	58	37	49
Zr	3	3	2	3	6	5	3	3	3	4	2	<2	<2

Appendix-Table 6: Concentration of major and trace elements in the vein-calcite from different localities.